UNIVERSITÀ DEGLI STUDI DI PADOVA
Dipartimento di Ingegneria Industriale
Corso di Laurea Magistrale in Ingegneria Aerospaziale

Simulations of oblique impacts on regular and hierarchical lattice structures

RELATORE: Prof. Ugo Galvanetto
CORRELATORE: Dr. Siamak Farajzadeh Khosroshahi

LAUREANDO: Matteo Destro 1147958

a.a. 2018/2019

UNIVERSITÀ DEGLI STUDI DI PADOVA
Dipartimento di Ingegneria Industriale
Corso di Laurea Magistrale in Ingegneria Aerospaziale

Simulations of oblique impacts on regular and hierarchical lattice structures

RELATORE: Prof. Ugo Galvanetto
CORRELATORE: Dr. Siamak Farajzadeh Khosroshahi

LAUREANDO: Matteo Destro 1147958

a.a. 2018/2019

ai miei genitori ed a Giorgia, che hanno sempre incoraggiato i miei sogni e che giorno dopo giorno mi hanno supportato senza farmi mai pesare nulla, rappresentando sempre un porto sicuro,

a tutti i miei nonni che sono stati sempre disponibili, preziosi complici e fonte di saggi consigli oltre che miei appassionati tifosi e pronti aiutanti,

a Rachele che con costanza, pazienza e determinazione mi ha incoraggiato, aiutato e accompagnato in questo percorso di studio così come al di fuori, spronandomi a dare sempre il meglio in vista del futuro.

INDEX

ABSTRACT

This study has considered twelve configurations of lattice structures subjected to oblique impacts (45 deg) with three different velocities: 6m/s, 7.5m/s and 9m/s.
The lattice structures studied are different for number of cells through the thickness, cell shape and cells relative dimensions (homogeneous or hierarchical schemes).

The interest in these structures is addressed to the improving of impact absorbing performances in application including the protective helmets. The lattice structures have demonstrated incredible potential if used as helmet liners instead of traditional foams [13].

This study aims to further investigate how the geometric parameters influence the performances of these structures under oblique impacts.

FEM analyses have been done using LS-Dyna software. The results processed with a specifically written MATLAB code are presented in chapter 3.

To define the best trade-offs it has been considered the deformation process of the specimens, their transmission of forces and their absorption of energy.
For all the result sets the best performing structures are those with five through-the-thickness tetrahedral-shape cells and that one with ten hierarchical through-the-thickness prismatic-shape cells.

1. INTRODUCTION

1.1 Helmets

Inside the wide branch of impact engineering, many efforts are made in order to provide effective solutions in design and production of personal protective equipment applied in impacts protection.

One type of such protective devices are helmets. They are mainly necessary to protect head and neck from impacts that might occur in sports, motorsports or during everyday life bicycle or motorbike rides.

During impacts, the most important parameters to take into consideration are the maximum impact energy and the transmitted loads in terms of forces and accelerations [1,2].

A helmet generally consists of a main dome surrounding the upper side, the rear side and the lateral sides of the head, a movable visor in front of the eyes zone and a chin-strap to fasten the helmet itself to the head of the person. Some helmets, mostly used by motorcyclists, extreme sports athletes and motorsports riders in general, have a main dome comprising a chin-bar. In this case they are called full-face helmets.

The main dome of a helmet is the main part associate with the impact-protection function. It consists of a rigid outer shell and a thick inner liner. The former part is generally made of thermoplastic materials such as polycarbonate (PC), acrylonitrile-butadiene-styrene (ABS) or composites like glass or carbon fiber in epoxy or polyester resins. The liners are generally made of expanded foams, typically expanded polystyrene (EPS) [1-3].

The main functions of the outer shell are:

• the distribution of impact load over the largest possible area in order to avoid concentrated loads and decrease the stress felt by the liner;

• the reduction of the likelihood that sharp objects and road obstacles might penetrate the helmet.

The liner is the most important part of the helmet for:

• the absorption of impact energy;

• the minimization of loads transmitted to the head.

These loads may cause cranial fractures considering the strain on the skull and brain injuries considering the accelerations exerted on the head [2,3].

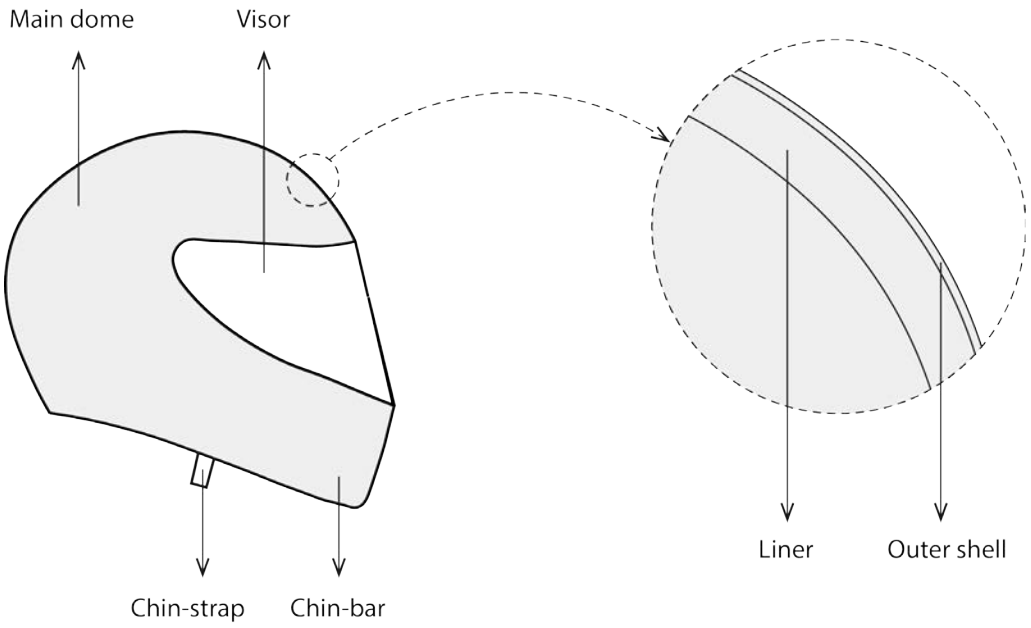

Figure 1: Schematic representation of a full-face helmet with zoomed sectioned view.

1.2 Foams

As stated, the liner is the most important part for the absorption of impact energy and for the reduction of transmitted loads.

EPS foam properties drive the performances of the liner. A foam is characterised by a complex microscopic structure made of few millimeters wide beads containing smaller closed cells whose dimensions are of the order of *100 μm*.

Looking at microscopic analyses performed in [1] it is clear that the manufacturing process of a foam cannot ensure a uniform cell distribution, leaving more dense cells at the boundaries of the beads.

The energy absorption capabilities are due both to bead walls and cell walls buckling.

Foams may also be called cellular solids and it is intuitive that their properties depend on microscopic structure parameters such as cell walls thickness and cell dimensions and on intrinsic features of the constitutive material.
Microscopic parameters and foam density are correlated. This lead to the fact that by varying the foam density it is possible to vary the microscopic parameters and, in consequence, the energy absorption capabilities [4].

The deformation mechanics of the liner material underpin the impact protection capability of the liner itself. In order to briefly summarize the deformation mechanics it is useful to consider the stress-strain curve.
A general stress-strain curve for an elastomeric foam may be subdivided in three main regions:

I. linear elastic;
II. plateau;
III. densification.

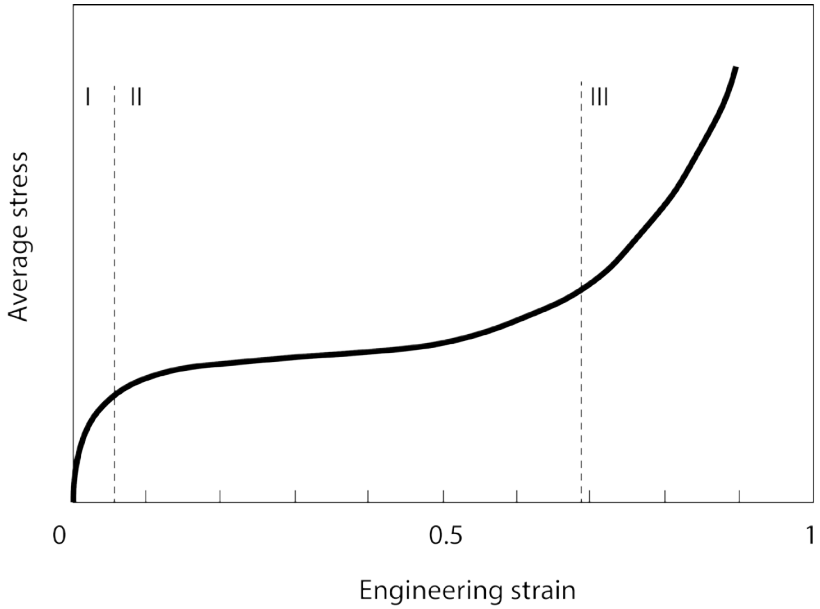

Figure 2: Typical compression stress-strain curve of a rigid foam. [1]

Linear elastic region characterised the small strains and it is driven by bending of cell edges, compression of gas trapped into the cells and by stretching of cell walls.
Plateau region is a wide region after the linear elastic one, that occurs when the stress reaches the yield point. This plateau is related to the occurrence of permanent hinges due to excess in bending moment acting at the cell walls, plastic stretching of cell walls and rising of gas pressure into the cells.
Densification region is relative to high strains where cells are completely collapsed and their opposite walls come into contact “creating” a bulk material whose stress increases with the strain following the slope given by the Young’s modulus of the constitutive material.

Different tests on EPS [1] show the density is the key parameter for the impact protection: high-density EPS absorb more energy than low-density EPS but transmit higher loads.
Lighter EPS has a larger amount of material contributing to the energy absorption than heavier EPS which respond only with cells close to the impact point.

All of these considerations suggest that the impact protection capabilities of foams may be enhanced both controlling macroscopic and microscopic properties.
Moreover, they suggest that using materials whose properties vary through the thickness may optimized the performances.
Since, as stated before, all properties may be changed by varying the density, different foams has been created in which the through-the-thickness density vary.

Such materials are layered foams and functionally graded foams (FGF).
Layered foams are made of overlapping uniform density layers, each one with its own density. These type of foam have a quite easy manufacturing process but the abrupt gaps of density at the interfaces between the layers may lead to concentrated stress and during impacts it might occur delamination or crack propagation [4-6].

In the FGF the through-the-thickness variation in density is made with continuous gradients. In this way the material does not have interfaces with strong discreteness and the just mentioned issues does not take place.
One possible trouble for FGF is the manufacturing process.

FGF show transmitted stress decrease through the thickness if the impact occur at the higher density side. A decreasing density gradient from impact side to inner side is the best choice for FGF in order to obtain major advantages in peak forces transmission.
In terms of absorbed energy, the comparison between functionally graded and uniform foams show substantial advantages under low-energy impacts for the former and nearly the same performances under high-energy impacts. This lead to prefer FGF because they offer overall higher performances. Furthermore, it is remarkable that the FGF reduce the duration of the highest accelerations [4,5].

Applied to helmet liners, FGF compared to uniform foams has demonstrated reduction in peak acceleration with increased contact area [7].

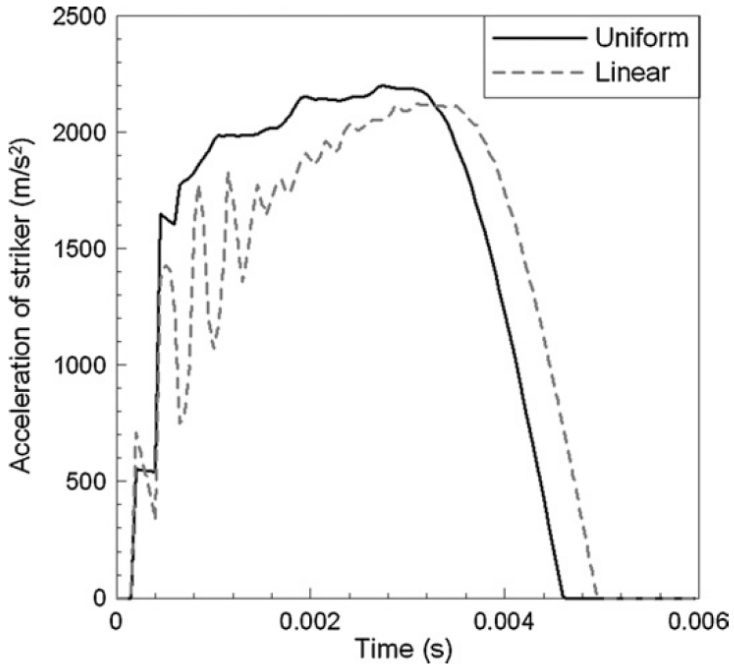

Figure 3: Example of acceleration of the impactor dropped on uniform foam block compared with linearly graded foam block. [4]

1.3 Lattice Structures

Many cellular materials are used for impact energy absorption purpose.
Lattice structures can belong to this category, their repeating geometry may be well-defined by the designer.
Making a parallel with foams, remembering that mechanical properties deeply depend also in microscopic features and hence in cell parameters, it is clear that it is possible to vary the mechanical properties of a lattice structure acting on its cell geometry.
This fact makes possible a further consideration: lattice structures offer much more control on mechanical properties than such a foam may do. This is a consequence of the microscopic geometry of foams that is stochastic instead of prior well-defined such as in lattice structures. Indeed, even if it is known how cells tend to distribute inside the beads, it is not possible to control the dimensions of each cell, wall, strut and bead.
The only current limitation in geometry design of lattice structures is related to the minimum possible manufacturing resolution.
Intricate geometries are possible using additive manufacturing technology that leave theoretically limitless freedom in geometry definition.
Additive manufacturing enables the creation of only open-cells structures because the presence of dividing walls between the cells would make it impossible the removal of the fabrication residuals.

Consequently, it is clear that lattice structures absorb energy with one main mechanism: buckling of struts. Only theoretically, work done pushing air out of the cells helps the energy absorption too but it is not so effective in lattice structure because the scale is too large to represent significant obstacles for the air flow.
Lattice structures, thanks to additive manufacturing, may be designed only looking at their final functionalities, giving the designer the freedom to tailor the internal architecture to the specific use and to the desired properties [8,9].
These considerations drive to affirm that using lattice structures may be more effective than the use of traditional materials.

Stress-strain curves obtained during compression tests show lattice structures have a behaviour similar to foams one. They present the initial linear elastic region, the wide plateau and the densification region for high strains.
The biggest difference is that lattice structures have an initial peak right before the

plateau starts. Abrupt drops mainly noticeable in high strain rate curves are caused by failures that occurs in the specimens, these failures are due to fracture of the struts near the nodes related to stress concentration and to buckling-induced fracture [8,10].

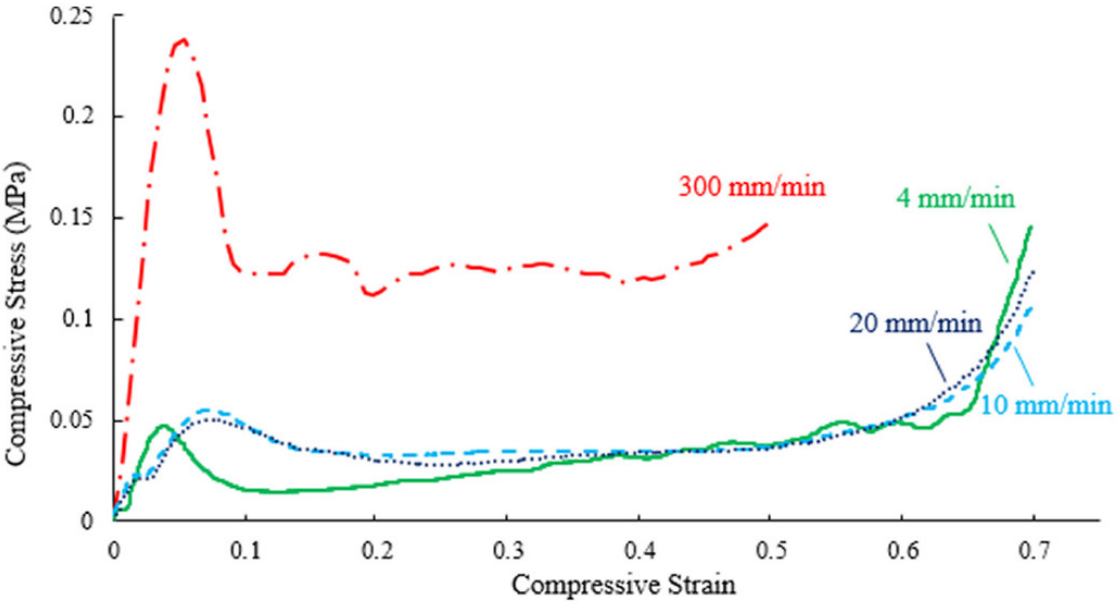

Figure 4: Stress-strain curves of varying strain rates for a specimen of lattice structure. [10]

Lattice structures thought to be obtained through additive manufacturing and applied as energy absorbing inner liner for helmets have been studied in [2]. In this application has been used square shape cellular structure with homogeneous cell dimensions.

The study show a decrease in peak translational accelerations and an increase in acceleration pulse durations when the density of the structure is reduced.

These significant results confirm that the use of this type of structure may lead to large improvements in impact protections.

Furthermore, the use of this cellular structure leads to savings in weight, size and material quantity with respect to the use of traditional foams.

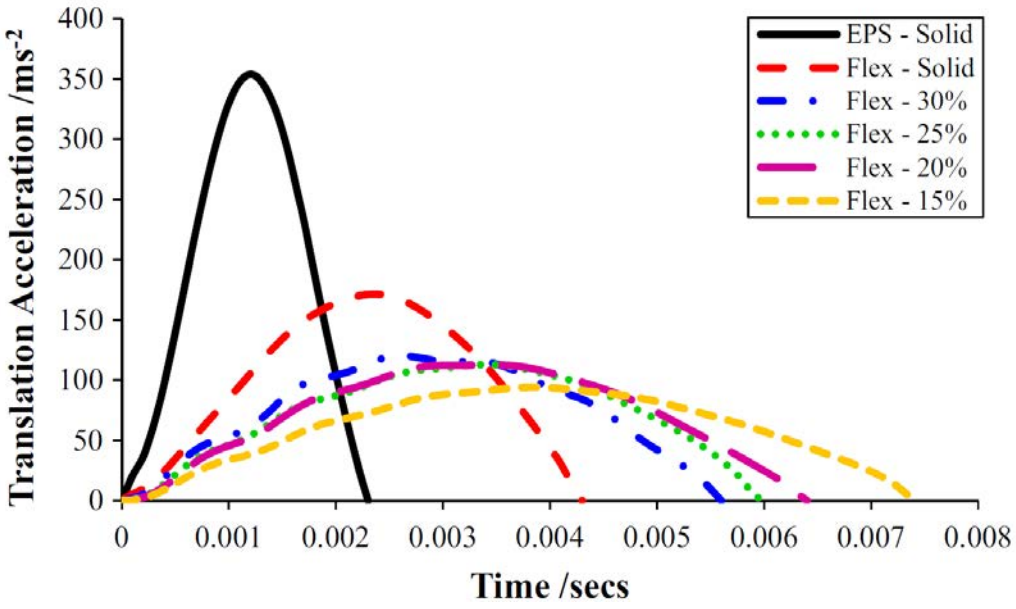

Figure 5: Comparing effects of helmets inner EPS liner with lattice liner (Flex) on headform translational acceleration. [2]

Many natural cellular materials can be included in lattice structures category. They are present in stiffness and lightweight demanding apparatus. Looking at several of them deeply, it is evident they consist of hierarchical architecture, made of repeating self-similar or different shape cells in smaller scales.

This fact give impulse to the study of hierarchical lattice structures in order to understand their effectiveness in applications like energy absorption.

Hierarchical lattice structures offers significant improvements in compressive strength especially for low density lattices of lower orders. These structures make possible to tailor stiffness and strength by varying shapes, scale lengths, and density for the best trade-offs in every single application.

Deformation mechanisms of lattice structures are heavily influenced by nodal connectivity.

It plays an important role determining how cells react during loading and hence determining the macroscopic properties of the structure [11,12].

Thus, energy absorption capabilities of lattice structures can be optimized using hierarchy and therefore be tailored on the different applications.

Taking into account the improvements of using hierarchy in structures, the

enhancing protection obtained with the application of lattice structures in helmets and remembering the effectiveness of vary the through-the-thickness properties in helmet's liners, it has been hypothesised the use of hierarchical lattice structures as inner liner materials for protective helmets [13].

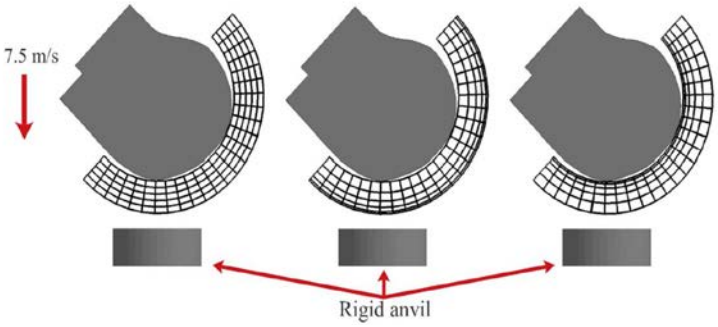

Figure 6: Schematic representation of helmets with regular lattice liner (left), with softer lattice layer close to the headform (middle) and with stiffer lattice layer close to the headform (right). [13]

Astonishing results are achieved in terms of impact protection. Peak linear acceleration is reduced by 44% to 60% in direct impacts and by 38% to 63% in oblique impacts using hierarchical lattice liner instead of different density EPS foams. Rotational accelerations are reduced too in case of using the hierarchical lattice liner by 55% to 70%.
Furthermore, hierarchical lattice liner may reduce brain injuries showing a reduction in brain strains and stresses.

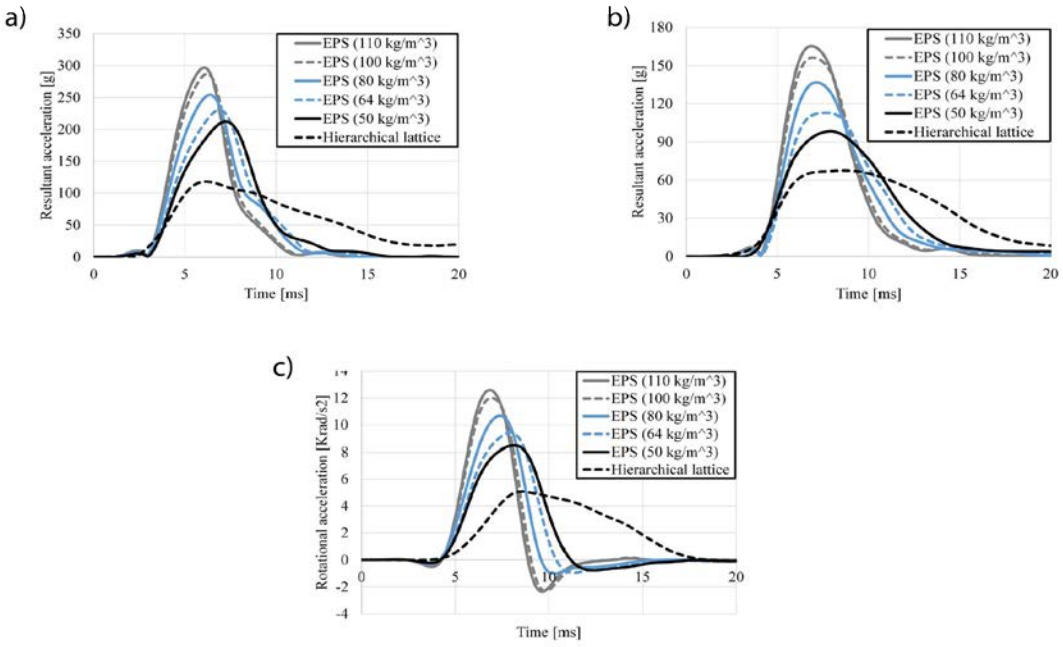

Figure 7: Resultant acceleration comparing EPS foams with hierarchical lattice. a) linear acceleration for direct impact, b) linear acceleration for oblique impact, c) rotational acceleration for oblique impact. [13]

1.4 Oblique Impacts

In real situations helmets rarely impact normal to the road surface. In many cases they impact with an angle different from 90deg. Impacts normal to road surface cause only compressive forces and linear accelerations on the head while oblique impacts cause both compressive and shearing forces on the helmet. These forces are related to simultaneous linear and rotational accelerations of the head.

It has been demonstrated that rotational accelerations give rise to brain damages of different entities depending on their values.

Peak rotational accelerations are mainly dependent on three parameters: the impact velocity component normal to the road surface, the friction coefficient between the outer shell of the helmet and the road surface and the impact direction that has influence on normal stress distribution across the inner surface of the liner and its deformation [14].

Oblique impacts tests on EPS foam specimens have been performed with a custom test rig in order to study combined compression-shear loading in [15,16].

Quasi-static tests show that biaxial loading reduce the compressive stress at yield compared to pure compression tests and that shear stress at yield is lower than compressive stress at yield.

High strain-rate dynamic tests are more interesting for impact study purposes.

Impacts with 2.2, 3 and 4 m/s velocities have been tested. At lower velocity, low density foams have flat plateau while for higher velocities the plateau become more inclined showing the strain-rate dependence.

These studies have shown that for oblique impacts compressive and shearing stress at yield are dependent from foam density and strain-rate.

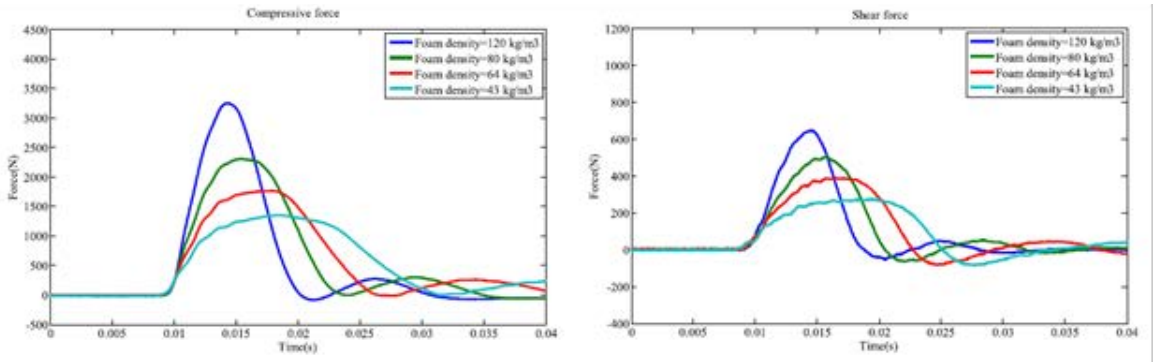

Figure 8a: Compressive and shear forces for oblique impacts on foams. v = 2.2 m/s. [16]

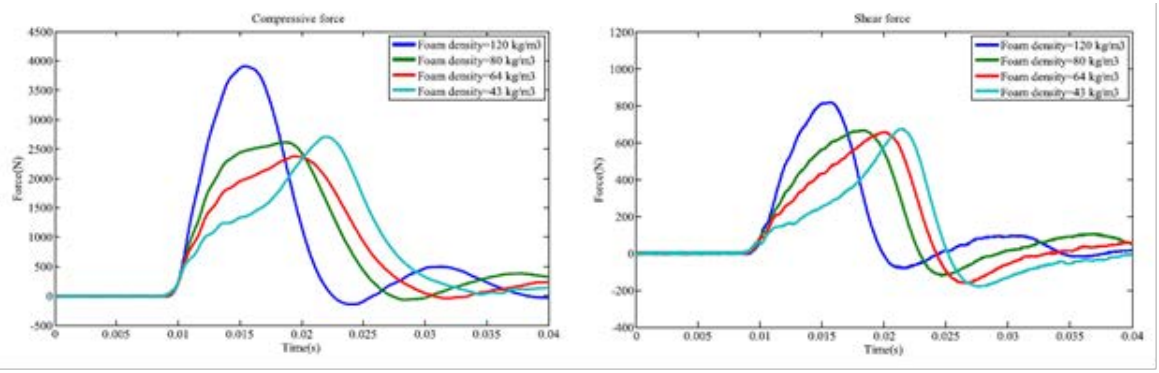

Figure 8b: Compressive and shear forces for oblique impacts on foams. v = 3 m/s. [16]

1.5 This Study Leading Arguments

This introductory report stated:

- the incredible possibilities to enhance the protection from impacts using lattice structures instead of foams;
- the additional improvement options given by the use of hierarchy providing many tailoring chances;
- the importance of studying oblique impacts that cause different loading conditions simultaneously.

From the conclusive considerations of [13], knowing the encouraging results that it shown, it is clear the need to make further research to deeply understand this type of structures with different characteristics under different conditions trying to find the best solutions.

The present study has the aim to compare different types of lattice structures for energy absorber applications under oblique impacts conditions.

The structures taken into account presents self-similar cells with two different topologies: prismatic and tetrahedral. Each topology is considered with regular and hierarchical architecture and they have been studied for three through-the-thickness number of cells: five, ten and twenty.

Moreover, three different impact velocities are applied: *6, 7.5* and *9 m/s*.

The chosen impact configuration is similar to that developed for [15] and modelled in [17], it consists of a specimen of lattice structure in contact with a rigid supporting anvil 45*deg* tilted, with a rigid impactor, tilted as the anvil, descending with vertical velocity.

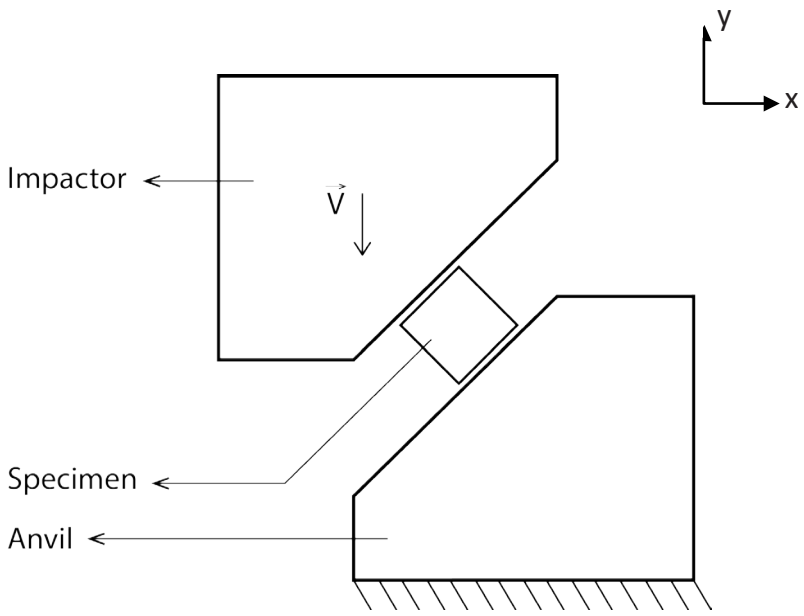

Figure 9: Model configuration chosen for this study.

2. MODELS DESCRIPTION

2.1 Geometry Description

As reported above, different lattice structures in term of cells shapes, cells dimensions and through-the-thickness number of cells were created.

Cells shapes are prismatic and tetrahedral, their dimensions are all equal for the regular structures and different for the hierarchical ones. All the specimens have the same dimensions of *40x40x40 mm* and, as stated before, they have five, ten or twenty through-the-thickness cells. Different numbers of through-the-thickness cells will be also called “densities” of the structure.

Combining the different explained features, the total number of different structures studied is twelve:

- Prismatic regular with five cells (P05R);
- Prismatic regular with ten cells (P10R);
- Prismatic regular with twenty cells (P20R);
- Prismatic hierarchical with five cells (P05H);
- Prismatic hierarchical with ten cells (P10H);
- Prismatic hierarchical with twenty cells (P20H);
- Tetrahedral regular with five cells (T05R);
- Tetrahedral regular with ten cells (T10R);
- Tetrahedral regular with twenty cells (T20R);
- Tetrahedral hierarchical with five cells (T05H);
- Tetrahedral hierarchical with ten cells (T10H);
- Tetrahedral hierarchical with twenty cells (T20H).

For the hierarchical structures were used the relations applied in [13]: the cells sizes follow $l=n\,\Delta l$ where l is the length of the considered n^{th} cell and $\Delta l= 2L/(N(N+1))$ with L as specimen thickness and N as number of cells through the thickness.

Tables 1-3 report struts lengths for hierarchical specimens.

5 CELLS - PRISMATIC		
Cell number	**Strut Length [mm]**	**Specimen Thickness [mm]**
1	2.667	40
2	5.333	40
3	8.000	40
4	10.667	40
5	13.333	40

Table 1: Dimensions of cells for 5 through-the-thickness cells specimen - Prismatic cells.

10 CELLS - PRISMATIC		
Cell number	**Strut Length [mm]**	**Specimen Thickness [mm]**
1	0.727	40
2	1.455	40
3	2.182	40
4	2.909	40
5	3.636	40
6	4.364	40
7	5.091	40
8	5.818	40
9	6.545	40
10	7.273	40

Table 2: Dimensions of cells for 10 through-the-thickness cells specimen - Prismatic cells.

20 CELLS - PRISMATIC		
Cell number	**Strut Length [mm]**	**Specimen Thickness [mm]**
1	0.190	40
2	0.381	40
3	0.571	40
4	0.762	40
5	0.952	40
6	1.143	40
7	1.333	40
8	1.524	40
9	1.714	40
10	1.905	40
11	2.095	40
12	2.286	40
13	2.476	40
14	2.667	40
15	2.857	40
16	3.048	40
17	3.238	40
18	3.429	40
19	3.619	40
20	3.810	40

Table 3: Dimensions of cells for 10 through-the-thickness cells specimen - Prismatic cells.

Tables 4-6 report diagonal strut lengths for tetrahedral cells specimens (struts which constitute cell dimensions are of the same lengths of prismatic cells specimens).

5 CELLS - TETRAHEDRAL Cell Number	Diagonal strut length [mm]
1	5.812
2	6.254
3	6.928
4	7.775
5	8.743

Table 4: Dimensions of diagonal struts for 5 through-the-thickness cells specimen - Tetrahedral cells.

10 CELLS - TETRAHEDRAL Cell number	Diagonal strut length [mm]
1	2.852
2	2.920
3	3.032
4	3.181
5	3.362
6	3.572
7	3.805
8	4.057
9	4.326
10	4.607

Table 5: Dimensions of diagonal struts for 10 through-the-thickness cells specimen - Tetrahedral cells.

20 CELLS - PRISMATIC	
Cell number	**Strut Length [mm]**
1	1.417
2	1.427
3	1.443
4	1.465
5	1.492
6	1.525
7	1.563
8	1.606
9	1.654
10	1.705
11	1.760
12	1.818
13	1.880
14	1.944
15	2.010
16	2.079
17	2.150
18	2.222
19	2.297
20	2.372

Table 6: Dimensions of diagonal struts for 20 through-the-thickness cells specimen - Tetrahedral cells.

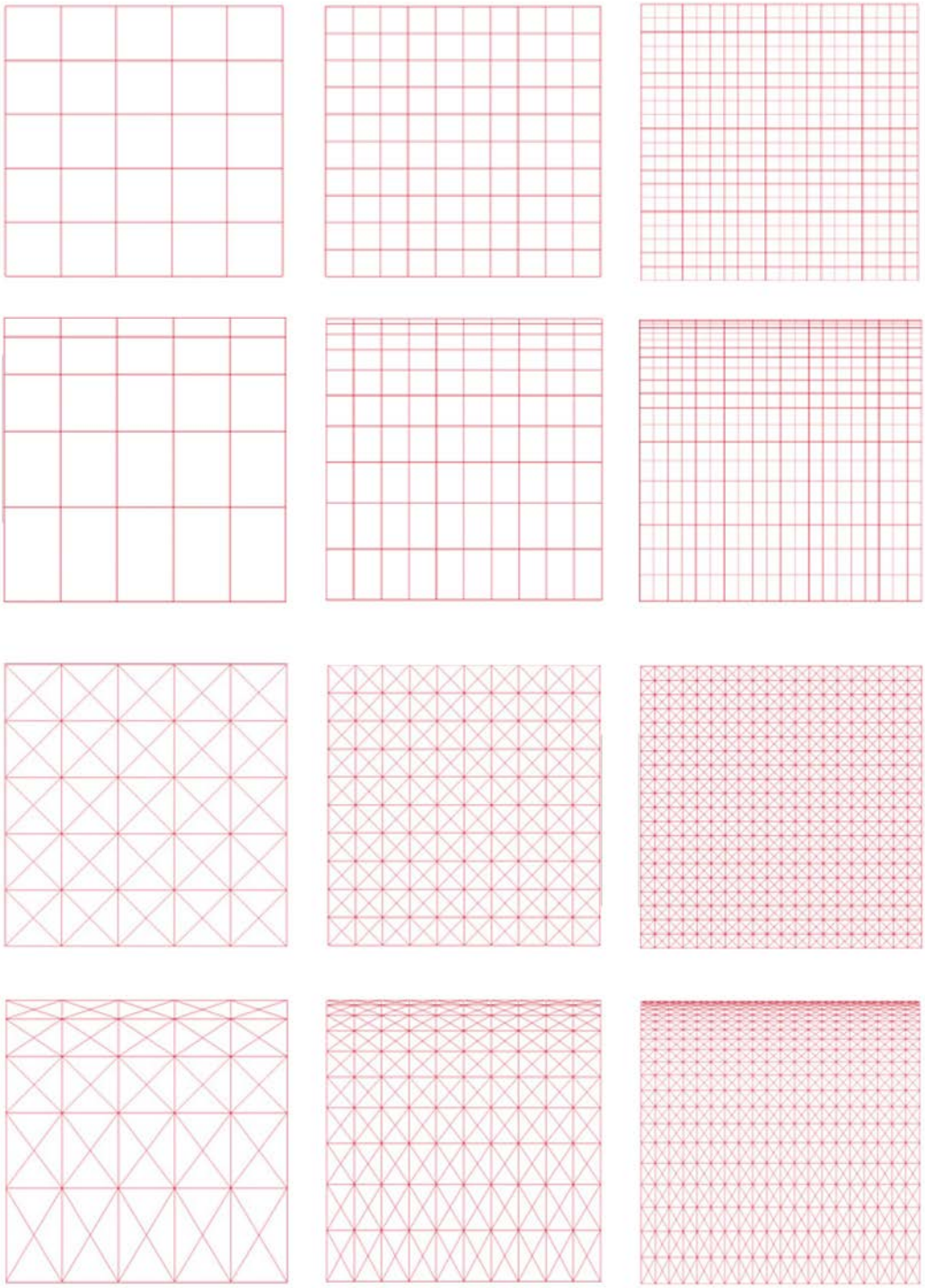

Figure 10: Geometries of the 12 different lattice structures studied. FIrst row: Prismatic regular cells. Second row: Prismatic hierarchical cells. Third row: Tetrahedral regular cells. Fourth Row: Tetrahedral hierarchical cells.

2.2 Material Description

Based on the material comparison made in [13], the material chosen for the structures in this work is Nylon (Polyamide 6), which is a good energy absorbing material because it presents plastic deformation during buckling.

Nylon mechanical properties implemented in the models are reported in Table 7.

MAT 24	
Density [kg/m3]	1100
Young's Modulus [MPa]	650
Poisson's Ratio	0.3
Yeld Stress [MPa]	10

Table 7: Nylon MAT24 mechanical properties.

The constitutive model used is Mat-24-Piecwise-Linear-Plasticity from LS-Dyna library with the Cowper-Symonds formulation adopted to include the effect of strain-rate; coefficients of this formulation were set to $C = 82\ s^{-1}$ and $P = 4.51$.

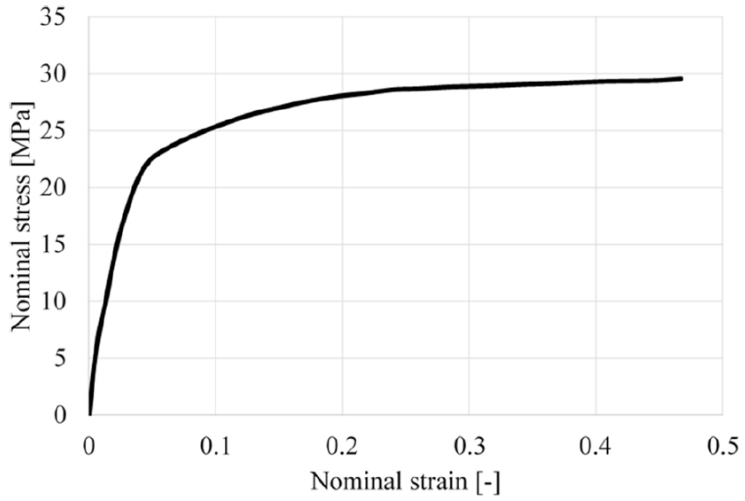

Figure 11: Stress-strain curve of Nylon (Polyamide 6). [13]

For the supporting anvil and the impactor, the material adopted is Mat-20-Rigid with the mechanical properties reported in Table 8.

MAT 20	
Density [kg/m3]	1173
Young's Modulus [MPa]	45
Poisson's Ratio	0.3

Table 8: MAT20 mechanical properties.

2.3 Elements and Mesh Properties

All the specimens are composed only of struts and so they can be modelled completely with beam elements.

The cross section of struts are circular solid with *1 mm* radius. Therefore, beam elements adopted for trusses modelling have a 1mm radius circular solid cross section too.

Because of adopting the same properties for beam elements, specimens with a greater number of trusses have also a greater mass.

Elements formulation implemented is Hughes-Liu with cross section integration.

Geometrical properties of beam elements are reported in Table 9:

Radius [mm]	1
Cross-section Area [mm^2]	3.124
Moment of inertia of the section [mm^4]	0.785

Table 9: Beam cross-section properties.

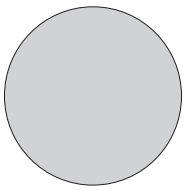

Figure 12: Beam cross-section.

With regards to the anvil and the impactor, the elements adopted are solids with constant stress formulation.

Each strut that composes the specimens is meshed in three elements. In this way, elements are not of the same size and this fact can be seen as a refinement of the

mesh from models with a lower through-the-thickness number of cells to the models with a greater number of them, if we consider regular specimens. Although if we consider hierarchical specimens, the refinement appear either in increasing through the thickness number of cells in the different specimens, either in proceeding from the base to the top of the same specimen.

2.4 Boundary Conditions

In the models there are two sets of single-point constraints as boundary conditions. The first one is to fix the anvil, so all of its nodes are blocked in six degrees of freedom (DOF); the second set is to permit the fall of the impactor, so its nodes are blocked in five DOF, leaving free only *Y* translation.

Contacts between anvil and lattice and between impactor and lattice are both automatic nodes to surface contacts in which the lattice are always set as slave following the convention that the stiffer body of a contact has to be set as master.
Friction is considered in order to represent as closely as possible an experimental test setup.

3. RESULTS

All the simulations have been made with LS-Dyna solver. With LS-PrePost software it was subsequently possible to access the results computed and to see the animations of the impacts.

Forces versus time and velocity of the impactor versus time data have been extracted using LS-PrePost and further processed and elaborated with a MATLAB code specifically written.

For the results evaluation it has been considered the master side of the anvil-lattice contact.

The focus of this work are the transmitted forces to the anvil and the absorbed energy. They are reported and discussed in order to understand the effectiveness of each type of the considered lattice structures in term of impacts protection.

3.1 Results Processing

The forces computed during the simulations in X e Y components has been rotated to obtain Normal and Shearing components.

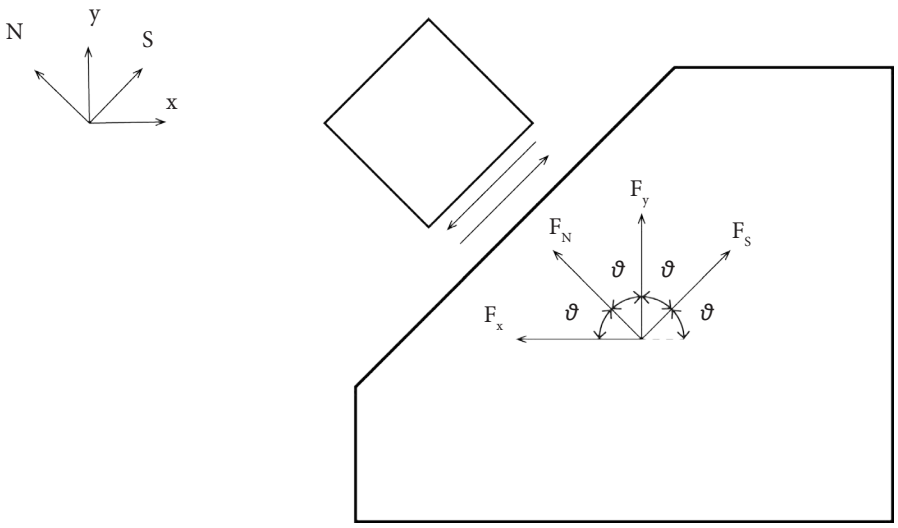

Figure 13: Reference system for forces rotation.

The equations applied to obtain the rotation, with reference to the above picture, are:

$$F_N = F_y \cdot \cos(\vartheta) + F_x \cdot \sin(\vartheta) \qquad (1)$$

$$F_S = F_y \cdot \sin(\vartheta) - F_x \cdot \cos(\vartheta) \qquad (2)$$

It has been evaluated the maximum values of the transmitted normal and shearing forces too. They represent the peak forces received by the anvil.

The absorbed energy has been computed as the difference between initial kinetic energy and final kinetic energy of the impactor:

$$E_{ab} = \frac{1}{2} m_{imp} v^2_{imp\text{-}init} - \frac{1}{2} m_{imp} v^2_{imp\text{-}fin} \qquad (3)$$

where *m* is the mass of the impactor and *v* is its velocity.
Because of the different masses of the specimens, it is interesting to compare the energy absorption capability related to the mass of the lattice structure. To do this, it has been computed the specific absorbed energy (SAE). SAE has been determined dividing the absorbed energy of each specimen by its own mass:

$$SAE = \frac{E_{ab}}{m_{spec}} \qquad (4)$$

3.2 Transmitted Forces

3.2.1 Comparison of different structure densities

a) 6m/s Impact Velocity

Following figures (from 14 to 21) show normal and shearing forces for the 6 m/s impact velocity and three successive animation frames of the simulations for each of the twelve structures. The frames are, from left to right, the initial time step of the impact, the instant at maximum deformation and, when possible, the first step after the detaching of the impactor or one of the last instants of the simulations.

Each force plot is relative to one type of structure (PR, PH, TR, TH). Hence, for given structure and impact velocity, each plot reports three curves relative to different through-the-thickness cells numbers.

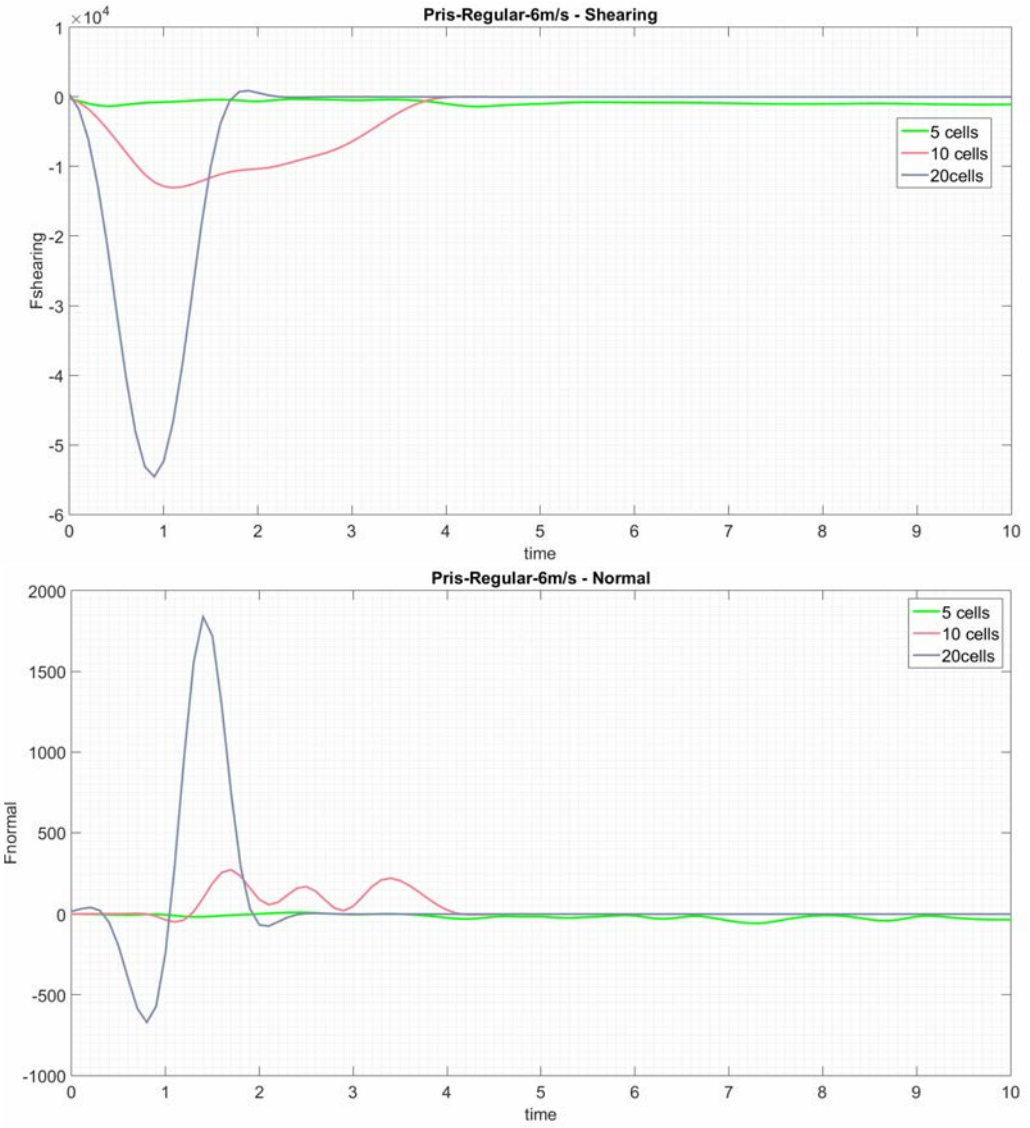

Figure 14: comparison of shearing and normal forces for different structures densities. PR - 6 m/s.

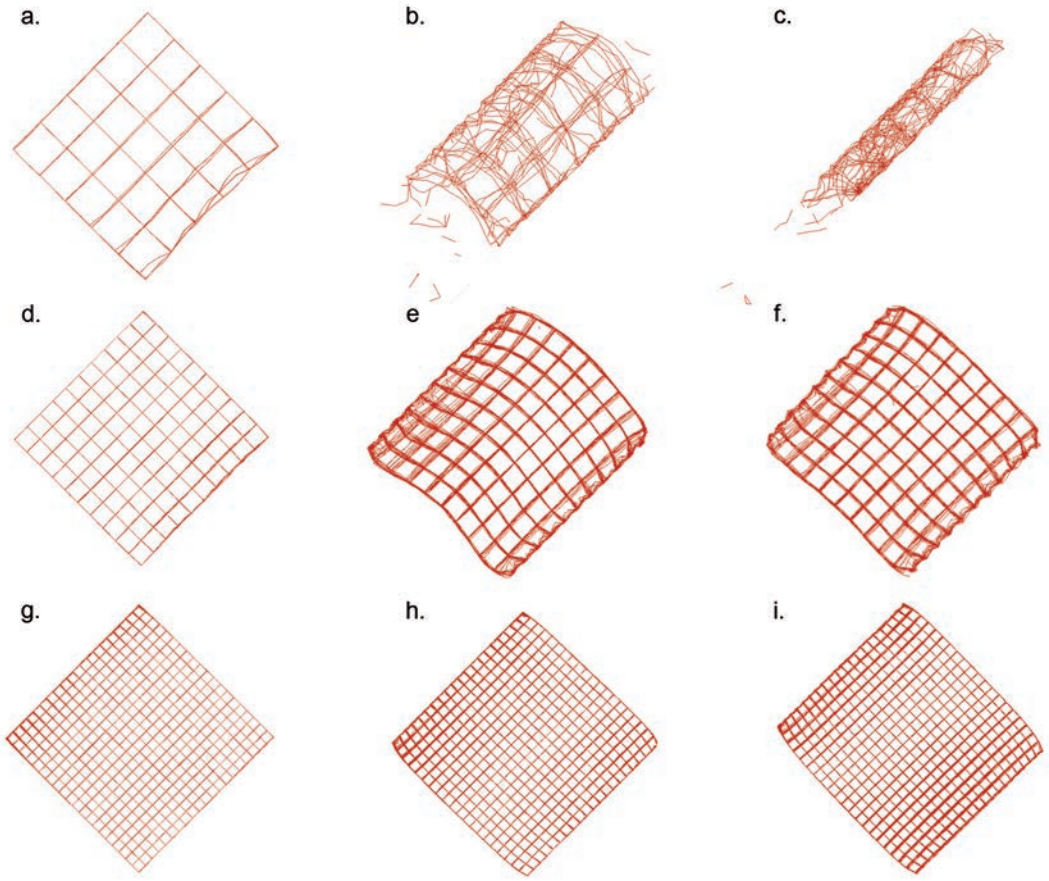

Figures 15: simulation frames for PR specimens during 6 m/s impact.

Figure 14 shows the Force-vs.-time plots for the specimens with prismatic-shape regular cells.

The five through-the-thickness cells structure seems to transmit very low loads. This is because the structure is too softer, it crushes completely during the impact, thus, it does not make resistance against the impactor. The complete crush is evident in figure 15c.

The peak in shearing force for the ten through-the-thickness cells number specimen correspond to the moment after which the structure starts to bend severely. For the twenty through-the-thickness cells number structure there is not significant bending because the cells are constituted from struts that are too small to buckle seriously. This lead to a stiff behaviour that cause an almost immediate rebound of the impactor.

The normal forces plot shows peculiar trends. It seems that the higher density structures are in stretching for a part of the impact duration. This is probably due to the shrinking occurs at the base of the specimens and to the rotation induced by the impact that may cause a hybrid situation between compression and tension in some

elements that leads to a resultant stretching.

From figures 15f and 15i it is visible how the higher density specimens recover some deformation occurred because most of their struts does not reach plastic strain. Hence, they present residual plastic strains after the detaching of the impactor localized at the base and top shrink zones.

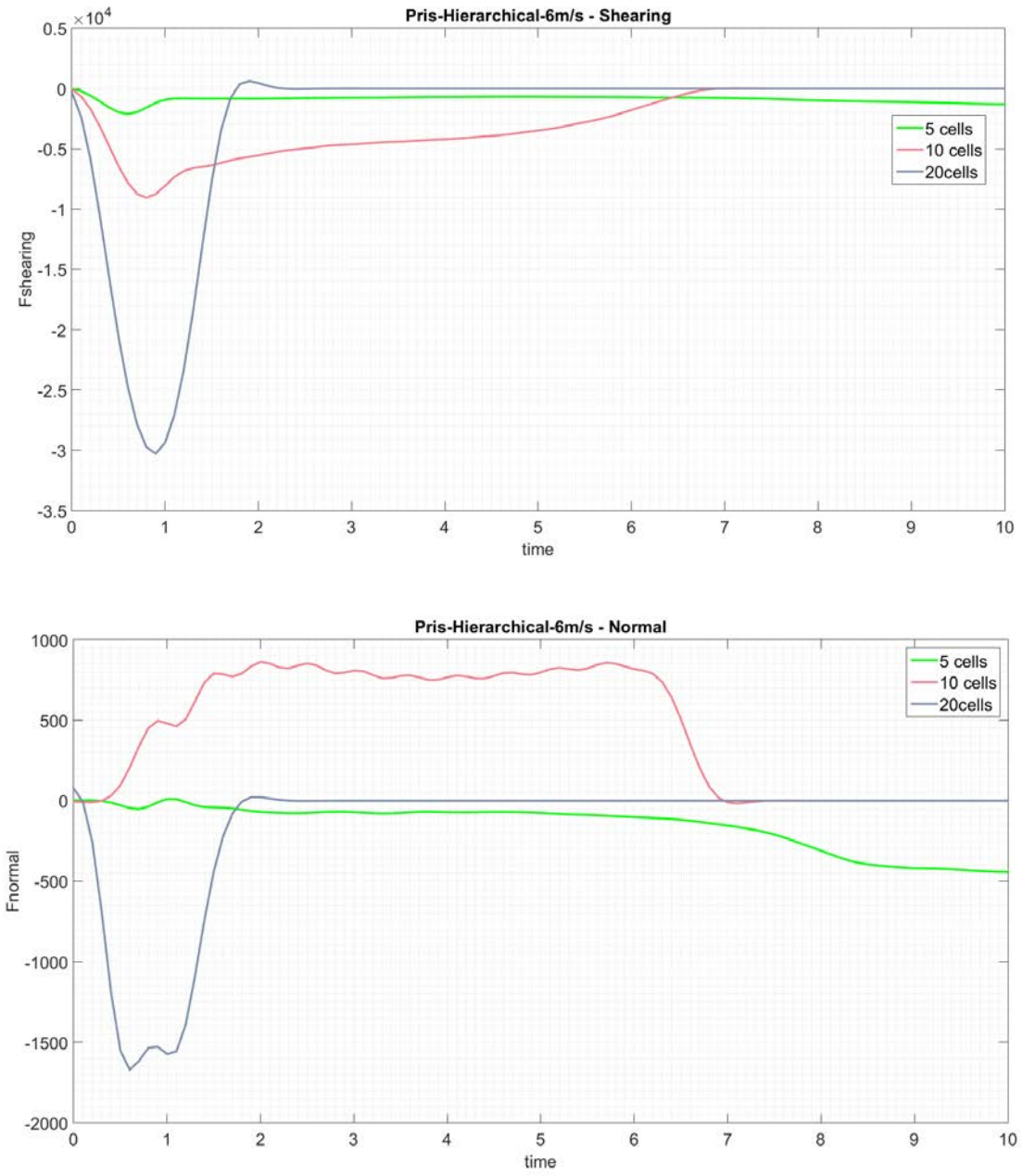

Figure 16: comparison of shearing and normal forces for different structures densities. PH - 6 m/s.

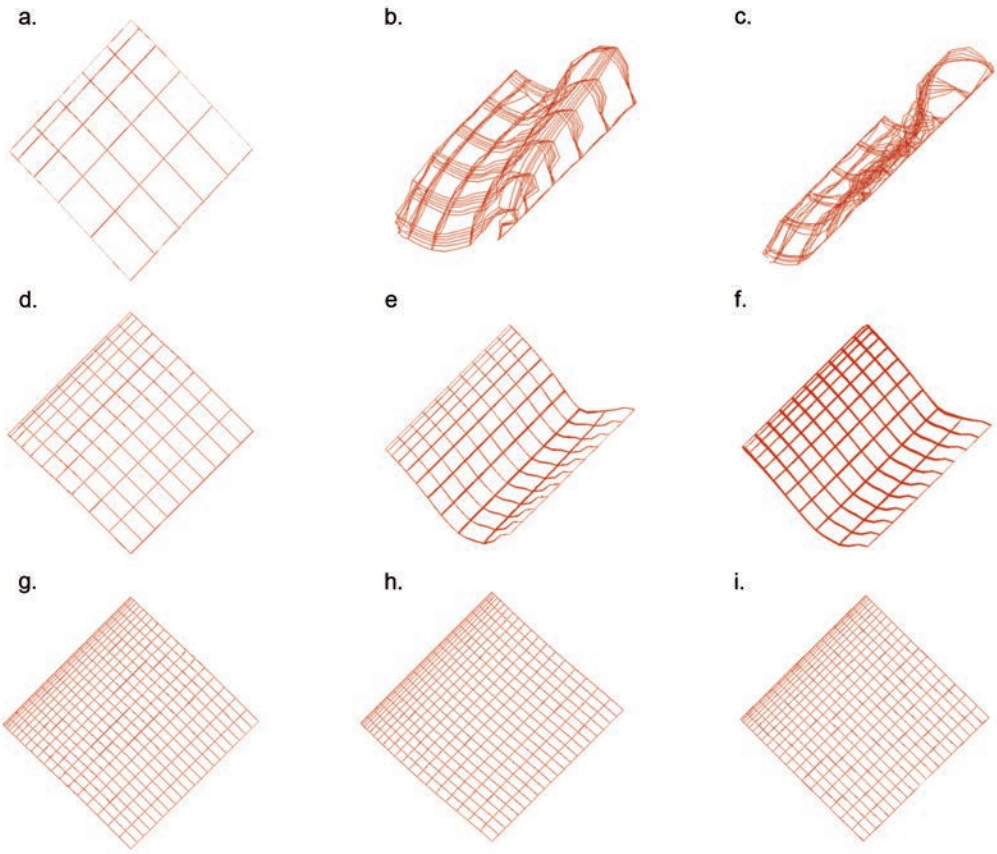

Figures 17: simulation frames for PH specimens during 6 m/s impact.

Forces plots for the prismatic hierarchical cells structures are reported in figure 16.

For the lowest density lattice structure, the hierarchy helps to make resistance against the impactor. The specimen reaches the maximum in shearing force right before the buckling starts, after the small drop the shearing force remains almost constant until the structure is completely folded on itself and smaller cells touch the anvil. In this moment both shearing and normal force increase until the end of the simulation. The normal force, before the just mentioned behaviour, has small values with slight fluctuations.

The hierarchy helps the ten through-the-thickness cells number specimen to buckle and hence to absorb the impact through the large deformations occurring. The shearing force increases until the buckling starts. The normal force trend is due to the rotation induced to the base of the specimen that leads to the overall stretching values.

The highest density structure forces trends show the peak in shearing force occur later with respect to the lower density structures. The high density of cells does not make the hierarchy modifying the shearing force trend even if it is evident the hierarchy

reduces the value of the peak. The normal force, on the contrary, reaches a higher compressive peak compared to the not hierarchical specimen.

From figure 17c appears that the specimen is completely folded and, probably, if the simulation continues it will appear a transmission of high forces due to the densification of the specimen that start to behave like almost a uniform solid block.

In figure 17f appears the specimen recover a little of deformation but remain largely plastic deformed.

For the twenty through-the-thickness cells specimen it seems the maximum deformation is very small and, at the detachment of the impactor, it looks there are none or very few plastic deformed elements.

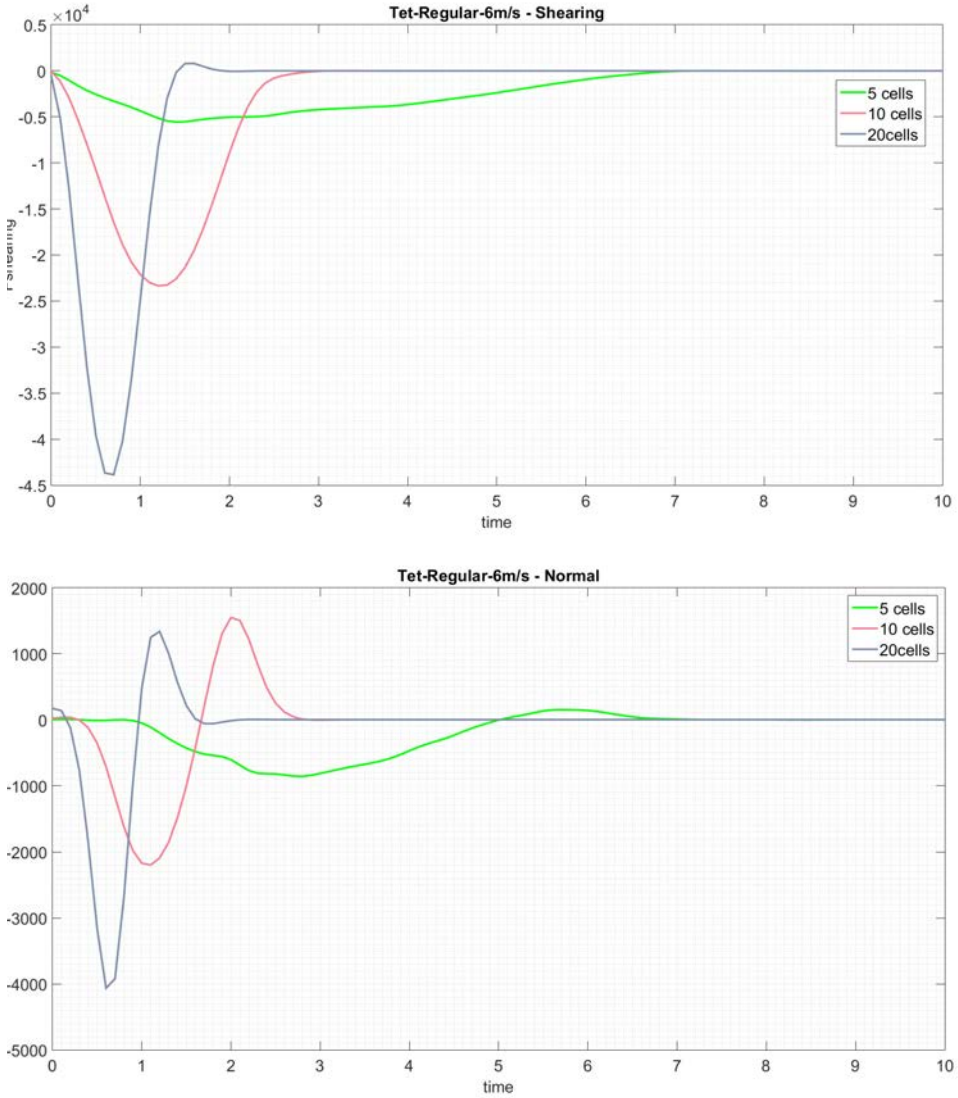

Figure 18: comparison of shearing and normal forces for different structures densities. TR - 6 m/s.

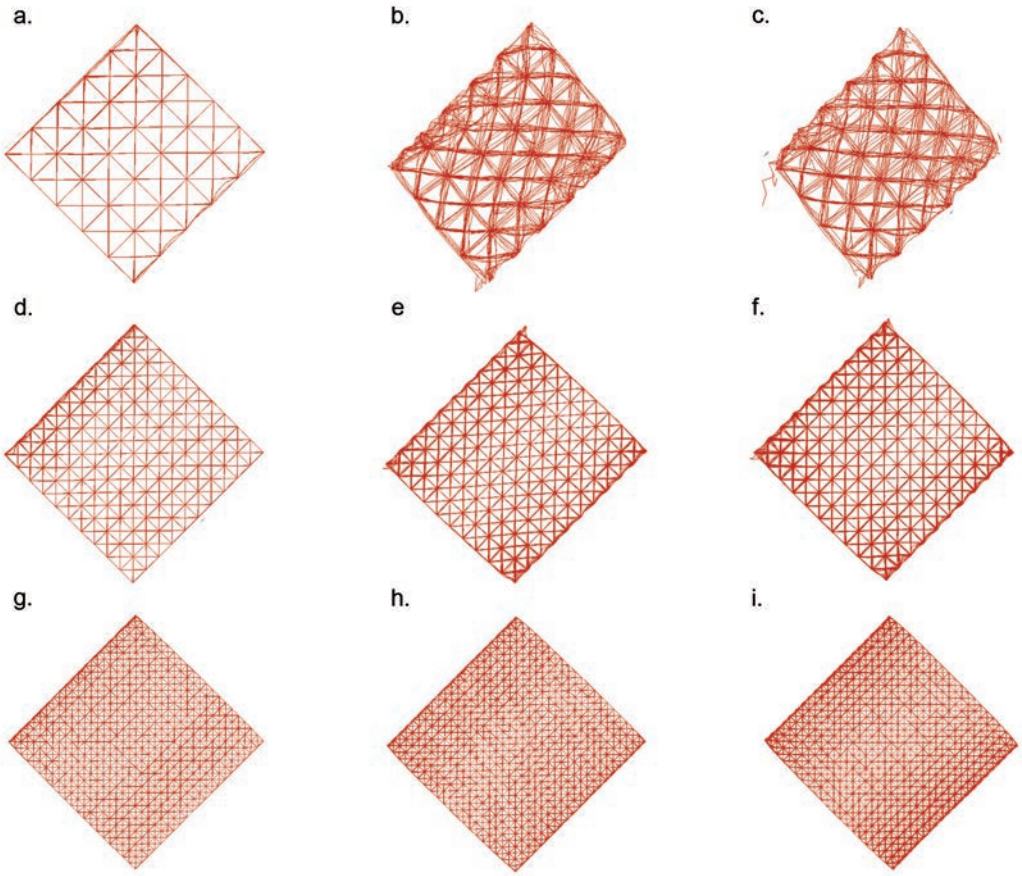

Figure 19: simulation frames for TR specimens during 6 m/s impact.

Considering the structures with tetrahedral-shape cells it is clear that they are stiffer because of the presence of diagonal struts.

Force vs. time plots of regular cells dimensions structures are reported in figure 18.

The lowest density specimen has the peak in shearing force that it is not at the start of the buckling; in this case shearing force increases until it exceed the friction force and the specimen start to slip.

The ten through-the-thickness cells and the twenty through-the-thickness cells specimens have similar trends both for normal and shearing forces. Main difference is that for the lower density structure the impact lasts more time. The peaks are reached for the normal force slightly before the shearing ones.

Looking at the figure 19c it is visible the partial crushing of the five through-the-thickness cells specimen that presents large plastic deformations too.

The ten through-the-thickness cells specimen shows a little crush with shrinks at the base and at the top that lead to plastic strains.

The highest density structure thanks to its stiffness presents very low plasticities mainly

localized at the base and at the top surfaces. The latter surfaces also present shrinks but smaller if compared to those of the just above described specimen.

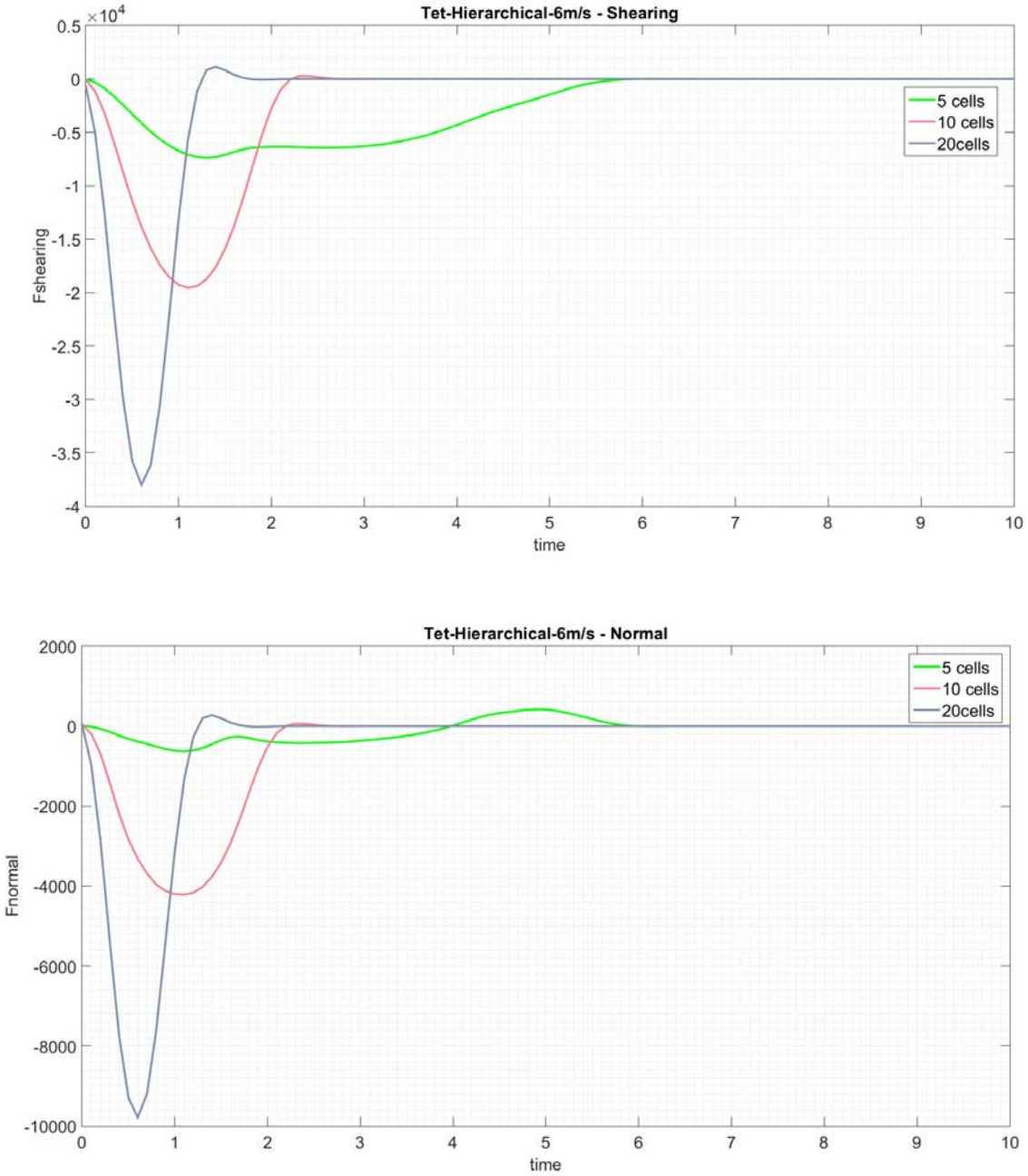

Figure 20: comparison of shearing and normal forces for different structures densities. TH - 6 m/s.

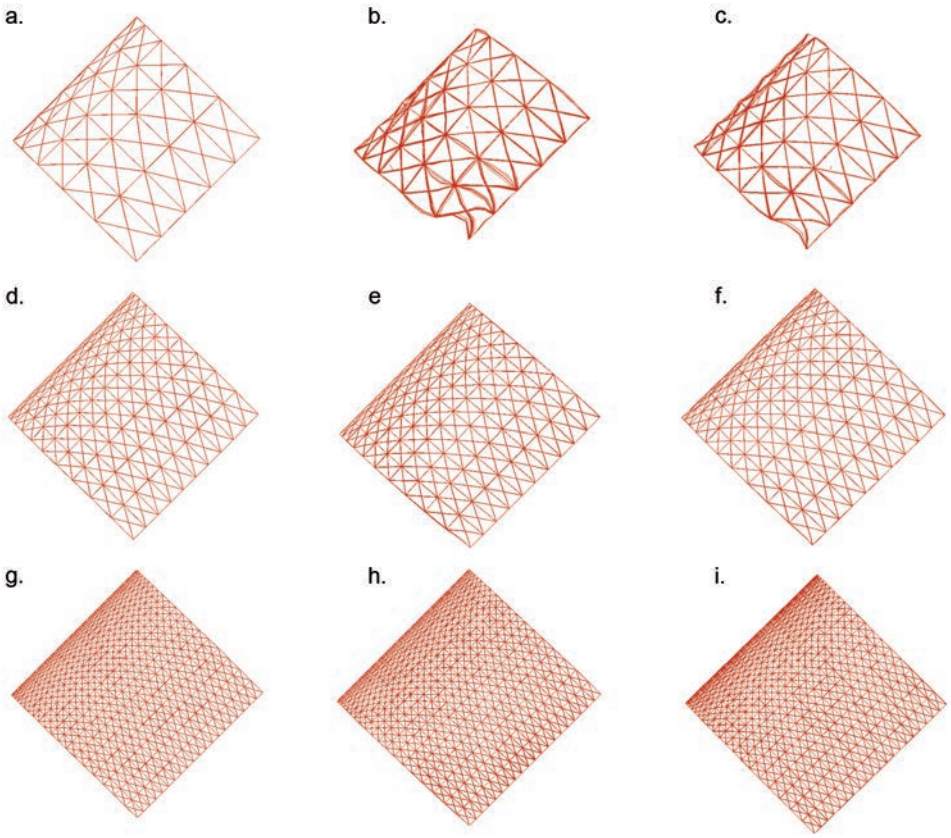

Figure 21: simulation frames for TH specimens during 6 m/s impact.

Figure 20 shows how hierarchy in tetrahedral-shape cells structures acts in transmitting forces.

The lowest density specimen reaches the peak in shearing force and after it, the buckling in some of larger cells become severe causing the shearing force to decrease gradually. Normal force remains low for the whole duration of the impact; its compressive peak is slightly before the shearing peak.

Similar to those for regular cells structures are the possible considerations for the higher density specimens. In this case the peaks of normal and shearing forces occur at the very same instant.

For these stiffer specimens, hierarchy does not make difference in term of during-the-impact behaviour because it is not sufficient to induce a severe buckling that causes a more gradual decrease of the forces like in the lowest density specimen. In terms of

peak values it is evident that hierarchy reduces the shearing peaks and increases the normal peaks.

As expected, at the end of the impact, the lowest density structure presents residual strain due to the reached plasticity. In figure 21b it is important to notice few of the smallest cells nearest to the impactor are totally collapsed in the wider underlying ones. These collapsed cells recover later with some failed struts. In the stiffer specimens, instead, the maximum deformations reached during the impact do not achieve the plastic region and hence the specimens recover their initial configurations.

6 m/s impact velocity resume

Looking at all the previous figures relative to the *6 m/s* impact, it is possible to do some general remarks.

It is highlighted that the transmitted forces, both normal and shearing, are higher for high-density lattices and lower for low-density lattices. This does not depend on the structure typology.

Parallel to the decrease in transmitted loads, decreasing the density of lattices tends to increase the duration of the impacts.

As expected, when the impact finishes, with the rebound and the detachment of the impactor from the specimen, the loads go to zero.

In case of prismatic-shape cells with five through-the-thickness cells specimens, both regular and hierarchical, it seems the impact does not finish within the simulation time. Those structures, in fact, are continuously crushing during the simulations. The time of simulation and the velocity of the impactor are not enough to see the impactor bouncing.

Each simulation shows that normal force is always lower than the shearing one. The difference may overlap an order of magnitude.

From the animation frames it is evident that in general the structures with regular dimensions of the cells, both prismatic and tetrahedral shape, have brittle behaviours leading to crushed specimens with a lot of failed struts. Hierarchical dimensions of the cells, instead, bring almost all the structures to deform without failing struts. The deformations, as seen, may be large and hence permanent or they may be not very large ensuring the initial configuration recovery of the structure. This depend on the cells density.

Comparing prismatic-shape with tetrahedral-shape cells it is evident the stiffer ones lead to obtain the force peaks earlier for the higher density specimens instead of earlier for the lower density ones like the prismatic-shape cells do.

b) 7.5 m/s Impact Velocity

Like for the *6 m/s* velocity, it is reported force vs. time plots and animation frames for each of the twelve different structures.

Each plot compares three different lattice densities for one fixed structure typology.

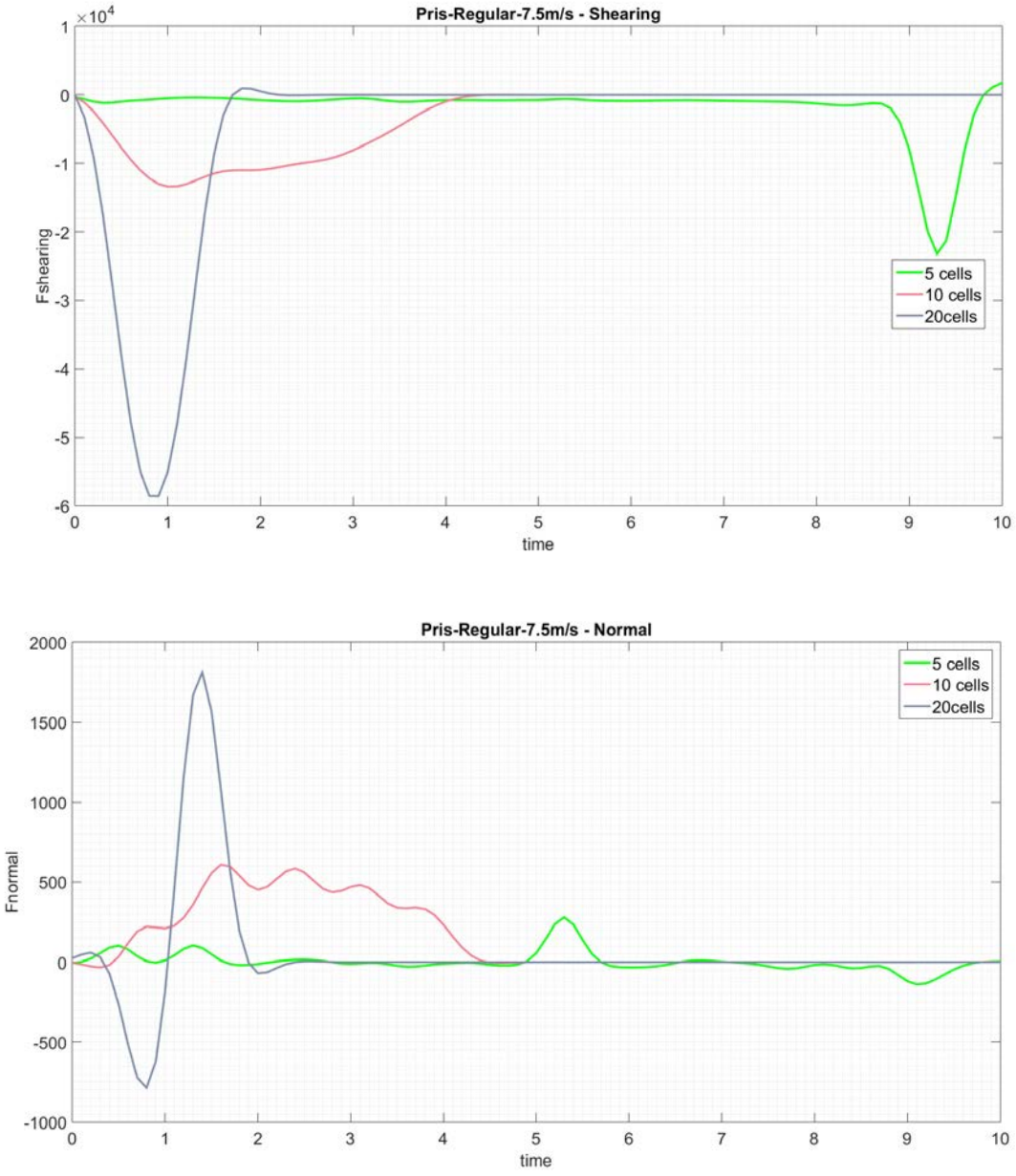

Figure 22: comparison of shearing and normal forces for different structures densities. PR - 7.5 m/s.

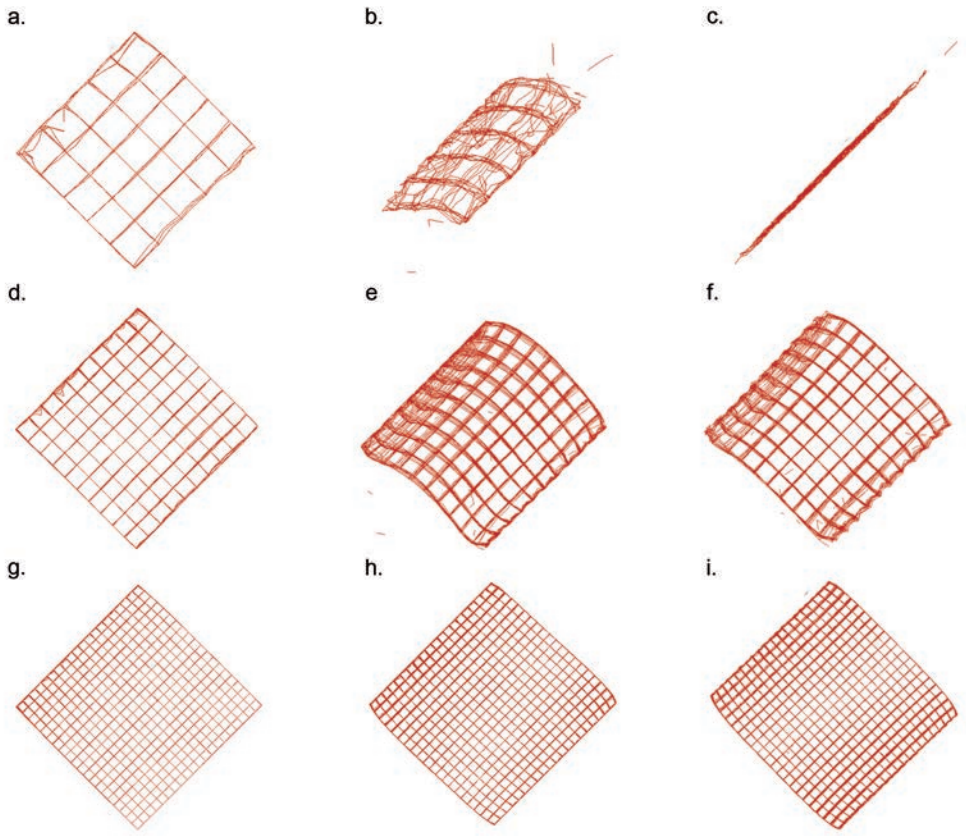

Figure 23: simulation frames for PR specimens during 7.5 m/s impact.

Let first consider the prismatic-shape in regular dimensions cells.

Force plots have similar trends to those for the *6 m/s* impact velocity. The main difference is in the lowest density structure that in this case presents a big peak in shearing force and a smaller one in the normal force near the end of the simulation time. Remaining the same time of simulation of the lower impact velocity, the impactor can go further in the crushing; this is clear looking at figure 23c.

The peaks mentioned above are probably due to the crushing of the struts that has turned into a solid layer of material.

As expected, while the trends remain similar, the transmitted forces values reached are bigger than those for the 6m/s impact.

In terms of residual deformations, it is more evident the ten through-the-thickness cells specimen has larger ones compared to the lower velocity impact and the upper level cells collapsed on the underlying one.

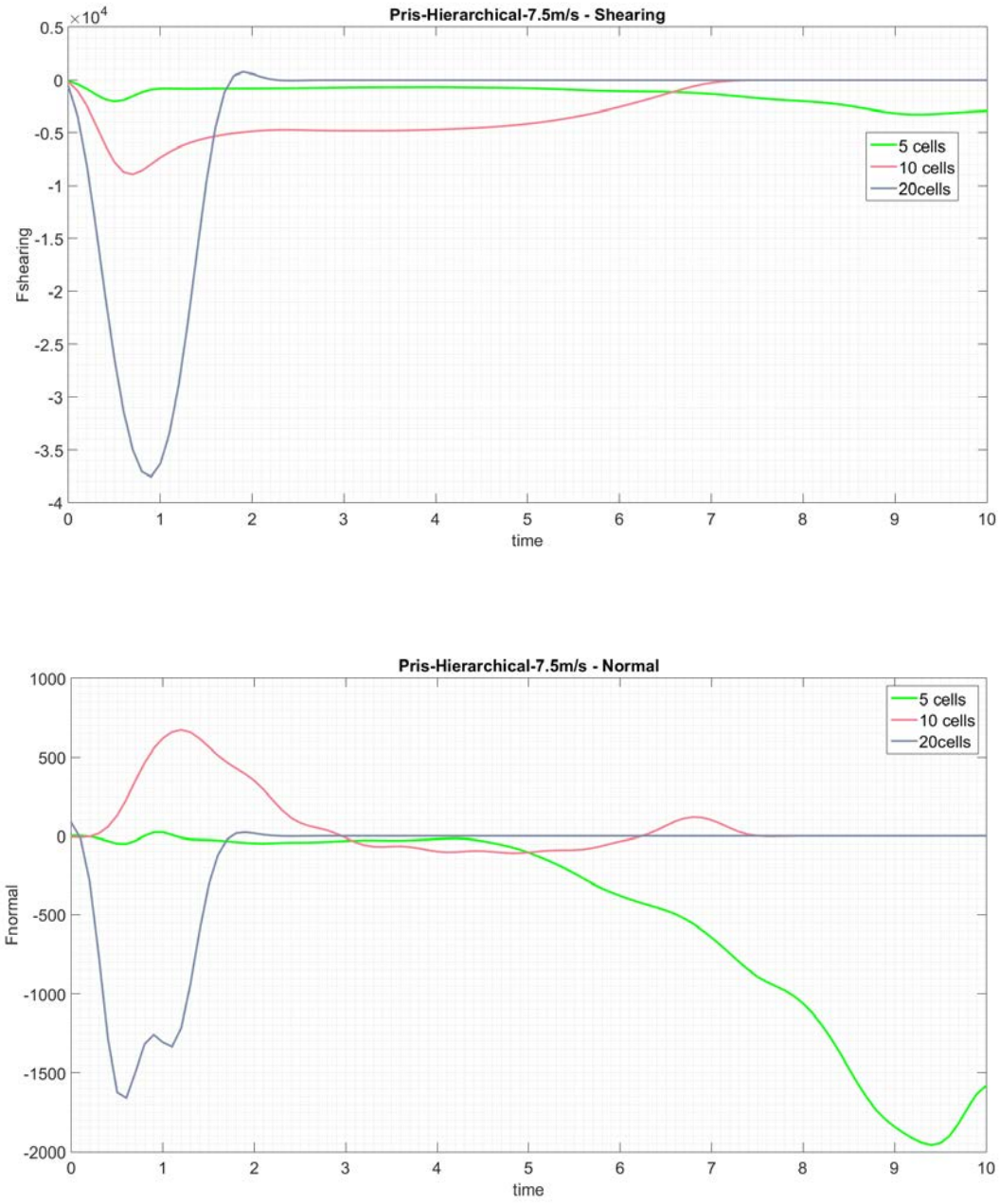

Figure 24: comparison of shearing and normal forces for different structures densities. PH - 7.5 m/s.

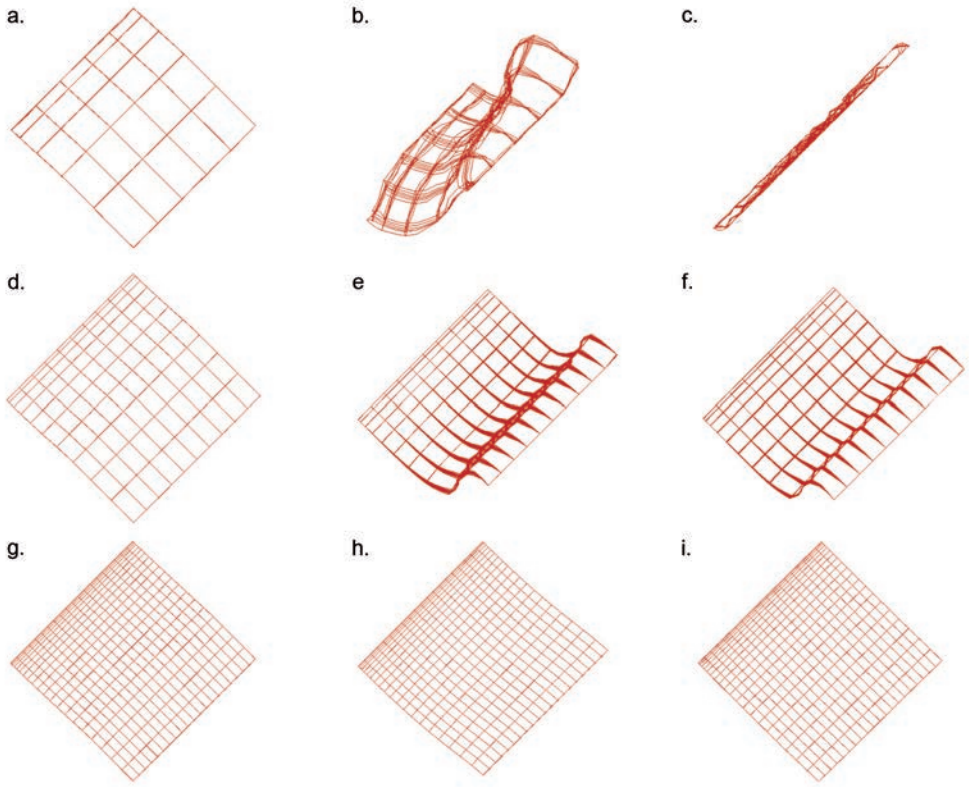

Figure 25: simulation frames for PH specimens during 7.5 m/s impact.

The hierarchy adopted in prismatic-shape cells leads to forces plot in figure 24.
Also for this type of structures the trends are similar to those for the lower impact velocity results. The main difference regards the normal force transmitted by the ten through-the-thickness cells specimen.
In this case too, the peaks of shearing forces, occurring at the starting of the buckling for the lower density specimens and at the instant right before the bouncing of the impactor for the highest density specimen, are at different moments of the impact. Increasing the density means the peak is reached later.
For the five through-the-thickness cells specimen is it evident the increasing of both shearing and normal forces in the last part of the simulation in a way that may represent the continuation of what starts at the end of the 6m/s impact. In this case, in fact, the higher velocity permit the visualization of the impact for a larger time.
As expected, the animation frames in figures 25e and 25f show a larger deformation at the maximum compression and a larger residual deformation at the end of the impact. In figure 25h there is a slight larger deformation while the differences at the end of the impact are neglecting with respect to the lower impact velocity.

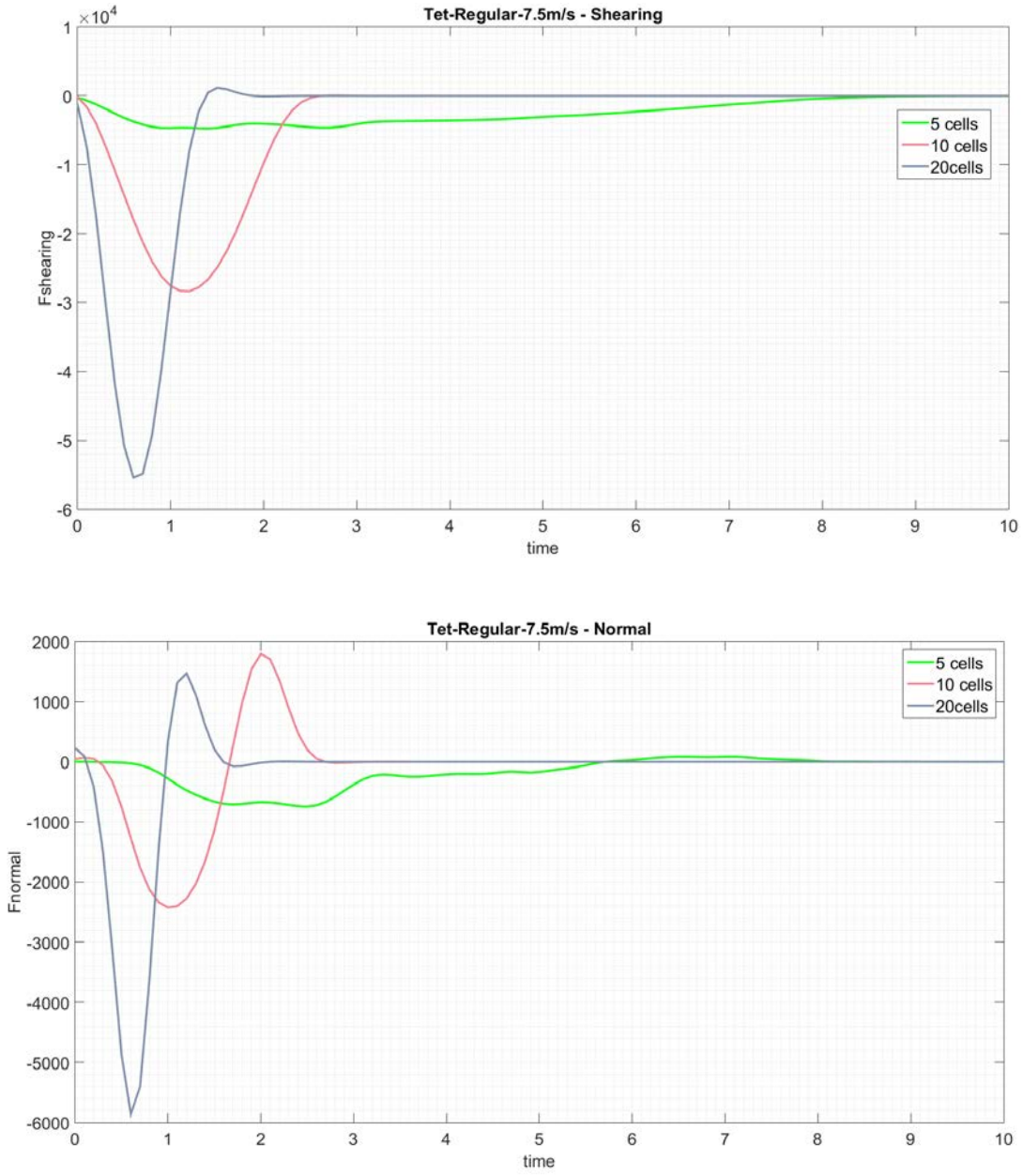

Figure 26: comparison of shearing and normal forces for different structures densities. TR - 7.5 m/s.

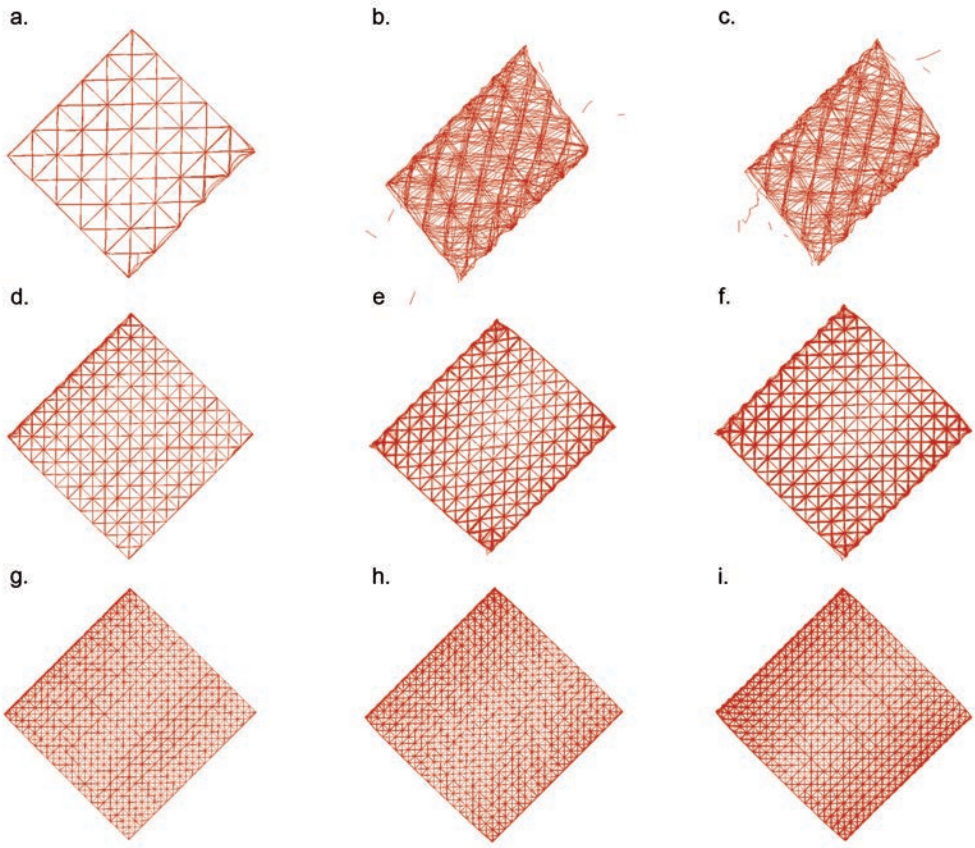

Figure 27: simulation frames for TR specimens during 7.5 m/s impact.

Tetrahedral-shape cells structures have a larger impact duration if it is considered the lowest density one while the higher density ones show shorter impact durations.
The five through-the-thickness specimen slips like in the *6 m/s* impact, it is severely crushed and transmitted low loads with respect to the stiffer specimens.
The latter do not show particular differences from the slower case in the deformation mechanisms during the impact.

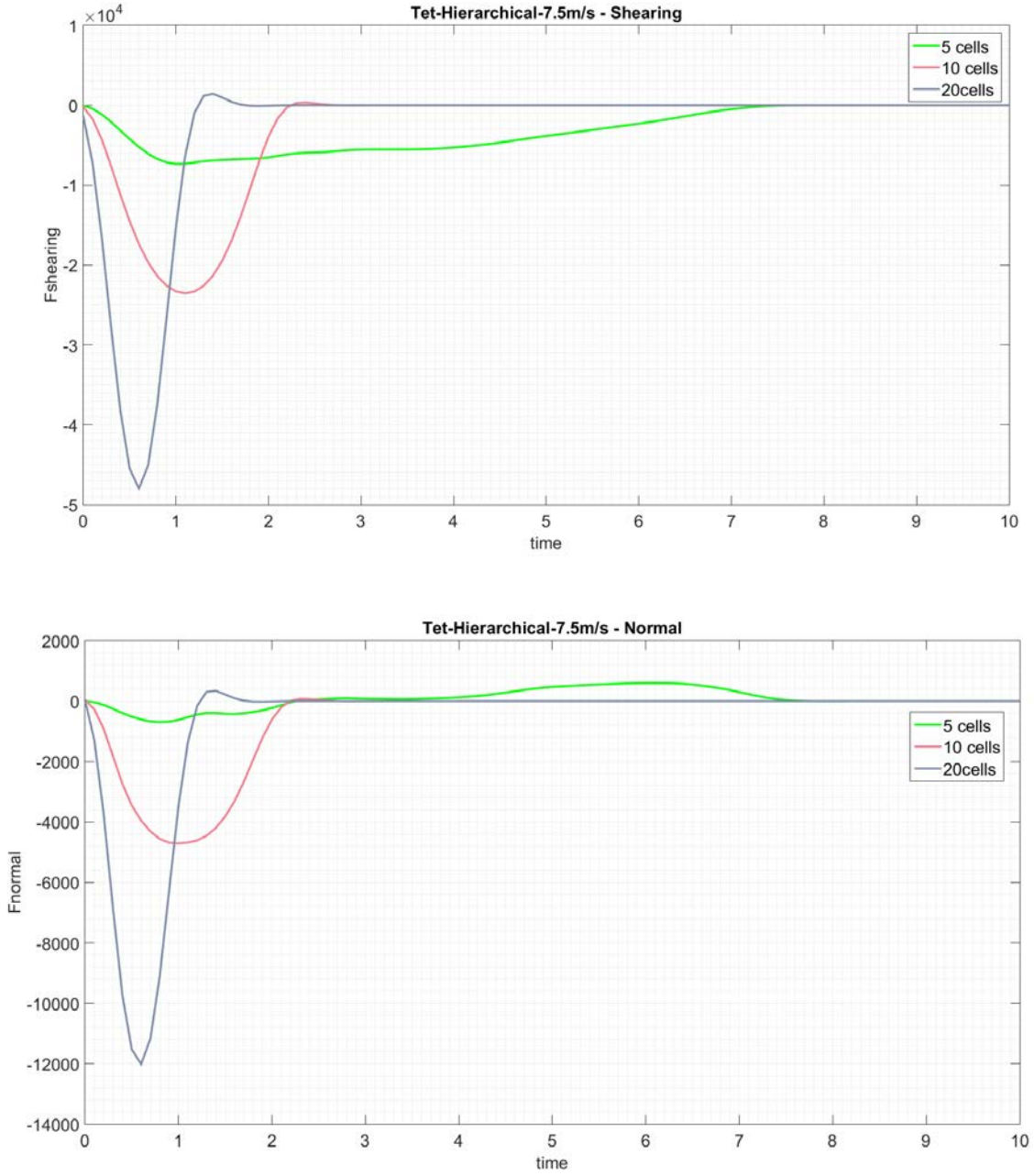

Figure 28: comparison of shearing and normal forces for different structures densities. TH - 7.5 m/s.

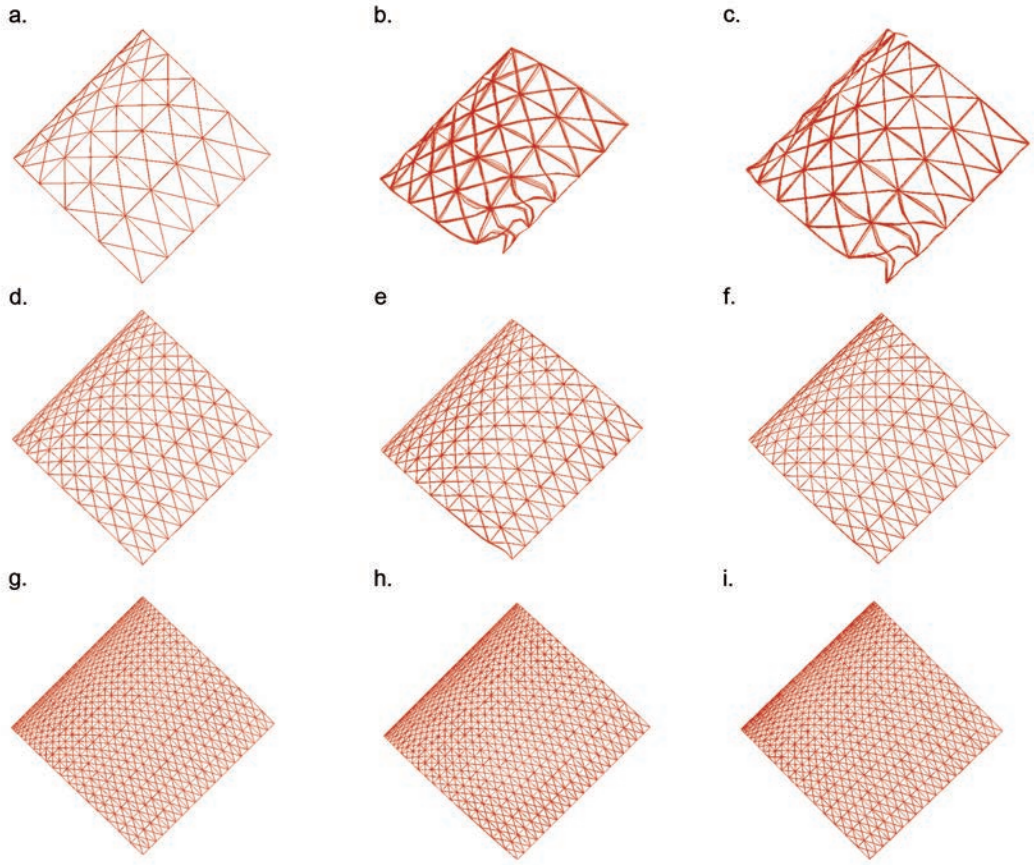

Figure 29: simulation frames for TH specimens during 7.5 m/s impact.

In this case too, the forces plots trends are very similar to the slower impact.
The impact durations remain almost the same for the stiffer specimens while it is increased for the softest one.
Looking at the animation frames, some differences are visible with respect to the same specimens impacted more slowly. The five and ten through-the-thickness cells structures show larger deformation both during the impact and at the end of it. Moreover, the softest shows cells of the two upper levels collapsed together on the underlying one. More failed struts in the upper smaller cells are visible after their recovering from the collapse.

7.5 m/s impact velocity resume

As a whole sight at the *7.5 m/s* impact velocity, it is remarkable the hierarchy helps to transmit smaller shearing loads than the corresponding regular dimensions same-shape cells structures.
Furthermore, the hierarchy leads to longer duration of the impact especially for the softest specimens.

It is evident even with this impact velocity that the simulation time is not enough to finish the impact in the softest prismatic cells structures.
Even for this faster impact, almost all of the hierarchical specimens do not show brittle behaviours, only the tetrahedral softest one shows evident failing at some cells.

c) 9 m/s Impact Velocity

Looking at the more energetic impact, with a velocity of *9 m/s*, it is reasonable to expect higher transmitted loads and more failures of the struts for the specimen that already had failures with less energetic impacts.

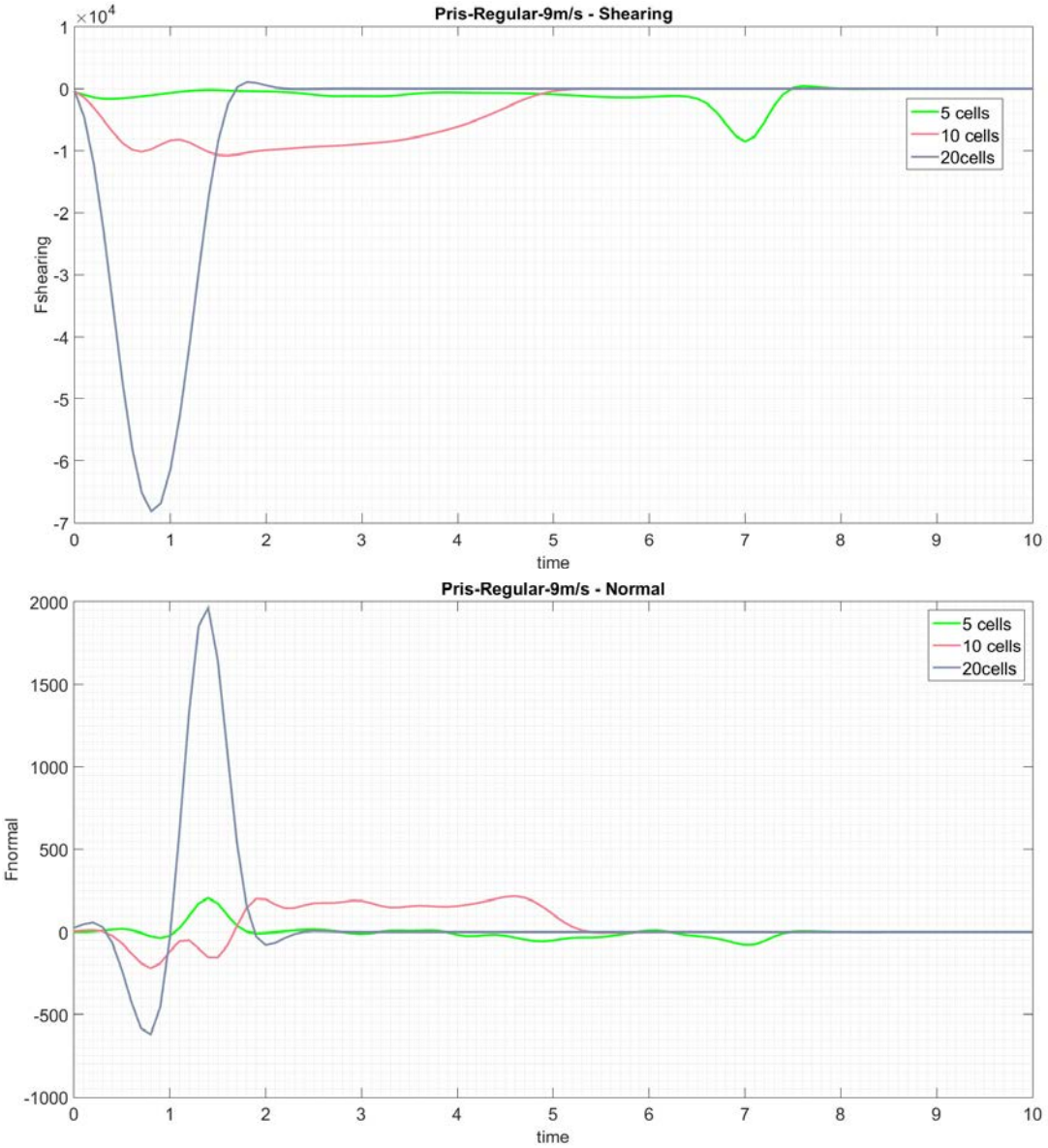

Figure 30: comparison of shearing and normal forces for different structures densities. PR - 9 m/s.

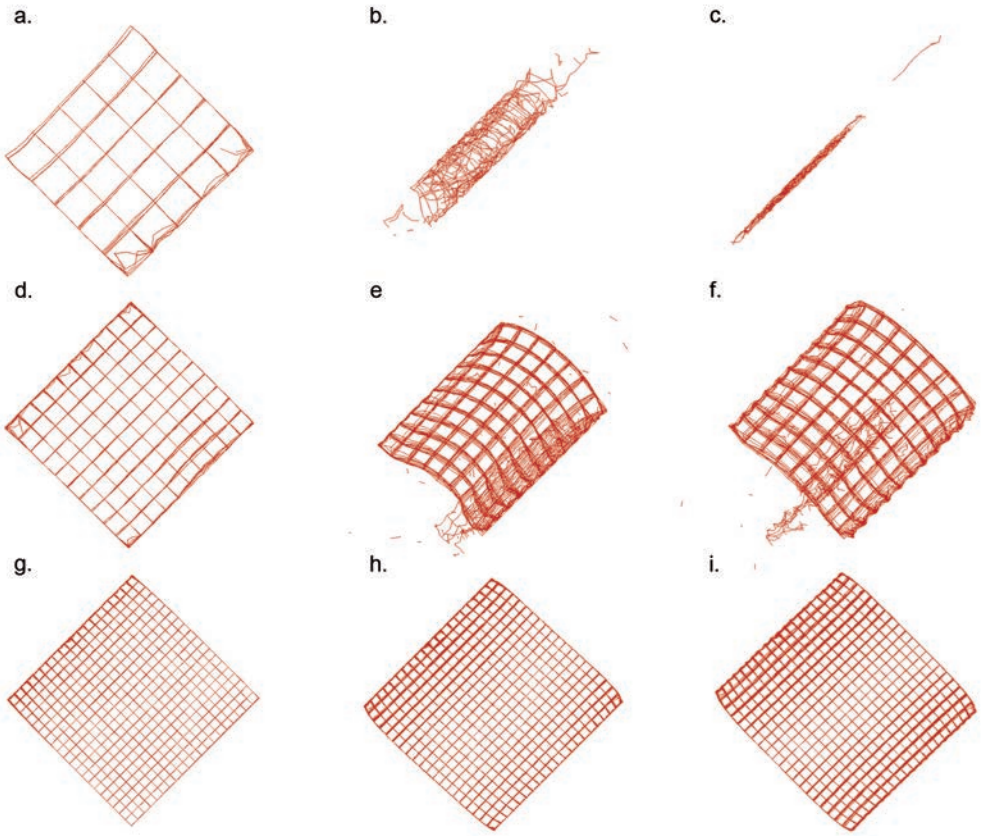

Figure 31: simulation frames for PR specimens during 9 m/s impact.

With the increased impact energy the trends of the force do not change widely; only the ten trough-the-thickness cells specimen has appreciable longer time impact and a shearing peak reached later.

This structure (P10R) is changing more its behaviour compared to the softer and the stiffer ones. It is evident from figures 31h and 31i how the faster impact cause more and severe failures also resulting in a complete detachment of the upper level of cells and making the new upper level to collapse with some cells on the underlying one. At the end of the impact, it recovers some deformations but it remains severe damaged.

The softest specimen is completely crushed like in the other impact velocities, it is not be able to provide protection from impacts.

The stiffest is, in this case, more plastically deformed.

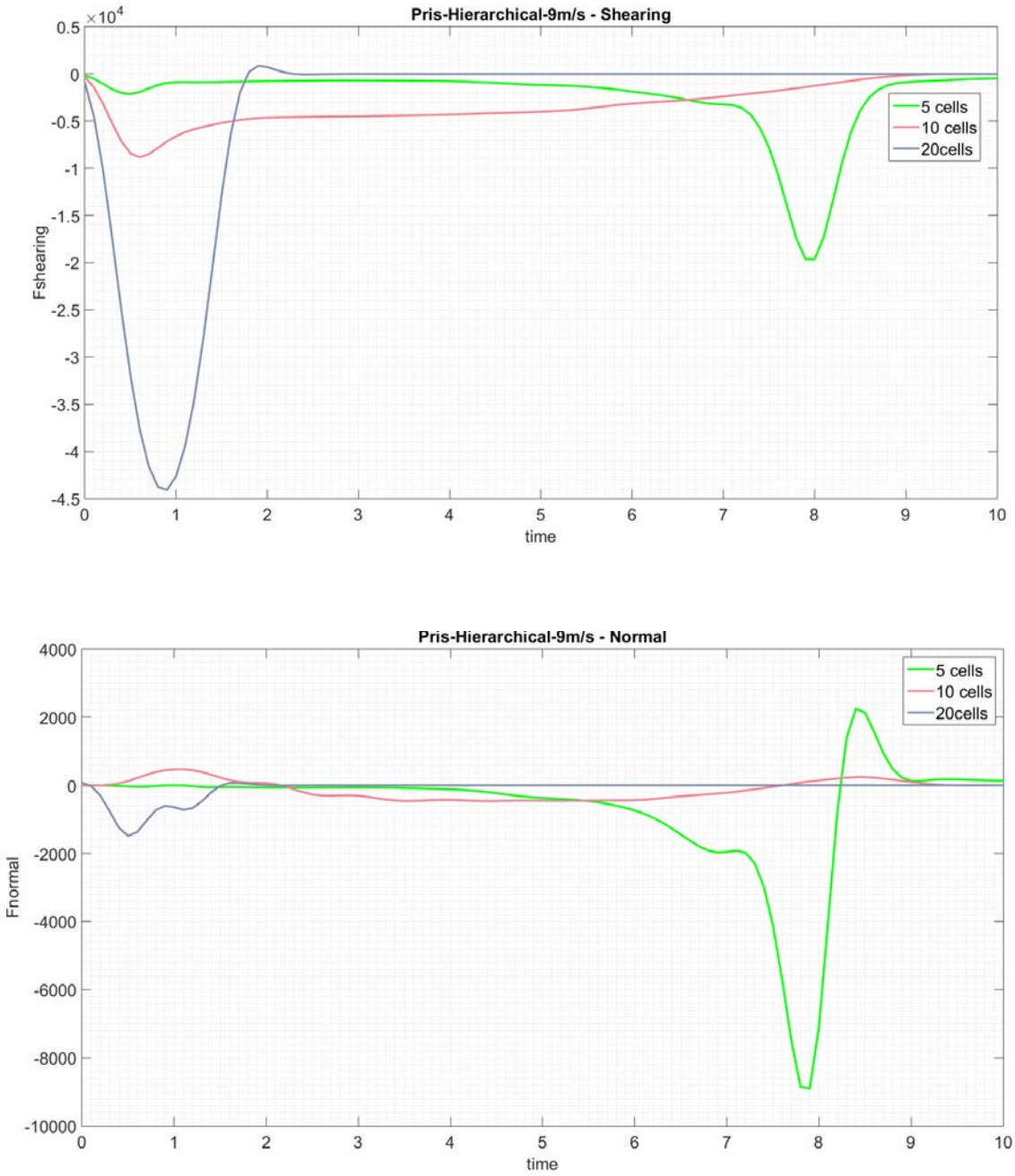

Figure 32: comparison of shearing and normal forces for different structures densities. PH - 9 m/s.

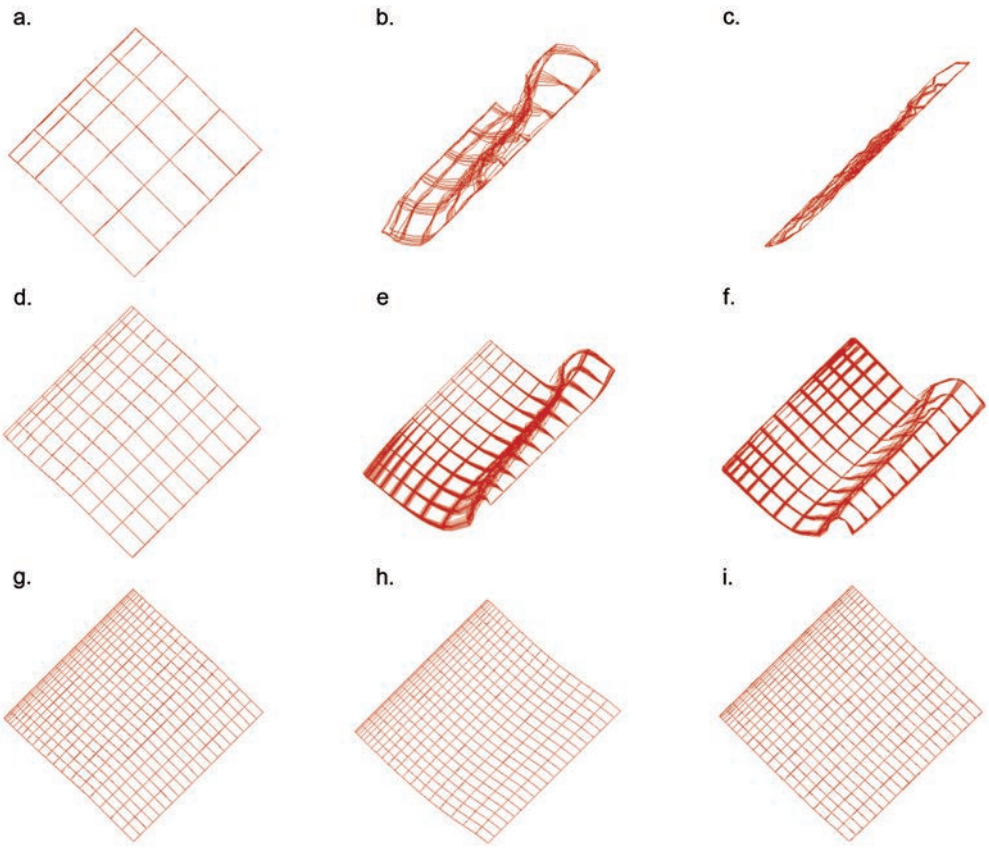

Figure 33: simulation frames for PH specimens during 9 m/s impact.

What is immediately evident from the forces plots (figure 32) for the prismatic-shape hierarchical specimens is the softest one possesses a sudden peak near the end of the simulation time. This peak, visible both in shearing and normal forces, is related to the bouncing of the impactor after the completely crushing of the structure. After the rebound the specimen starts to recover (figure 33c). It is not possible to understand how much it will recover because the simulation ends with the specimen that is continuing to change shape. The raising in transmitted forces change slope every time some folded material touches the anvil.

For the higher density specimens there are more deformations during the impact and more residual strains at the end, this is compatible with the more energy possessed by the impactor, that the specimens have to absorb.

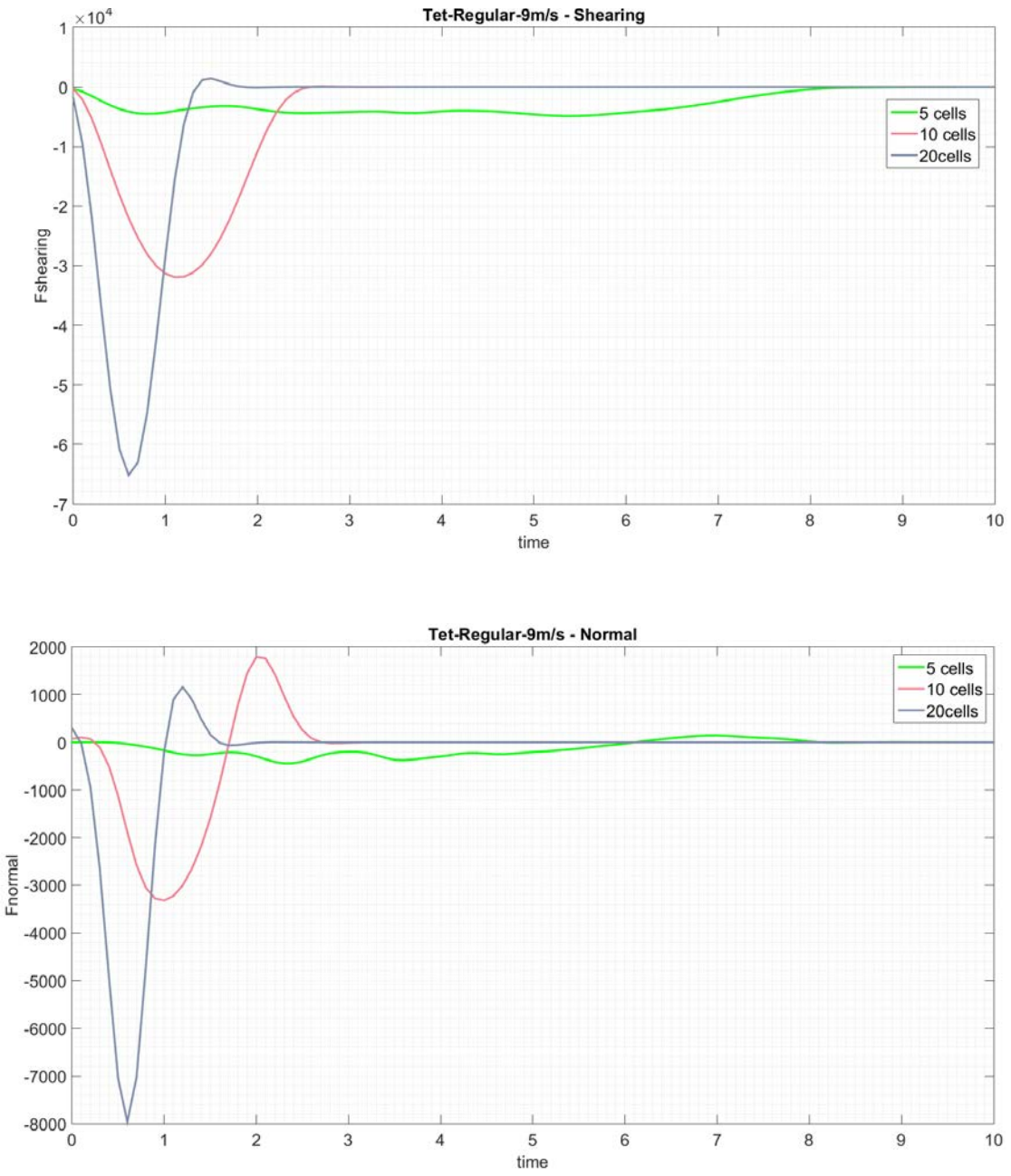

Figure 34: comparison of shearing and normal forces for different structures densities. TR - 9 m/s.

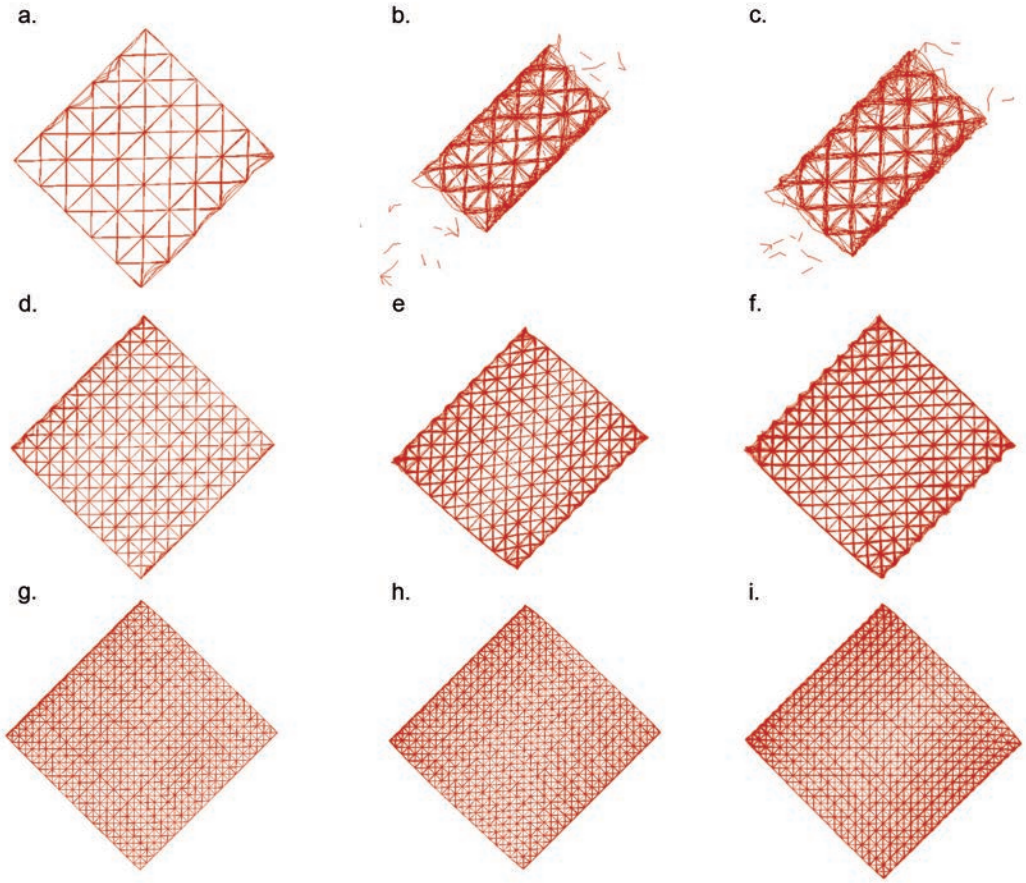

Figure 35: simulation frames for TR specimens during 9 m/s impact.

For the specimens with tetrahedral-shape regular dimension cells, there are not peculiar differences in force trends for this high energetic impact with respect to lower energetic ones.

The animation frames show the lowest density specimen crushing with a lot of failed struts leading to the finish of the impact with only three layers of cells remained.

The stiffness of the higher density specimens make the during-the-impact behaviours to do not show particular differences compared to lower velocities impacts.

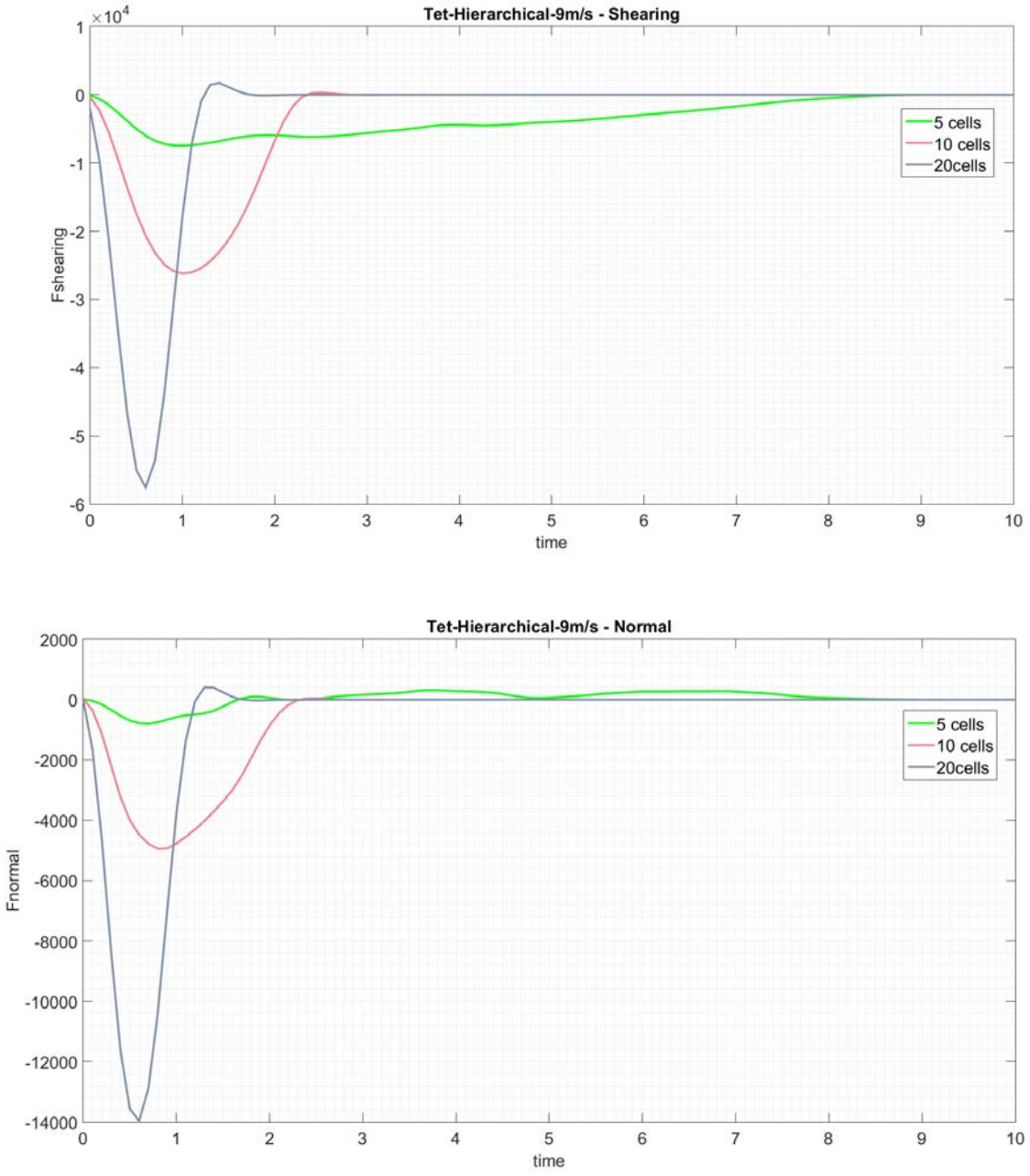

Figure 36: comparison of shearing and normal forces for different structures densities. TH - 9 m/s.

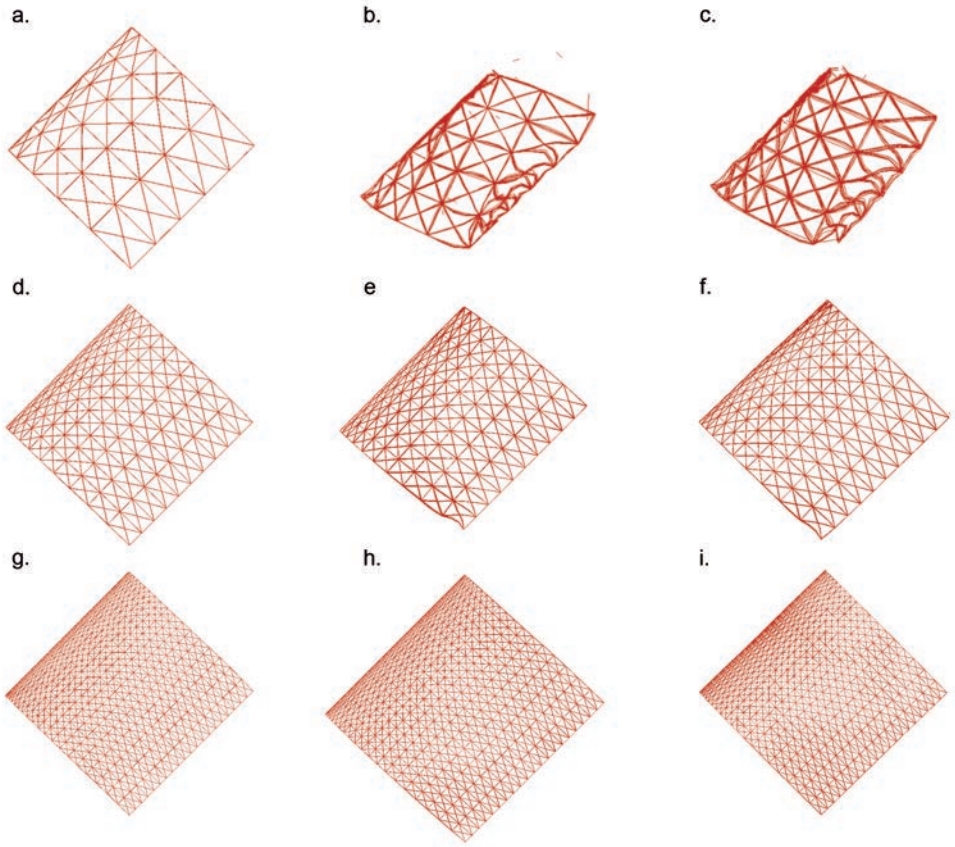

Figure 37: simulation frames for TH specimens during 9 m/s impact.

If compared to *6 m/s* and *7.5 m/s* impact velocities, evident longer impact time for the lowest density specimen is obtained in this high velocity impact on structures with tetrahedral-shape hierarchical cells.

From the animation frames it is evident how the high velocity impact causes many damages on the softer specimens, especially the softest one. It is highly crushed and deformed with the majority of cells of the two upper layers completely collapsed during the impact. They are not able to recover properly after the impactor rebound. They also show more failures and the lower layer shows serious plasticity.

The ten through-the-thickness cells specimen too, shows more damages with this velocity impact. The lower layer of cells is deformed plastically. The upper layers collapse during the impact and causes failure of some struts.

9 m/s impact velocity resume

In general the results in terms of forces and deformations for the *9 m/s* impact are compatible with what deduced from the slower impacts.

The force peaks are reached later for the denser specimens in case of prismatic-shape cells and earlier for the denser specimens with tetrahedral-shape cells.

d) General Discussion

From this comparison, it is evident that independently on the cells shape, as the density of the structures increases, the transmitted loads rise too, the impacts last less time and the damages made on the structure itself are less serious.

The main purpose of this comparison is the comparison between different through-the-thickness number of cells. Focusing strictly on this, for the prismatic-shape cells it may be highlighted:

- Five cells through the thickness with uniform dimensions make a structure too brittle causing an almost complete failure;
- Ten cells through the thickness with uniform dimensions make the structure stiff enough to stop the impactor but it may has failures and it remain with residual deformations;
- Twenty cells through the thickness with uniform dimensions stiffen the structure more than the previous but do not ensure the absence of plastic residual strains; the transmitted forces are greater than the structures with ten through-the-thickness cells;
- Five cells through the thickness with variable dimensions following a hierarchical scheme help to transmit low loads thanks to the induced buckling on longer struts but create structure that are not stiff enough to do not permit the impactor to descend to the anvil yet;
- Ten cells through the thickness with variable dimensions following a hierarchical scheme are sufficient to stop the impactor but their residual deformations are very large;
- Twenty cells through the thickness with variable dimensions following a hierarchical scheme stiffen the structure and do not leave large residual strains; however, the transmitted forces are much more high with respect to the lower density structures

Focusing on the tetrahedral-shape cells, their topology, thanks to their diagonal struts, ensure to reach a stiffness that always stop the impactor before touching the anvil. The highlights are:

- Five cells through the thickness with uniform dimensions make the most fragile structure of this type, but also make the transmitted forces to be the smallest;
- Ten cells through the thickness with uniform dimensions leave the possibilities to have failures of struts and the residual strains but less than the previous one;

however, with ten cells, the structure transmits higher forces;

- Twenty cells through the thickness with uniform dimensions make a very stiff structure, negligible residual deformations but allow transmission of the highest shearing forces together with the analogous prismatic-shape cells structure;
- Five cells through the thickness with variable dimensions following a hierarchical scheme lead to have a highly deformed structure at the end of the impact; this structure transmits low forces and lasts the impact for long time.
- Ten cells through the thickness with variable dimensions following a hierarchical scheme stiffen the structure ensuring not large residual strains;
- Twenty cells through the thickness with variable dimensions following a hierarchical scheme lead to negligible plastic strains but lead also to transmit high forces.

3.2.2 Comparison of Different Types of Structures

This section is intended to make a comparison between the four different types of structures for given through-the-thickness cells number and impact velocity.
This comparison not only allows to understand which cell topology is better but also if the hierarchy is more effective with respect to the regular dimension cells.
Moreover, it allows to comprehend if the number of through-the-thickness cells and the impact velocity influence differently the effectiveness of cell topology and hierarchy.
Each of the following plots shows four curves of shearing or normal force for every type of structure. Each plot is related to one number of through-the-thickness cells and one velocity.

a) 6 m/s Impact Velocity

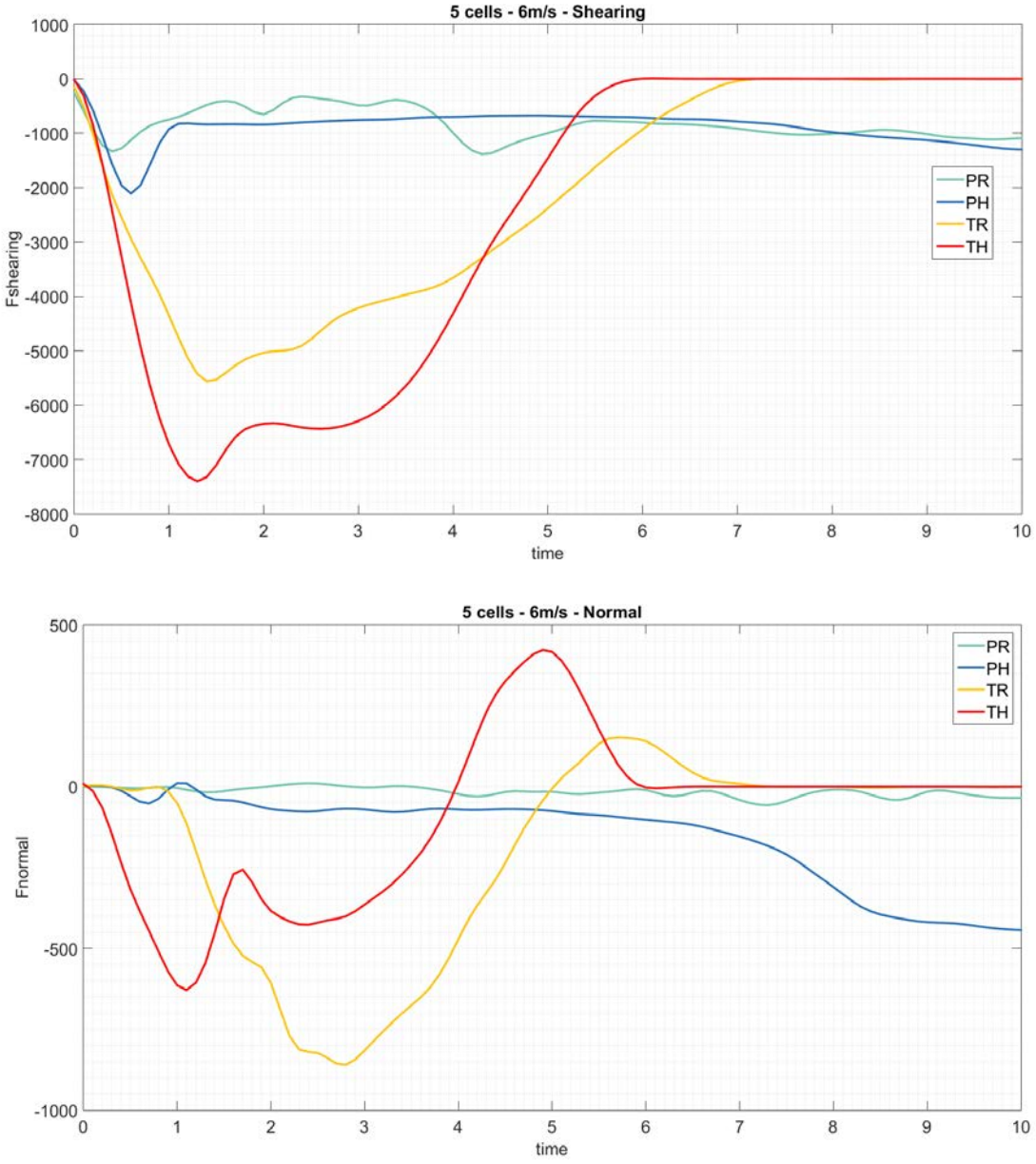

Figure 38: comparison of shearing and normal forces for different structures types. 5 cells - 6 m/s.

For the *6 m/s* impact velocity and five through-the-thickness cells number it is visible how the topology of the cells leads to different trends and values of transmitted forces. Remembering the regular dimensions cells structure is completely crushing during the impact, the only prismatic-shape cells worthy to consider is the hierarchical. It maintains the forces very low but it tends to completely crushed configuration too but without brittle behaviour.

Tetrahedral-shape cells structures have curves different from the previous, transmitted forces reach larger values but they do not collapse entirely. In this case the hierarchy is better than the regular dimensions cells only for the normal force.

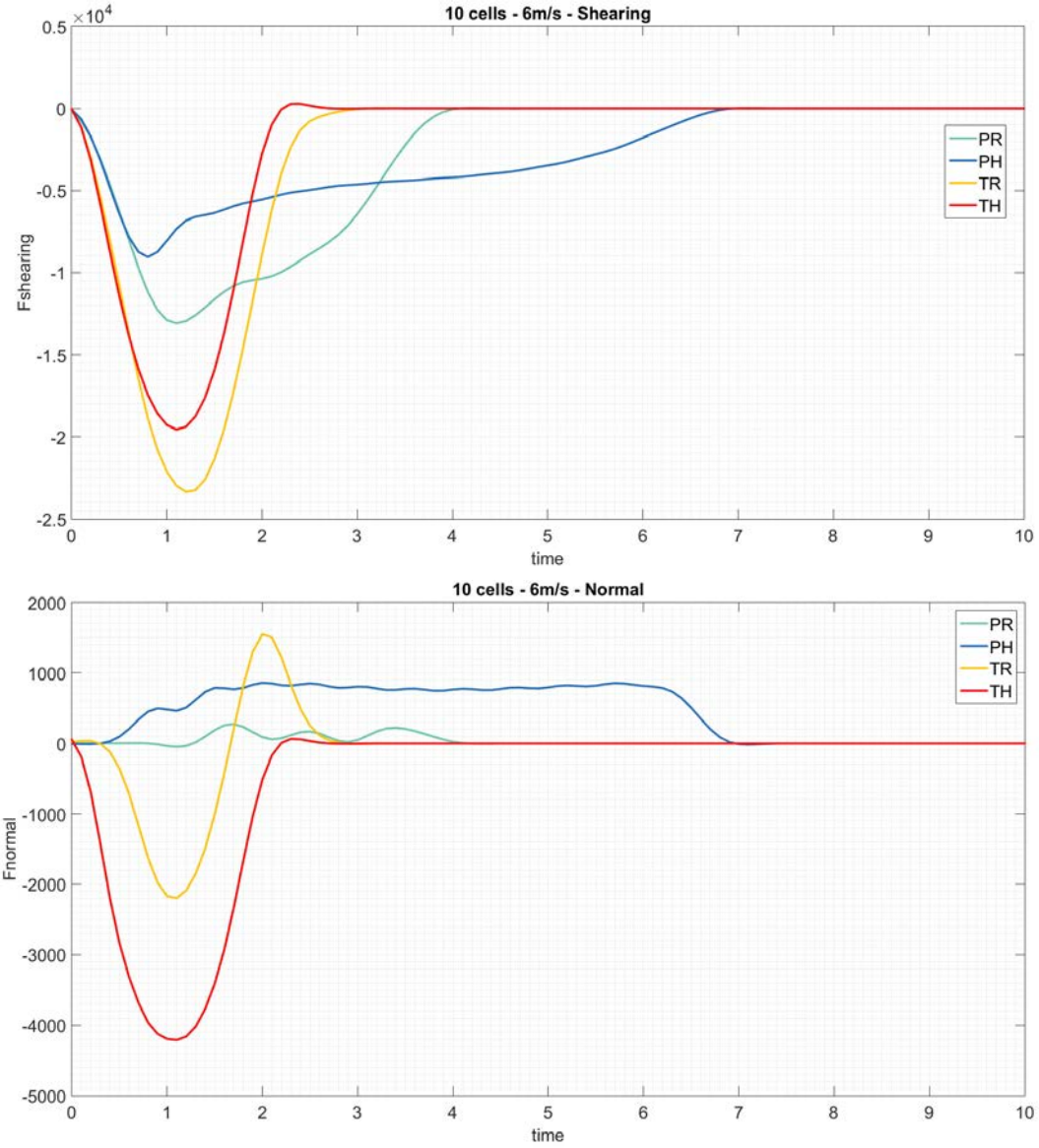

Figure 39: comparison of shearing and normal forces for different structures types. 10 cells - 6 m/s.

For the ten through-the-thickness cells specimens, it is clear the advantages brought by hierarchy for the shearing forces while for the normal ones, the regular dimensions cells are better.

With respect to the less dense specimens curves, there is an inversion in which is the best between the regular and the hierarchical dimensions for the tetrahedral-shape cells structures. In this case in fact, the hierarchy helps to transmit lower shearing force but higher normal force.

For this higher density structures too, prismatic-shape cells specimens transmit lower forces, both shearing and normal.
The hierarchy, with respect to regular dimensions cells, make the impact lasts more for the prismatic cells specimens and less for the tetrahedral cells ones.

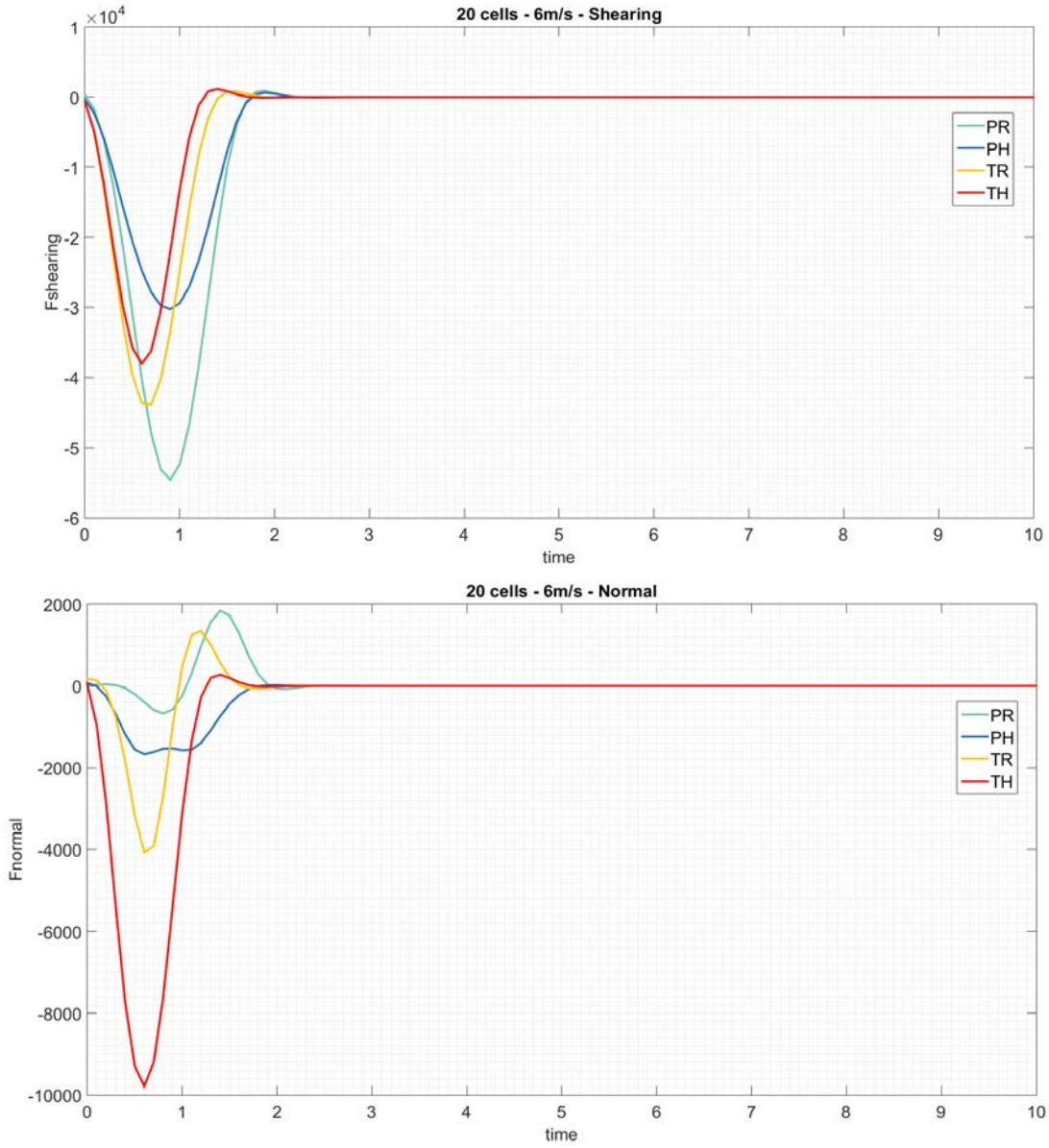

Figure 40: comparison of shearing and normal forces for different structures types. 20 cells - 6 m/s.

For the highest density cases, the hierarchical structures lead to lower shearing transmitted forces but larger normal ones with respect to their analogous homogeneous dimensions cells structures.
With this density, the prismatic-shape regular dimension specimen transmits the highest shearing force, overlapping the tetrahedral-shape structures.

b) 7.5 m/s Impact Velocity

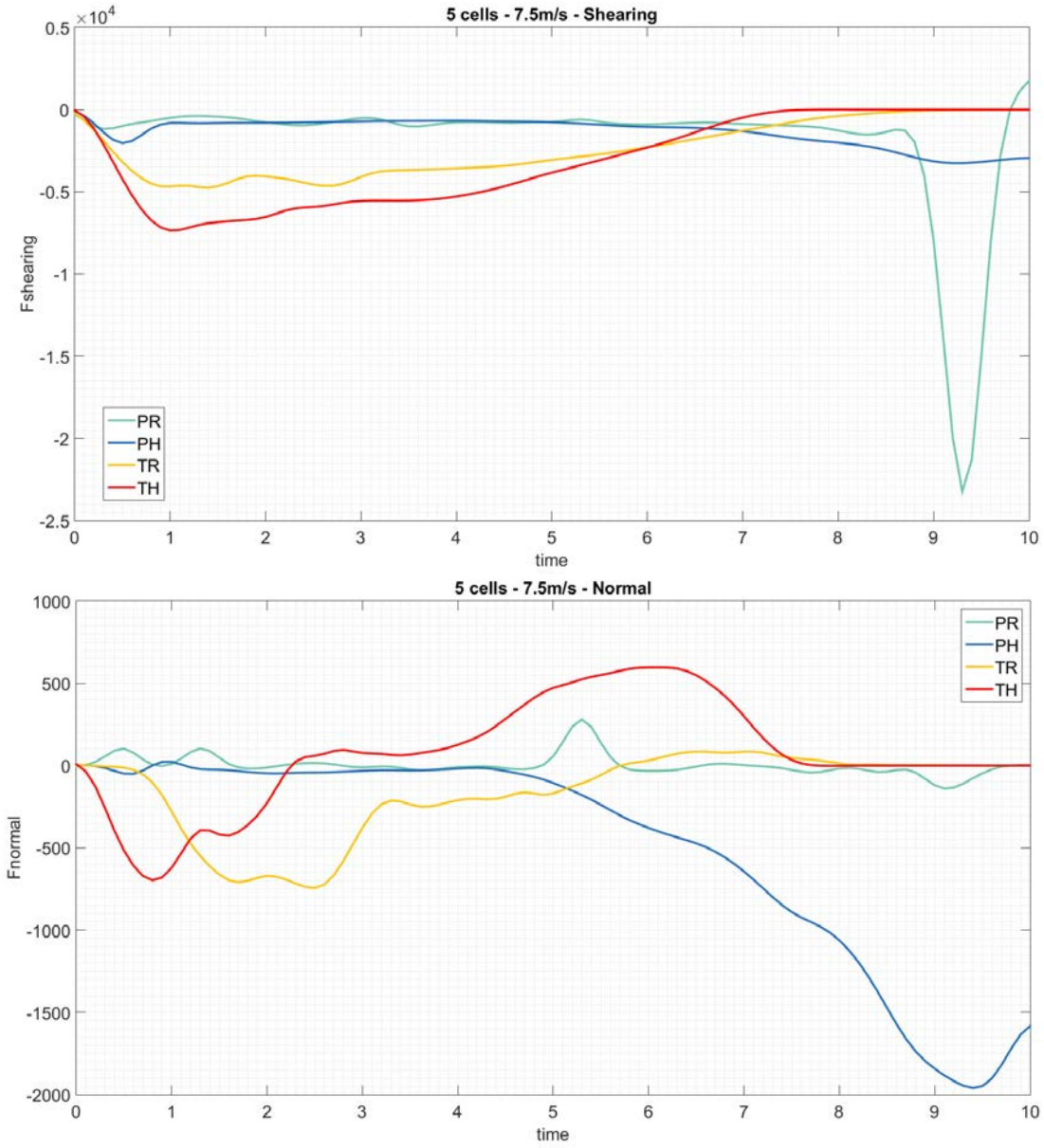

Figure 41: comparison of shearing and normal forces for different structures types. 5 cells - 7.5 m/s.

Remembering the prismatic-shape cells specimens possess the peaks at the end of the impact for the touching between the impactor and the anvil, the other parts of the plots highlight the hierarchical structures are less effective for the shearing force. Curves for tetrahedral-shape cells specimens confirm, for this impact velocity too, the regular dimensions of cells transmit lower shearing forces with respect to the use of hierarchy.

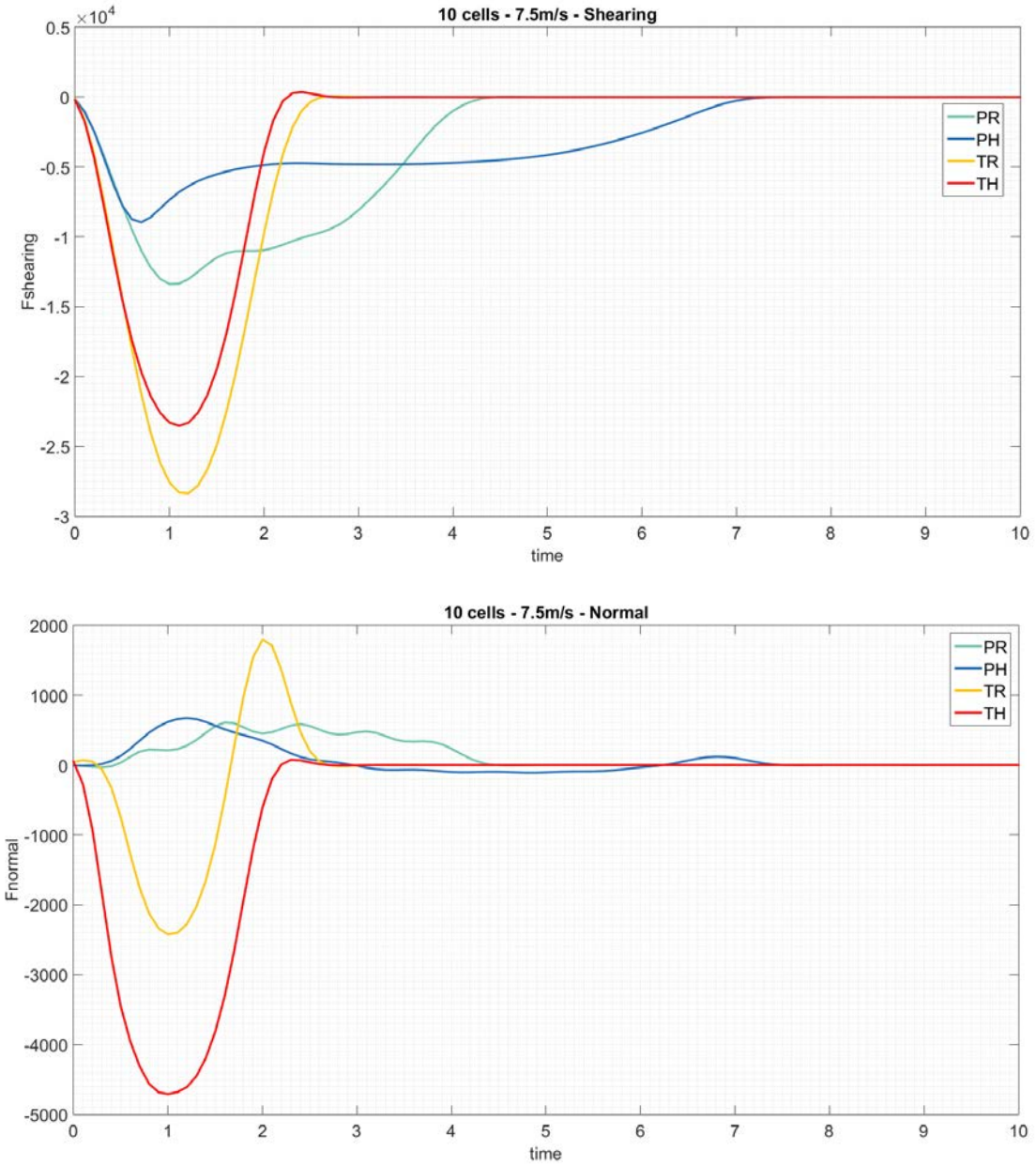

Figure 42: comparison of shearing and normal forces for different structures types. 10 cells - 7.5 m/s.

In this higher energetic impact too, as the cells density is increased, the hierarchy brings advantages for the shearing forces and disadvantages for the normal forces.
The prismatic-shape cells, thanks to their minor stiffness compared to the tetrahedral-shape ones, reach smaller values and make the impact lasting more time.

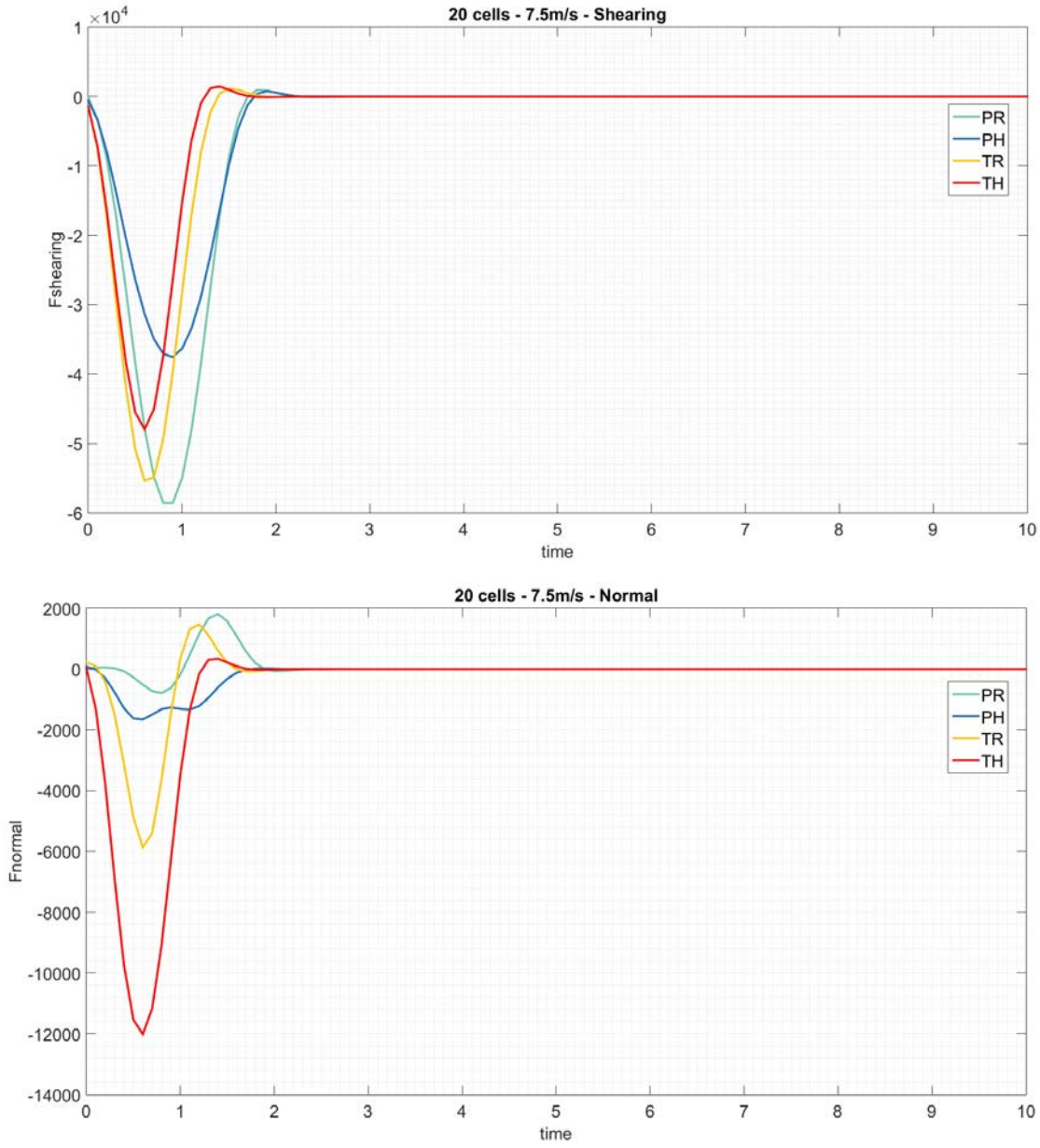

Figure 43: comparison of shearing and normal forces for different structures types. 20 cells - 7.5 m/s.

With twenty through-the-thickness cells, hierarchical specimens continue to be more effective than the regular dimensions ones for the shearing forces. The prismatic-shape cells specimens, because of the increased stiffness given by the high density of cells, have shearing curves that are becoming more similar to the tetrahedral-shape cells specimens.

The prismatic-shape regular dimensions specimen is still the worst in transmitting shearing force, even if compared to the stiffest tetrahedral-shape cells specimen.

c) 9 m/s Impact Velocity

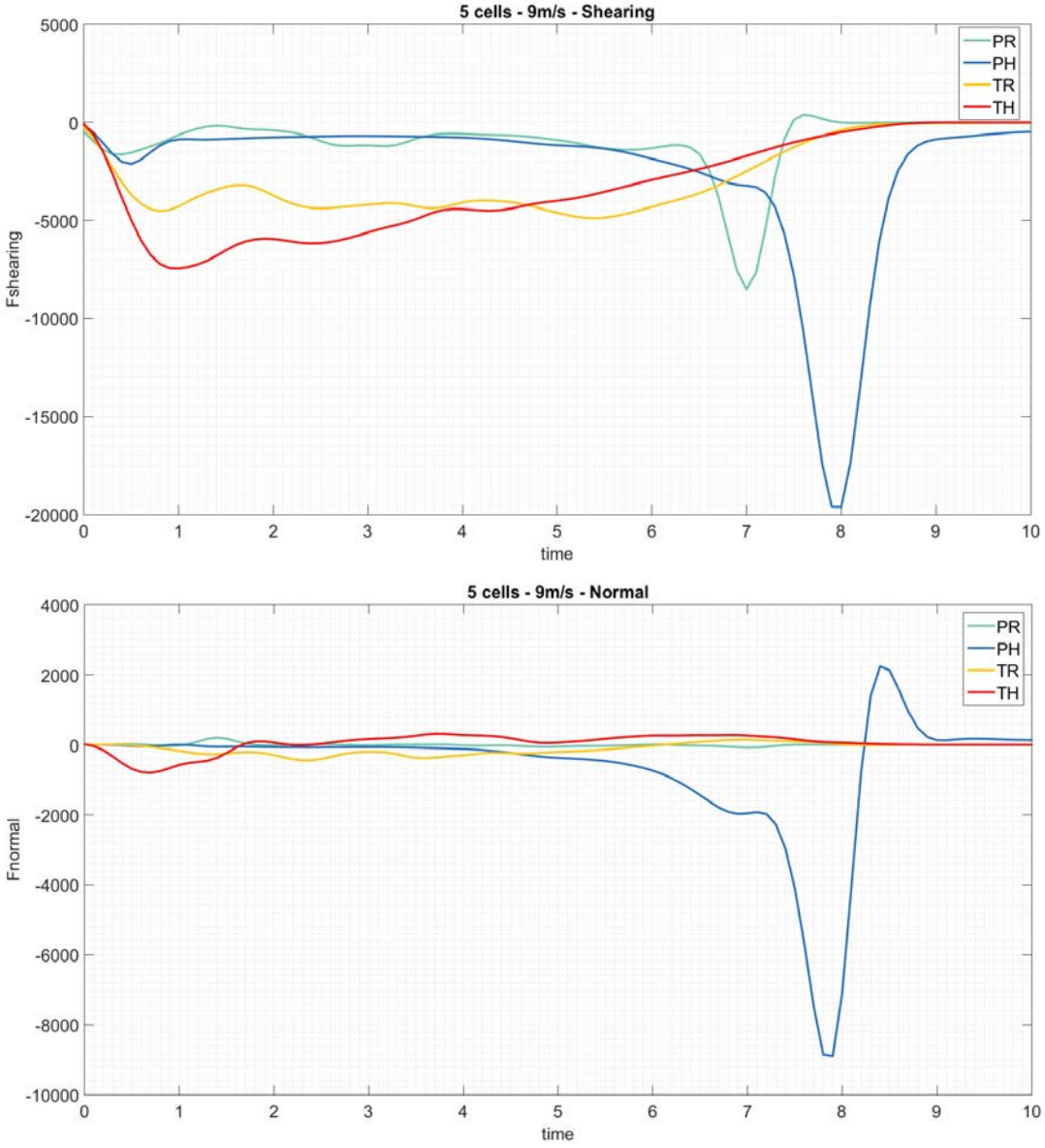

Figure 44: comparison of shearing and normal forces for different structures types. 5 cells - 9 m/s.

With the highest impact velocity the hierarchical specimens with the lowest density of cells, are still generally worse than the regular dimension cells ones.

The stiffness of the tetrahedral-shape cells continues to drive to higher peak values with respect to prismatic-shape ones.

The highest peaks for the prismatic-shape curves are due to the fact the impactor crushes the lattices until they form a thin layer, between the impactor itself and the anvil, that does not act as an absorber.

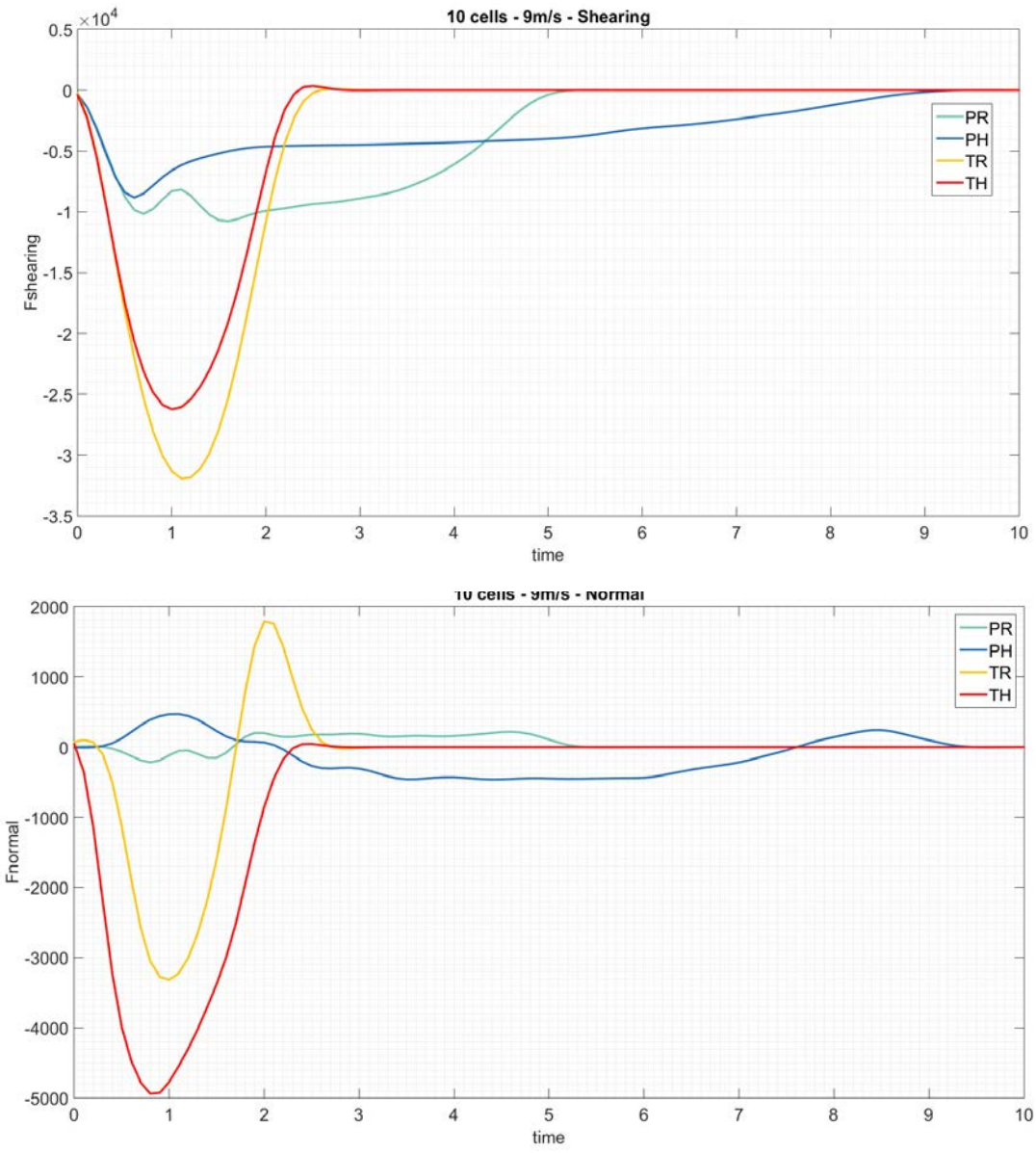

Figure 45: comparison of shearing and normal forces for different structures types. 10 cells - 9 m/s.

Even with this *9 m/s* impact velocity, it is clear the cells density changes the behaviour of the different structures: with this density the behaviour of the structures changes its trends compared to the lower density previous described.

The hierarchy induces a more effective buckling, the longer struts at the base of the specimens can highly transversely deform transmitting lower shearing forces.

The largest deformations are induced in the prismatic-shape cells because of their minor stiffness. These largest deformations bring to the longest impacts evident in the plots.

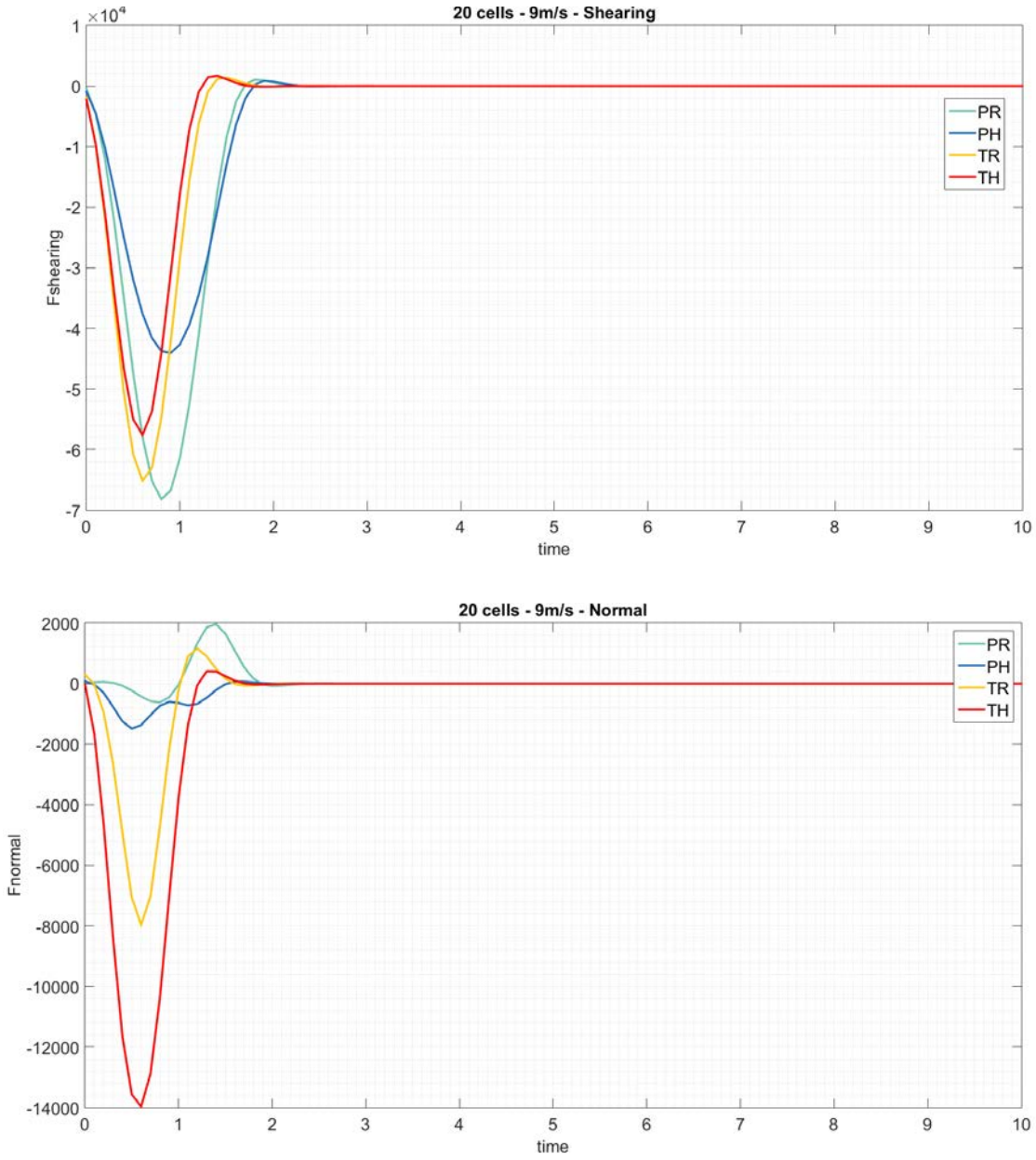

Figure 46: comparison of shearing and normal forces for different structures types. 20 cells - 9 m/s.

With twenty cells through the thickness, the hierarchy leads to more effective solutions to minimize the shearing forces.

With regard to the normal force, the prismatic-shape cells drive to the lowest peaks and the hierarchy continues to be worse than the regular dimensions cells.

d) General Discussion

From this comparison it is interesting to do some considerations.

First of all it is clear, looking at the plots for different impact velocities, that the behaviour of every single structure does not depend so much on the velocity itself. In fact, each of the twelve different structures maintain similar curves for the three different impact energies. The most important difference from different impact velocities are the reached values of transmitted forces.

For five trough-the-thickness cells the hierarchy makes the structure worse for the transmission of forces. The prismatic-shape cells are too soft and make the specimens transmitting low forces but completely crushing during the impact. The tetrahedral-shape cells are stiffer and hence they do not make the specimens completely failing or folding but transmitting higher forces.

When the cells density is increased, both ten and twenty trough-the-thickness cells, there is an inversion on the effectiveness in the use of the hierarchy. Cells with hierarchical dimensions make the specimens transmitting low shearing forces and higher normal forces with respect to the regular dimensions ones. Increasing the density means to stiff the structures and this hardening of the structure makes the impacts last less time and leads to have curves approaching a bell-like shapes.

These effects of the hardening are also visible looking at the difference between prismatic-shape and tetrahedral-shape cells in the same plot. The tetrahedral-shape cell is in fact stiffer because of the diagonal struts.

Looking at the force values, the shearing force is always about an order of magnitude greater than the normal force. Hence, it is reasonable to think the disadvantages in the transmitted normal forces brought by the use of the hierarchy are much less important than the advantages brought in the shearing forces by the usage of it.

3.2.3 Comparing forces peak values and resultant forces

In this section only the peak values of the transmitted forces are considered.

Surfaces in 3D plots are useful to compare at the same time how the cells geometry and the cells density influence the peaks of the forces for a fixed impact velocity.

The surfaces are also useful to look at the trends established by the variation of the parameters.

With these 3D plots it is possible to have a wide and complete view and to identify which parameters affect more the maximum transmitted forces.

These types of plots, in presence of some structure specific constraints and requirements permit the immediate filtering of the suitable and unsuitable structures.

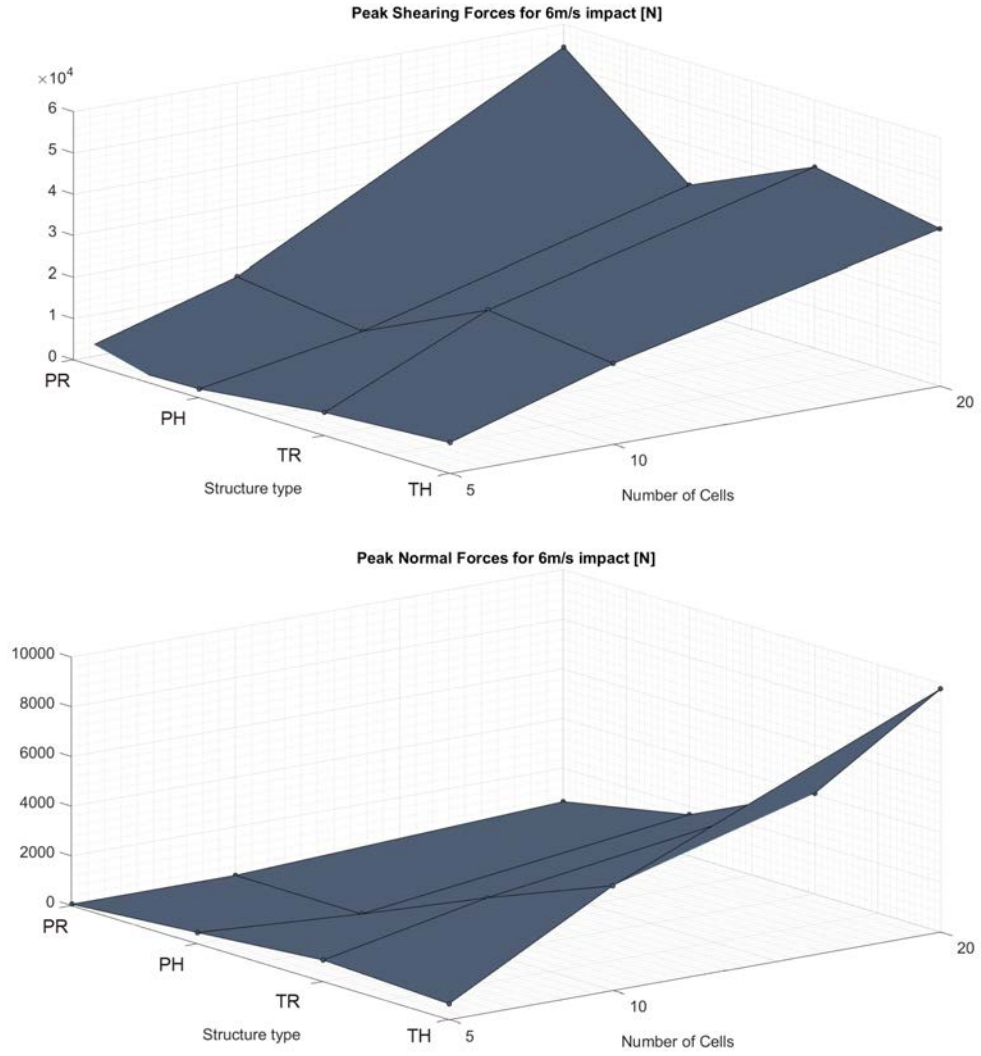

Figure 47: peak values of shearing and normal forces for 6 m/s impact velocity.

For the *6 m/s* impact it appears the peaks increase as the density grow up. Moreover, it is confirmed that at constant number of through-the-thickness cells, the hierarchical structures are almost always better compared to their analogous with regular dimensions cells for the shearing peaks. For the normal peaks it is confirmed too that the hierarchy makes the peaks larger.

Except the highest density structure with prismatic-shape regular cells, it is clear the cells with tetrahedral shape are always worse than the prismatic-shape ones.

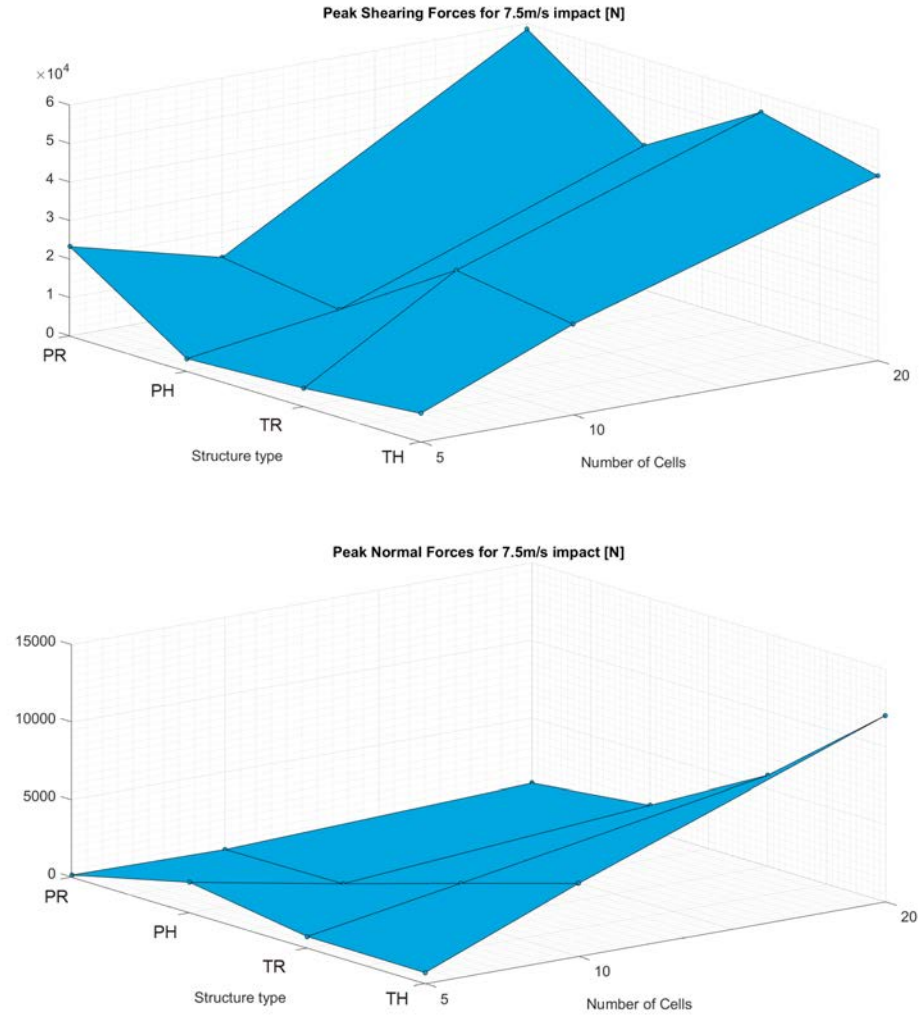

Figure 48: peak values of shearing and normal forces for 7.5 m/s impact velocity.

For the *7.5 m/s* impact, previous considerations are still generally applicable.

In this case, however, there are some things to mind: the structure with five through-the-thickness prismatic-shape cells are showing peaks greater than the others because

the increased velocity may makes the crushing of those specimens too heavy and the impactor finishes close the anvil.

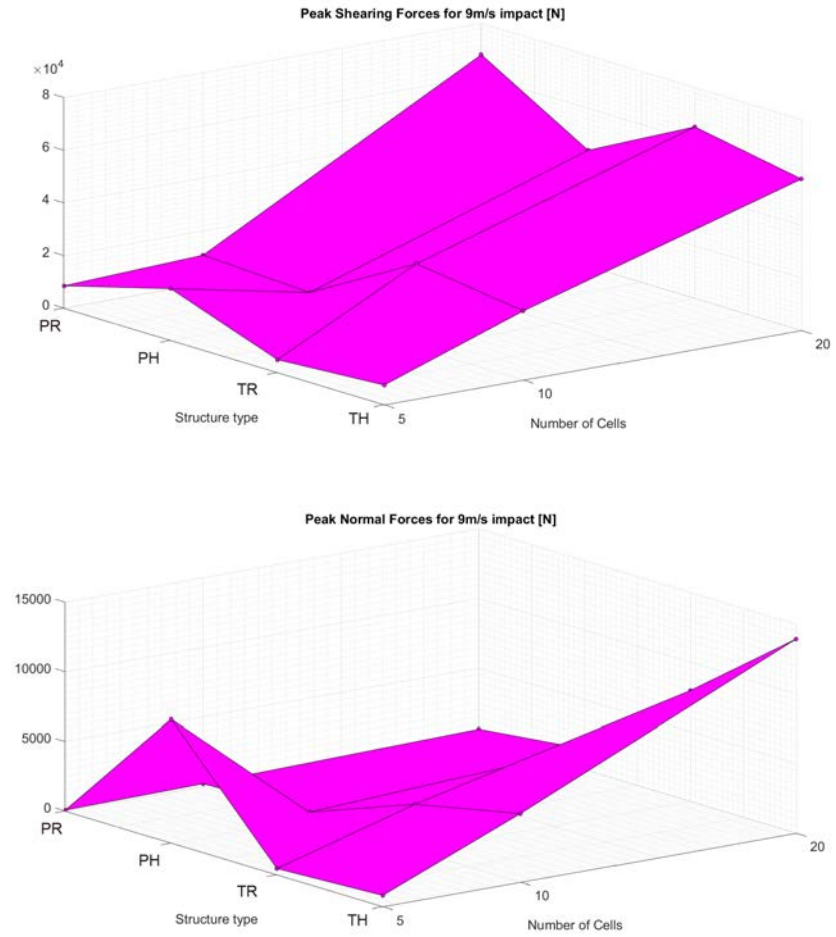

Figure 49: peak values of shearing and normal forces for 9 m/s impact velocity.

Also for the highest impact velocity, the same considerations just made continue to apply well.
The peaks obviously differ in absolute values when the impact become more and more energetic.

Successive 2D plots are sections of the surfaces shown above, they help to extract more quantitative details for the identification of the structures representing the best trade-offs in terms of forces transmission.
For each impact velocity is also reported a table indicating the peak values for every structure.

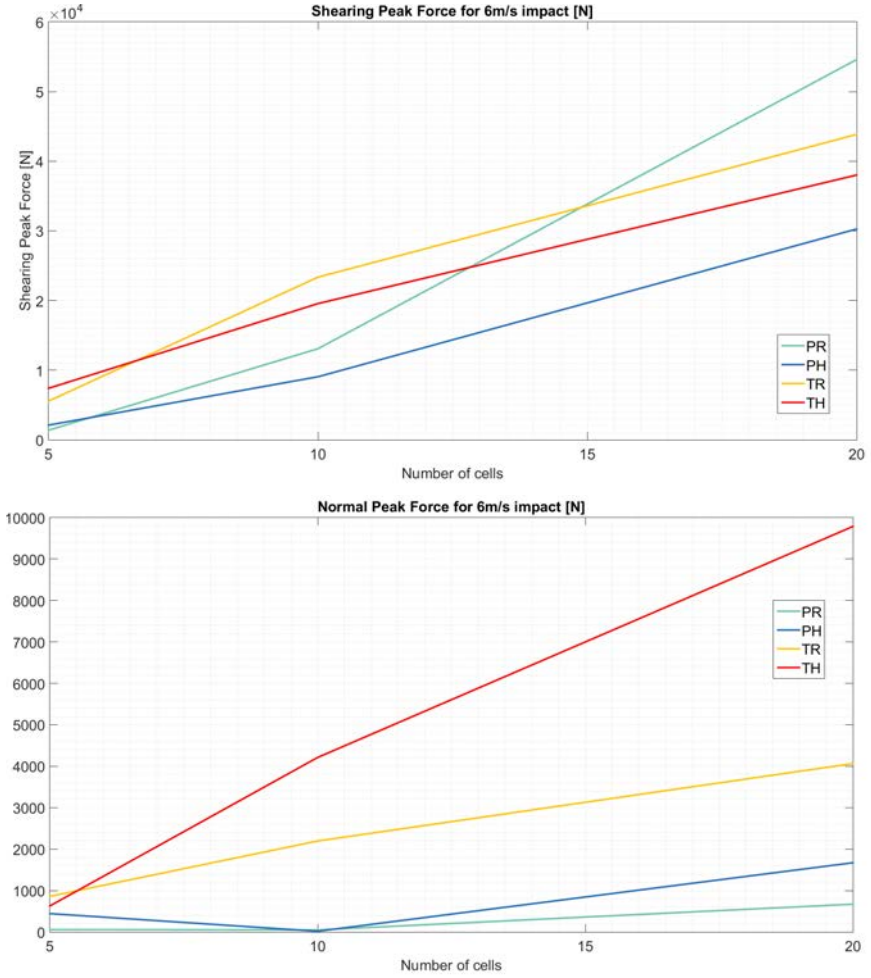

Figure 50: 2D plots for peak values of shearing and normal forces for 6 m/s impact velocity.

STRUCTURE TYPE Prismatic-shape cells	**Peak of normal Force [kN]**	**Peak of Shearing Force [kN]**	**Peak of Resultant Force [kN]**
P05R	0.057	1.383	1.384
P05H	0.443	2.108	2.109
P10R	0.049	13.080	13.080
P10H	0.017	9.051	9.062
P20R	0.671	54.600	54.603
P20H	1.671	30.268	30.306
Tetrahedral-shape cells			
T05R	0.860	5.560	5.572
T05H	0.629	7.399	7.419
T10R	2.196	23.351	23.444
T10H	4.211	19.558	20.007
T20R	4.064	43.853	44.028
T20H	9.787	38.019	39.259

Table 10: numerical values of forces peaks. Impact Velocity 6 m/s.

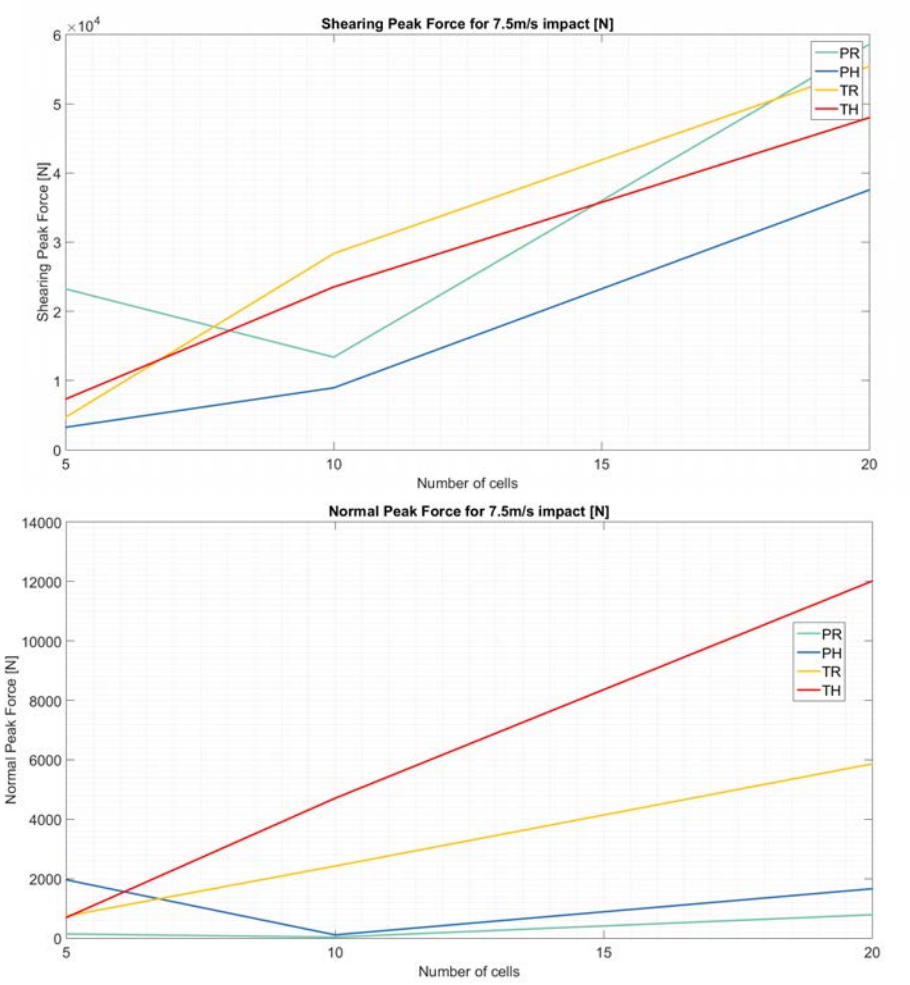

Figure 51: 2D plots for peak values of shearing and normal forces for 7.5 m/s impact velocity.

STRUCTURE TYPE Prismatic-shape cells	**Peak of normal Force [kN]**	**Peak of Shearing Force [kN]**	**Peak of Resultant Force [kN]**
P05R	0.139	23.233	23.233
P05H	1.960	3.264	3.800
P10R	0.033	13.390	13.391
P10H	0.109	8.960	8.967
P20R	0.787	58.608	58.612
P20H	1.661	37.556	37.577
Tetrahedral-shape cells			
T05R	0.744	4.749	4.788
T05H	0.697	7.354	7.380
T10R	2.425	28.365	28.456
T10H	4.708	23.540	24.001
T20R	5.863	55.406	55.716
T20H	12.015	47.993	49.474

Table 11: numerical values of forces peaks. Impact Velocity 7.5 m/s.

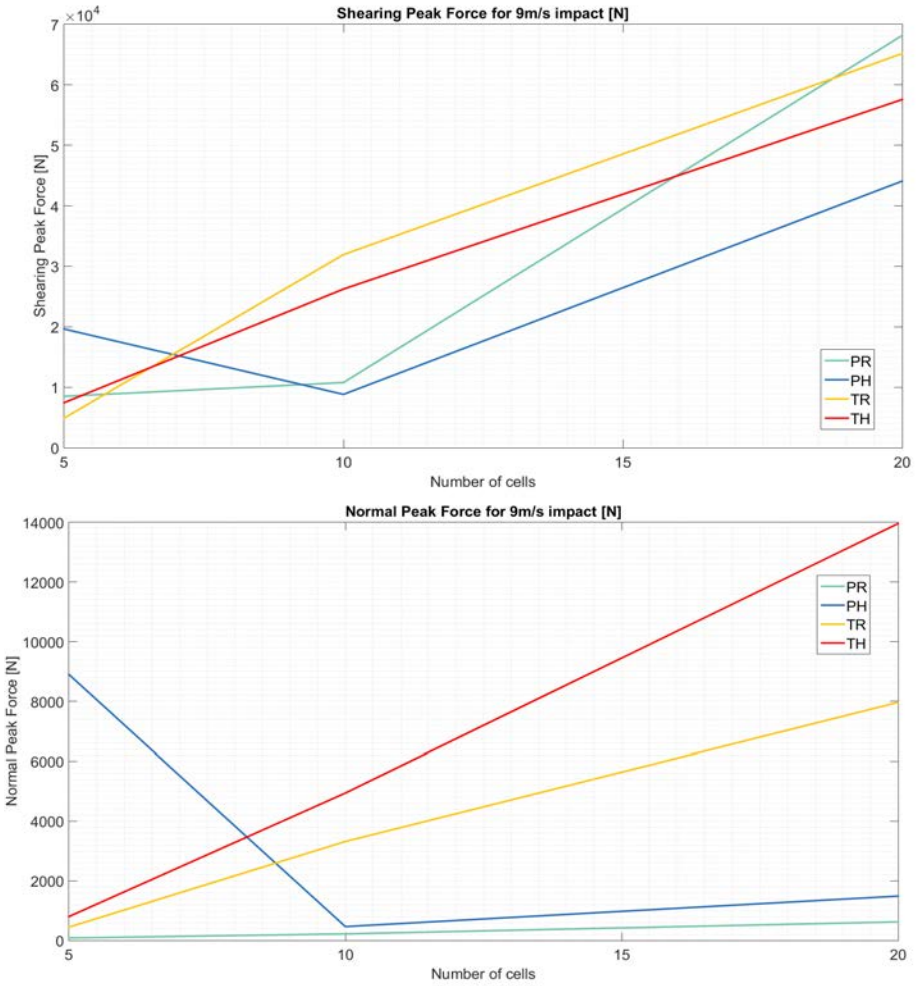

Figure 52: 2D plots for peak values of shearing and normal forces for 9 m/s impact velocity.

STRUCTURE TYPE Prismatic-shape cells	**Peak of normal Force [kN]**	**Peak of Shearing Force [kN]**	**Peak of Resultant Force [kN]**
P05R	0.079	8.504	8.504
P05H	8.898	19.628	21.540
P10R	0.218	10.773	10.773
P10H	0.463	8.820	8.822
P20R	0.620	68.172	68.175
P20H	1.485	44.088	44.092
Tetrahedral-shape cells			
T05R	0.444	4.890	4.893
T05H	0.799	7.449	7.471
T10R	3.317	31.931	32.094
T10H	4.941	26.232	26.662
T20R	7.963	65.184	65.669
T20H	13.962	57.581	59.250

Table 12: numerical values of forces peaks. Impact Velocity 9 m/s.

The columns with the peaks of resultant forces show values close to the shearing peaks, this is a consequence that the shearing force for the majority of the structures is about an order of magnitude greater than the normal force. This means the plots of the resultant forces are very close to the shearing force plots.

The following plots (figures from 53 to 58) are analogous of those in section 3.2.1 and report the resultant forces in order to show their similarities with the shearing forces.

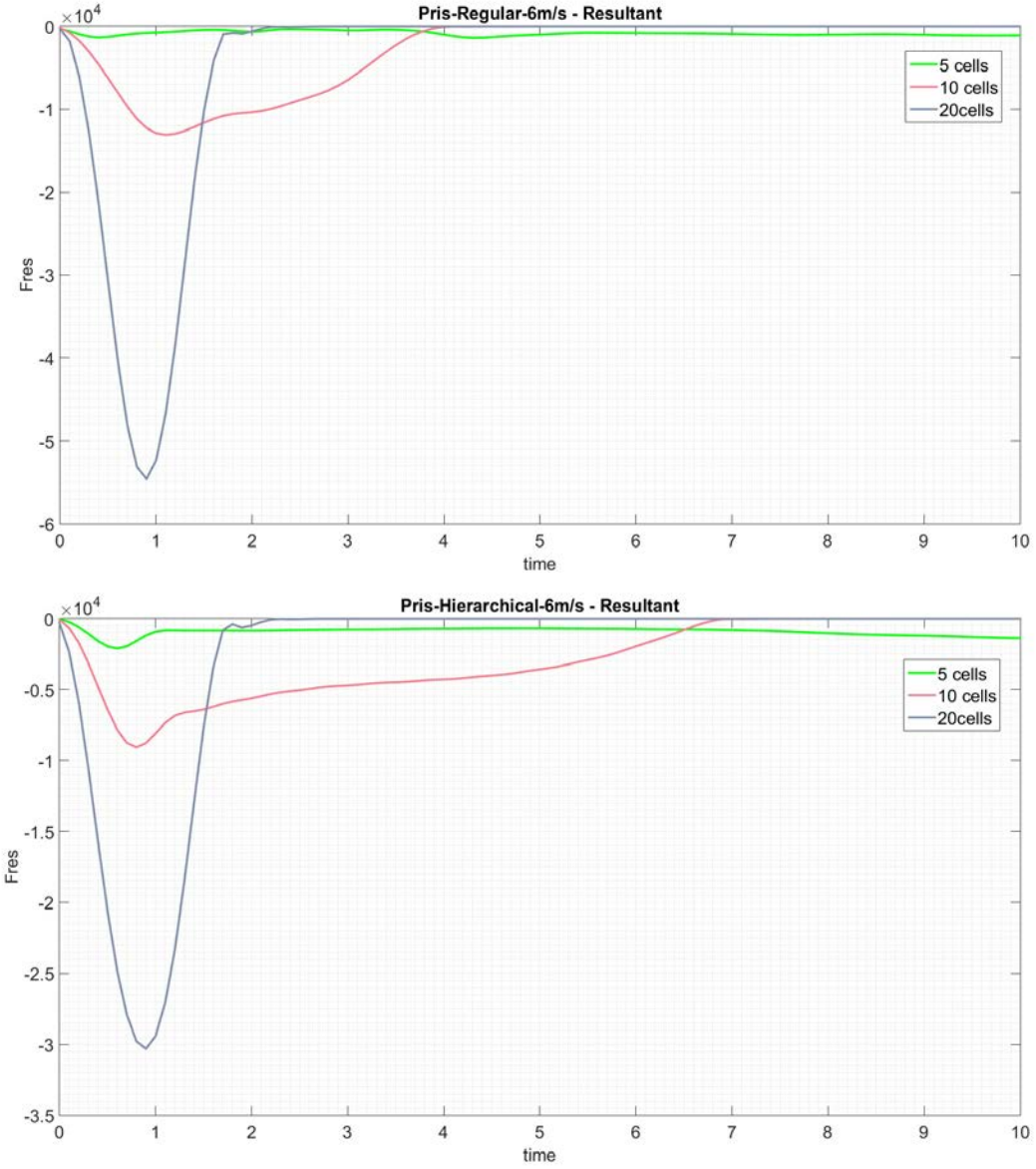

Figure 53: comparison of resultant forces for different structures densities. PR and PH - 6 m/s.

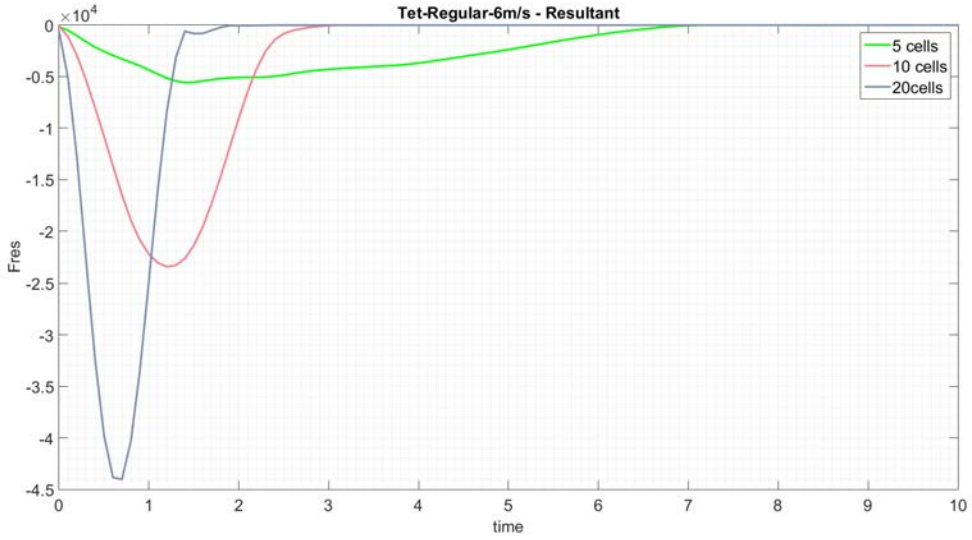

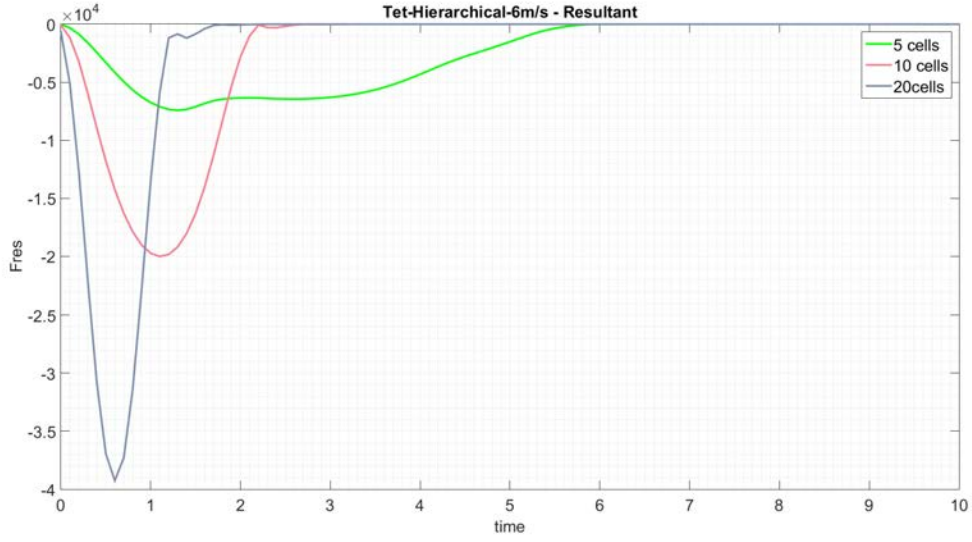

Figure 54: comparison of resultant forces for different structures densities. TR and TH - 6 m/s.

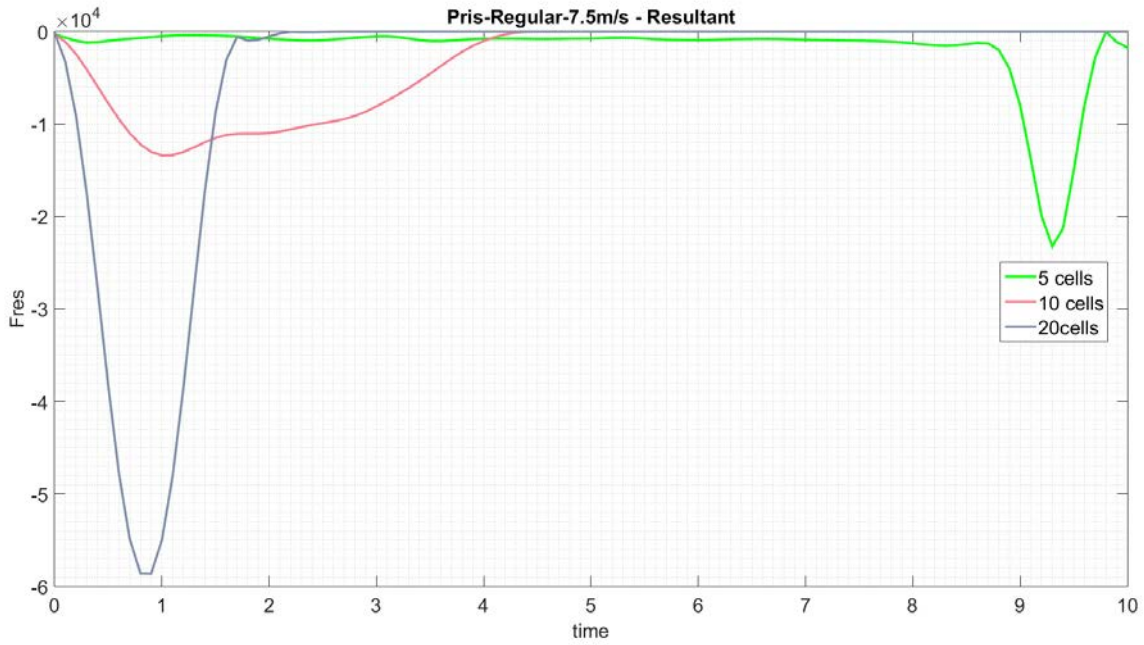

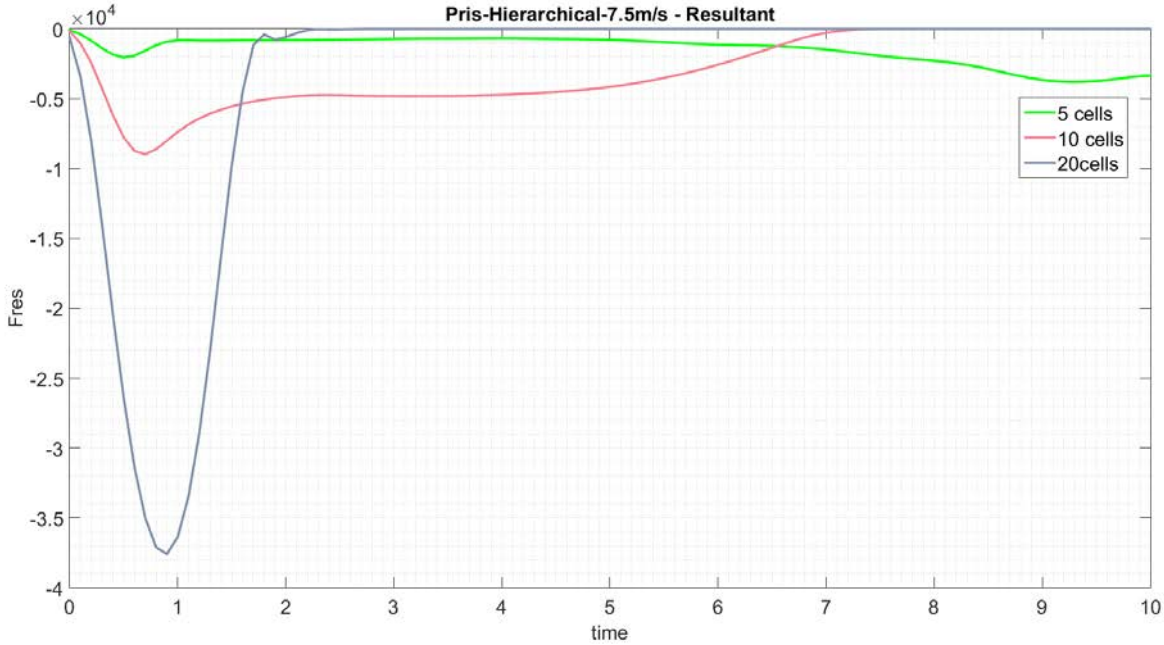

Figure 55: comparison of resultant forces for different structures densities. PR and PH - 7.5 m/s.

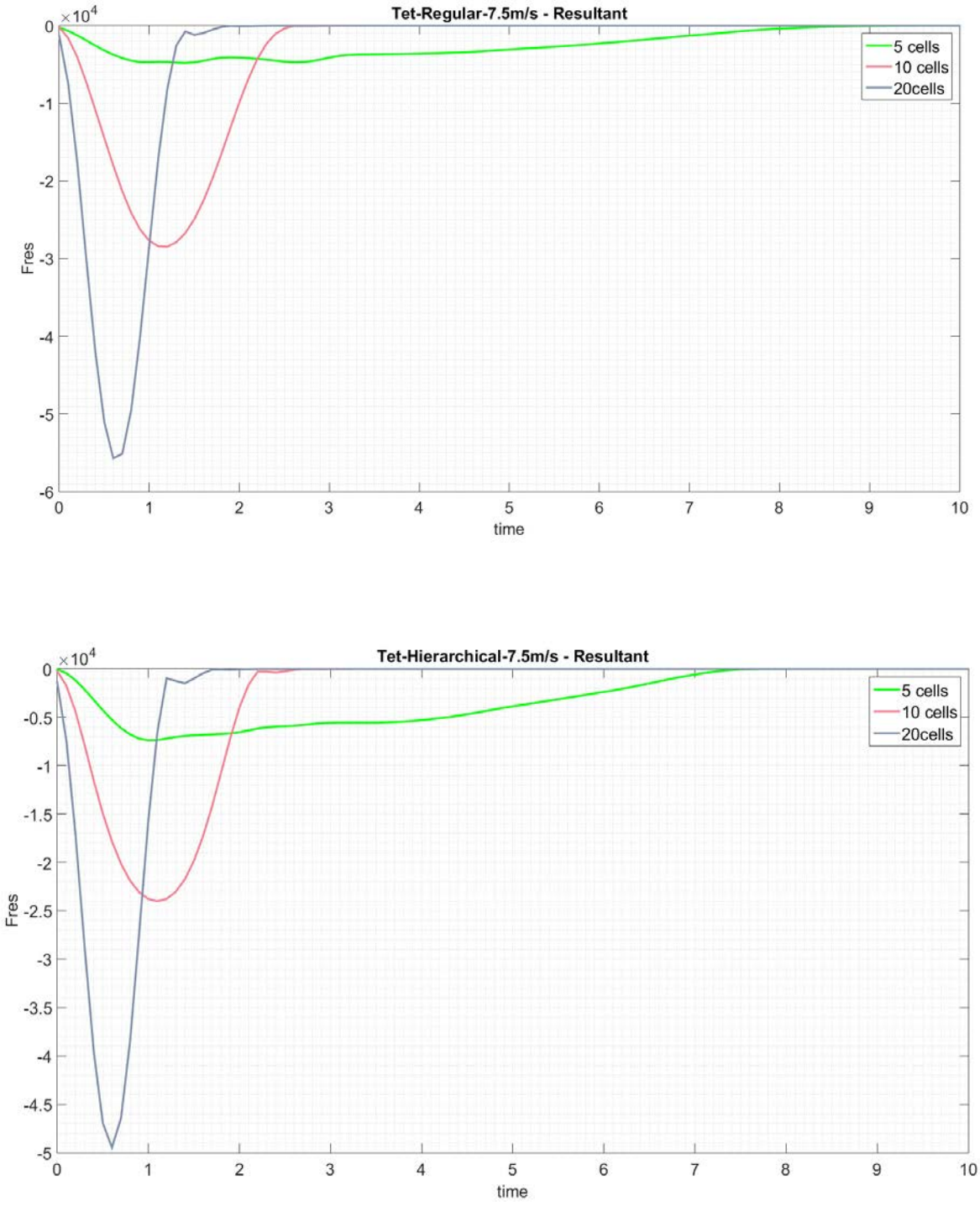

Figure 56: comparison of resultant forces for different structures densities. TR and TH - 7.5 m/s.

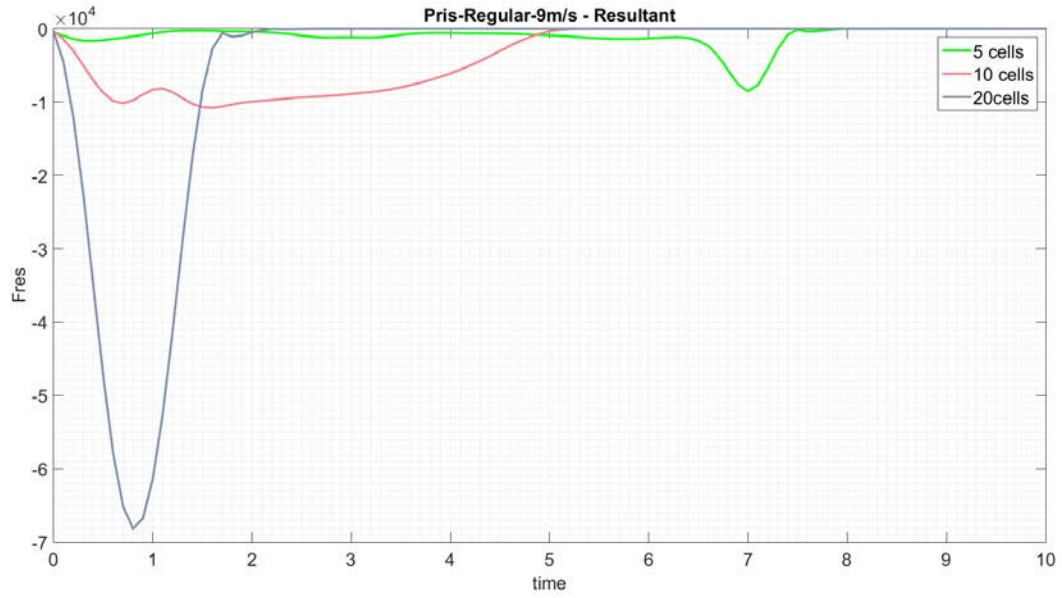

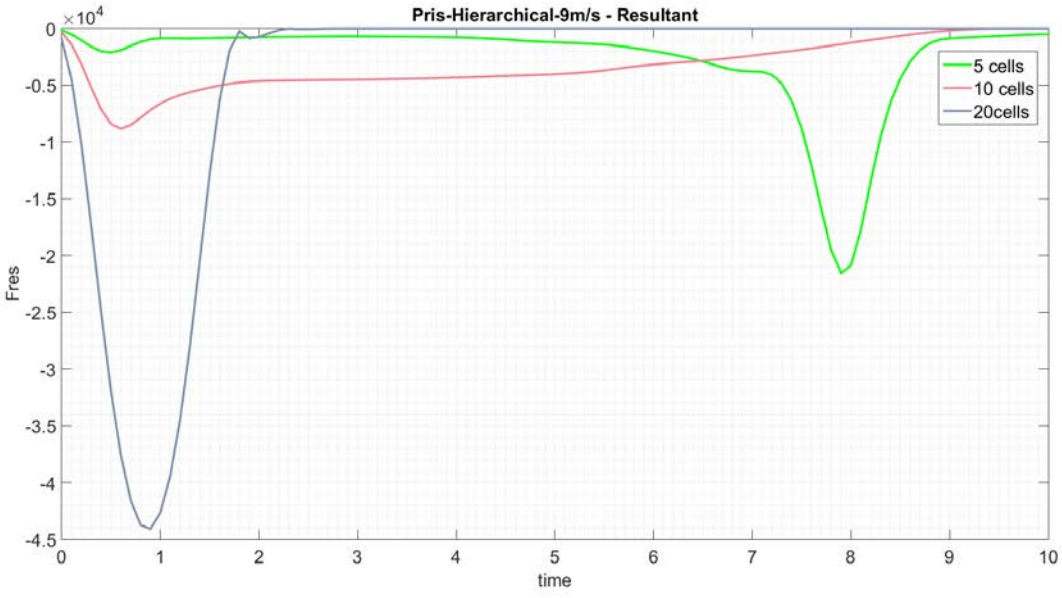

Figure 57: comparison of resultant forces for different structures densities. PR and PH - 9 m/s.

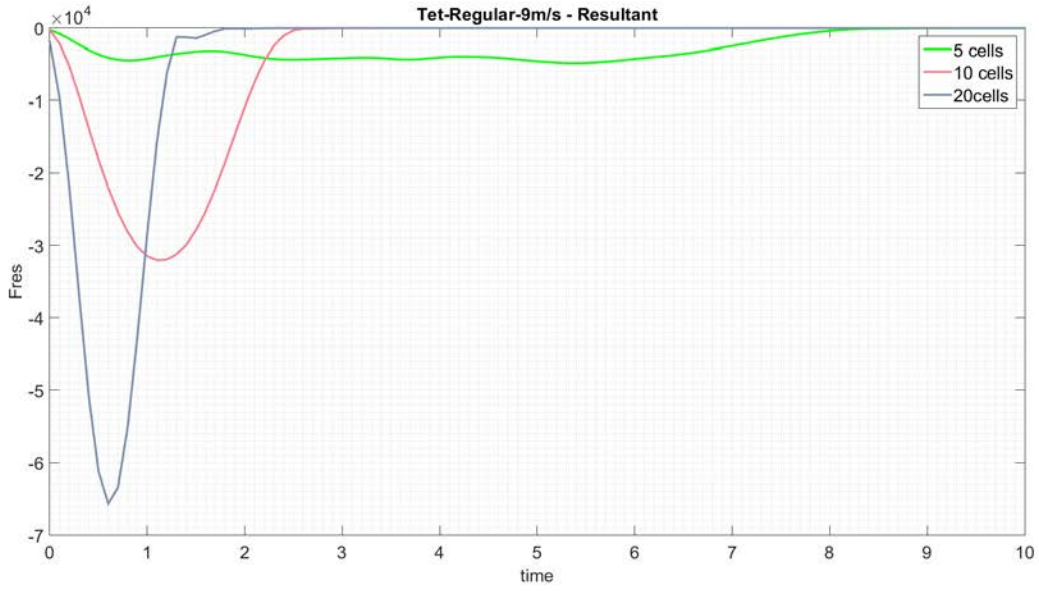

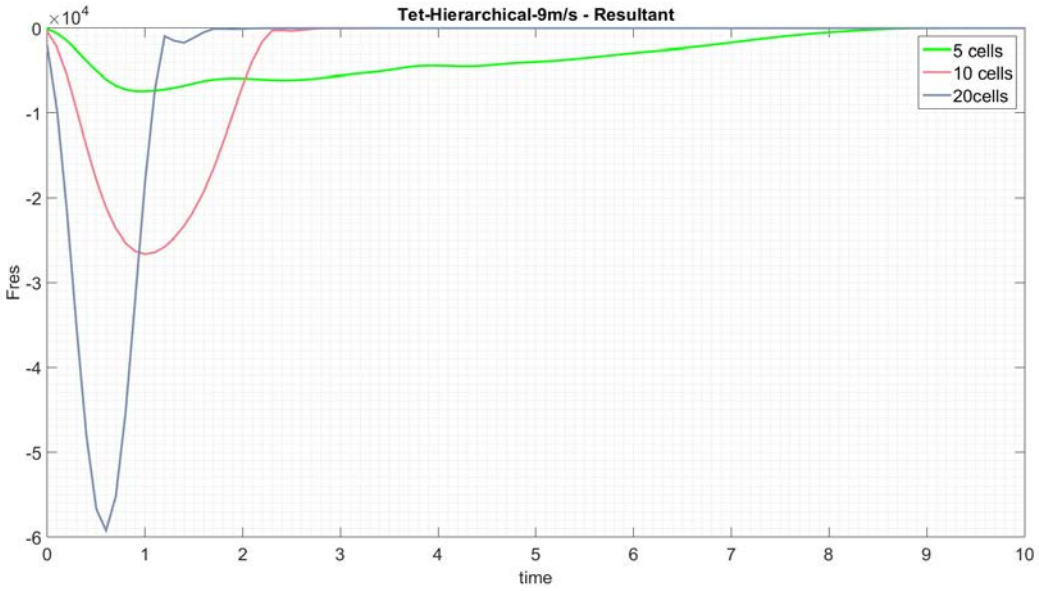

Figure 58: comparison of resultant forces for different structures densities. TR and TH - 9 m/s.

It is then presented the surface plots for the resultant forces for the purpose of comparing them with those in figures 47-49.

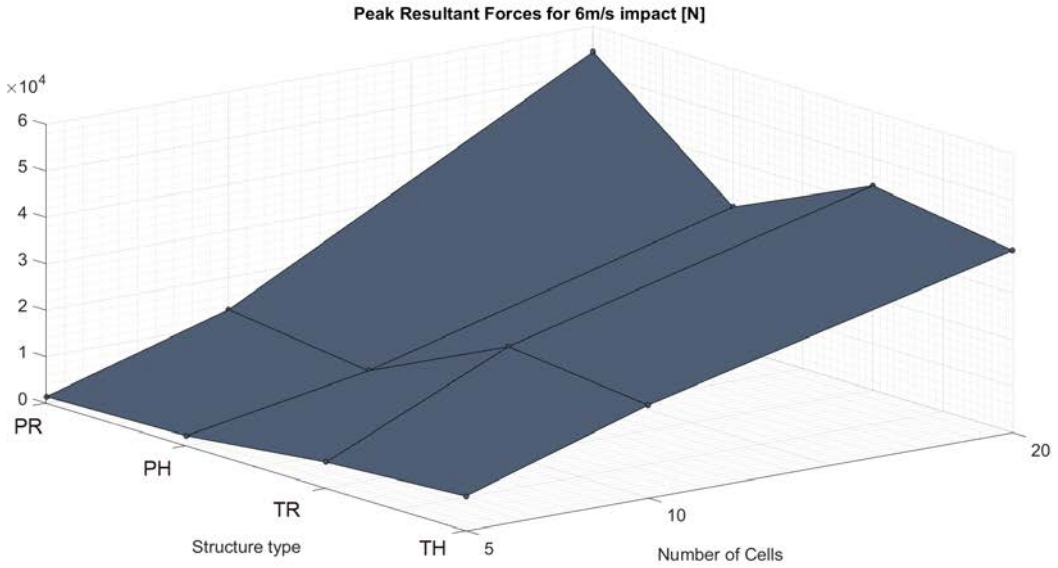

Figure 59: peak values of resultant forces for 6 m/s impact velocity.

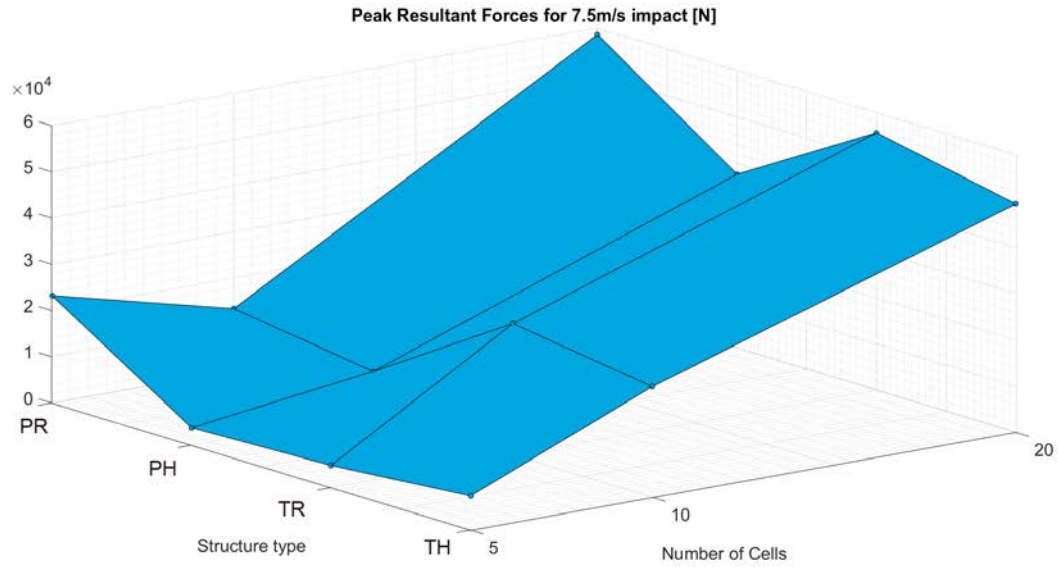

Figure 60: peak values of resultant forces for 7.5 m/s impact velocity.

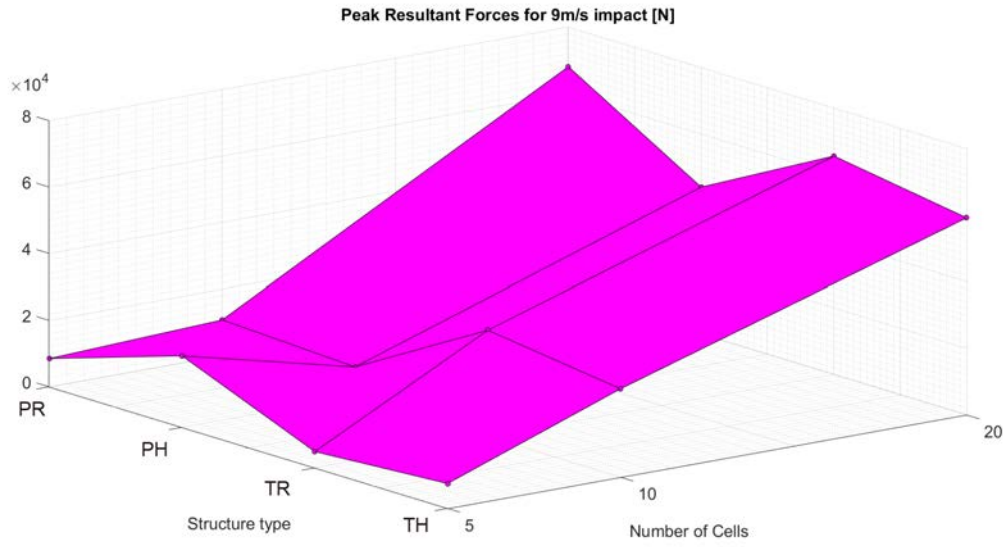

Figure 61: peak values of resultant forces for 9 m/s impact velocity.

These extreme similarities, both in trends and in values, confirm the normal forces have low effects on the resultant transmitted forces.

The peak values comparison may be also done using percentage of peak transmitted forces reduction. In this way the tables above are more immediate to read and to evaluate which structures represent the best trade-offs.
Taken the highest peak values for each of the normal, shearing and resultant forces as the 100%, the reduction is calculated as:

$$reduction\ \% = 100 - 100 \cdot \frac{peak\ in\ exam}{highest\ peak} \quad (5)$$

A reduction of 0% is obviously reported in the cells correspondent to the structure having the highest peak used as 100%.

STRUCTURE TYPE Prismatic-shape cells	Reduction in Normal Force [%]	Reduction in Shearing Force [%]	Reduction in Resultant Force [%]
P05R	99.42	97.47	97.47
P05H	95.47	96.14	96.14
P10R	99.50	76.04	76.05
P10H	99.83	83.42	83.40
P20R	93.15	0.00	0.00
P20H	82.93	44.56	44.50
Tetrahedral-shape cells			
T05R	91.21	89.82	89.79
T05H	93.58	86.45	86.41
T10R	77.56	57.23	57.06
T10H	56.97	64.18	63.36
T20R	58.48	19.68	19.37
T20H	0.00	30.37	28.10

Table 13: percentages of reduction in forces peaks. Impact Velocity 6 m/s.

STRUCTURE TYPE Prismatic-shape cells	Reduction in Normal Force [%]	Reduction in Shearing Force [%]	Reduction in Resultant Force [%]
P05R	98.84	60.36	60.36
P05H	83.69	94.43	93.52
P10R	99.72	77.15	77.15
P10H	99.10	84.71	84.70
P20R	93.45	0.00	0.00
P20H	86.17	35.92	35.89
Tetrahedral-shape cells			
T05R	93.81	91.90	91.83
T05H	94.20	87.45	87.41
T10R	79.82	51.60	51.45
T10H	60.82	59.83	59.05
T20R	51.20	5.46	4.94
T20H	0.00	18.11	15.59

Table 14: percentages of reduction in forces peaks. Impact Velocity 7.5 m/s.

STRUCTURE TYPE Prismatic-shape cells	Reduction in Normal Force [%]	Reduction in Shearing Force [%]	Reduction in Resultant Force [%]
P05R	99.44	87.53	87.53
P05H	36.27	71.21	68.40
P10R	98.44	84.20	84.20
P10H	96.69	87.06	87.06
P20R	95.56	0.00	0.00
P20H	89.36	35.33	35.33
Tetrahedral-shape cells			
T05R	96.82	92.83	92.82
T05H	94.28	89.07	89.04
T10R	76.24	53.16	52.92
T10H	64.61	61.52	60.89
T20R	42.97	4.38	3.68
T20H	0.00	15.54	13.09

Table 15. percentages of reduction in forces peaks. Impact Velocity 9 m/s.

Looking at the more interesting columns of shearing and resultant forces, it appears:

- the stiffest structures, with 20 cells through the thickness, which transmit the highest peaks in all the cases, by the variation of their cell geometry or dimensions, may reach a reduction that almost stands between 3% and 45%; the maximum reduction is for the hierarchical dimensions cells;
- the specimens with ten through-the-thickness cells achieve reductions between 52% and 87%; the hierarchical specimens are still the best;
- Five through-the-thickness cells structures may reduce the peaks by a minimum of 68% until a maximum of more than 92% (the specimens with prismatic-shape cells are not considered because of their complete failures and folding).

3.3 Energy Absorption Evaluations

3.3.1 Absorbed Energy

Absorbed energy is the other interesting set of results computed in order to understand how the lattice structures in exam react to impacts.

The final kinetic energy of the impactor should be computed when its velocity returns to be constant after the impact. In the cases where the simulation time is not enough to make the velocity of the impactor returning constant, the absorbed energy values computed are not reliable and they cannot be used.

The kinetic energy possessed by the impactor for the different impact velocities are reported in table 16:

IMPACTOR MASS [Kg]	IMPACT VELOCITY[m/s]	KINETIC ENERGY OF IMPACTOR [J]
2.00616	6.0	36.11088
2.00616	7.5	56.42325
2.00616	9.0	81.24948

Table 16: impactor kinetic energy for different impapct velocities.

Absorbed energy has been analysed for different structures for each impact velocity. Surfaces with absorbed energy has been plotted to have wide views on how the different parameters act. The *number of cells* axis of the plots has reverse direction with respect to the 3D plots of peak forces for a better view.

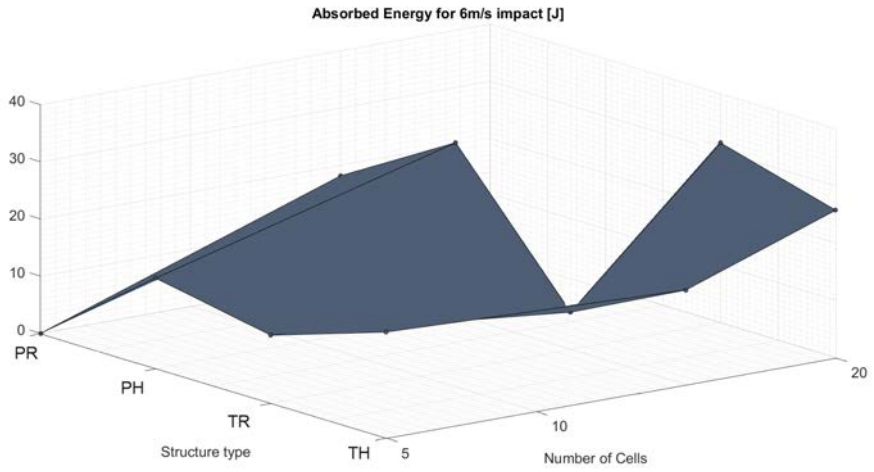

Figure 62: absorbed energy values. 6 m/s impact velocity.

This plot does not report the values for the P05R and P05H specimens because the related simulations do not last enough to get back constant velocity of the impactor.

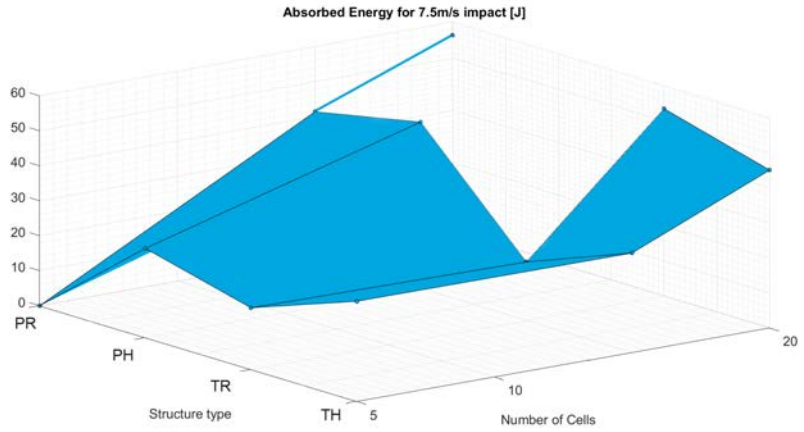

Figure 63: absorbed energy values. 7.5 m/s impact velocity.

The P05H specimen, in this case too, has not been included for the same reason of the *6 m/s* velocity.

For the impact on the P05R specimen, the impactor, after the crushing, continues towards the anvil with reduced constant velocity. Its absorbed energy value are reported even if the specimen is completely failed.

For the T05R and T05H specimens the velocity of the impactor has not yet returned perfectly constant but it is very close to. For this reason the absorbed energy values of these structures are reported; the main targets of these surface plots are, in fact, to understand the trends and to compare qualitatively the different types of considered structures.

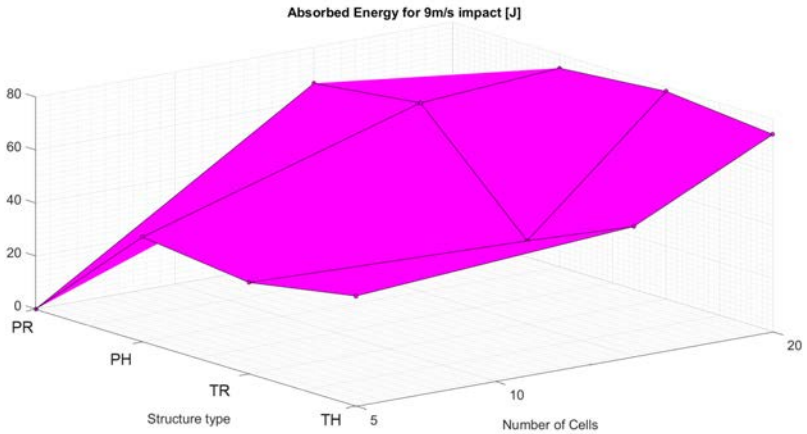

Figure 64: absorbed energy values. 9 m/s impact velocity.

With the highest velocity, almost all of the simulations have enough time to make the impactor having constant final velocity.
With the P05R specimen, the impactor behave like in the *7.5 m/s* impact and hence the related value of absorbed energy is reported.
Instead, with the P05H, P10H, T05R and T05H specimens, the impactor has not get back to constant velocity but it is very close to. Thus, like in the *7.5 m/s* impact simulations with T05R and T05H specimens, the absorbed energy values are left in the plot.

Giving some general comments on these surfaces, it may be stated:

- these surfaces show the hierarchical structures absorb more energy than their analogous specimens with shape-similar but not-hierarchical cells;
- a general trend, valid for the majority of the structures, is the decreasing of the absorbed energy stated by the increasing of the through-the-thickness cells;
- it is evident the biggest differences are for the ten through-the-thickness cells specimen; those with prismatic shape are much more effective than those ones with tetrahedral shape;
- for the highest densities specimens it appears the tetrahedral-shape cells make the structures more effective than the prismatic-shape cells do, considering separately the comparison between regular dimensions and hierarchical dimensions.

All of these discussions are applicable to all the impact velocities.

In figures 65- 67 are visible the sections of the surfaces in figures 62-64. These plots give quantitative details about the values of energy absorbed by the structures in exam. It should be remembered the results relative to the simulations in which the impactor does not reach a perfectly constant value of final velocity are affected by errors. Anyway, they are reported in the following plots because it is reasonable to think the errors made are not so large. This may be affirmed because, as stated before, the velocities are very close to be constant.
For each plot, there is a table reporting the results for every simulation in terms of absorbed energy values and in terms of percentage of absorbed energy where the 100% is the impactor initial kinetic energy.

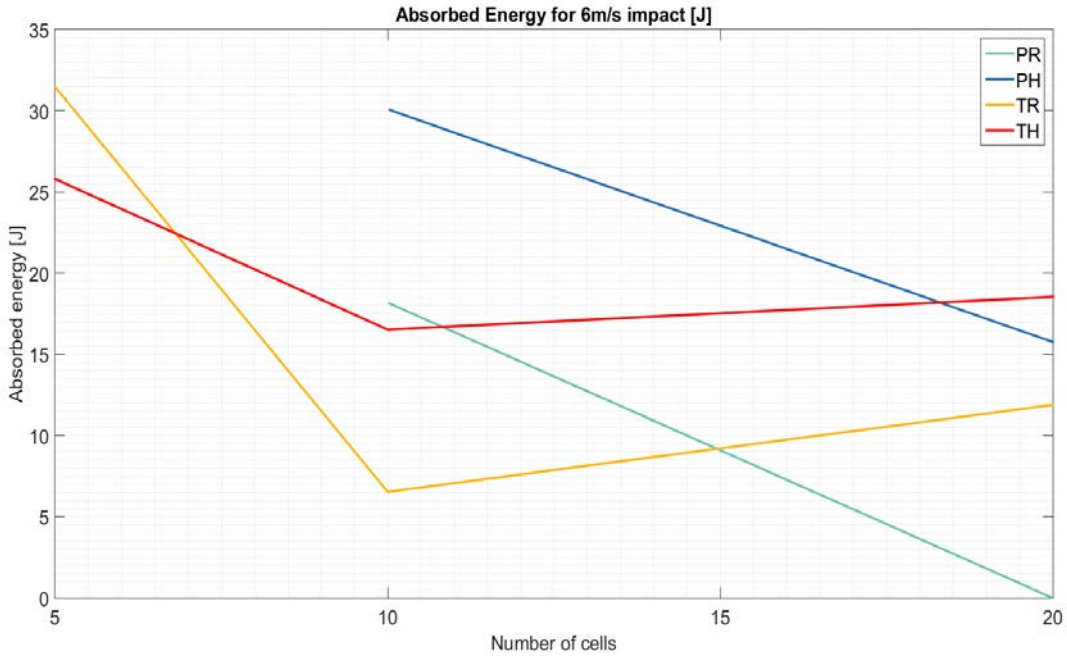

Figure 65: 2D plots for absorbed energy values. 6 m/s impact velocity.

STRUCTURE TYPE **Prismatic-shape cells**	**Absorbed energy [J]**	**Absorbed percentage [%]** **Impactor initial kinetic energy = 100%**
P05R	-	-
P05H	-	-
P10R	18.19	50.37
P10H	30.09	83.31
P20R	0.00	0.00
P20H	15.76	43.65
Tetrahedral-shape cells		
T05R	34.46	95.44
T05H	25.80	71.45
T10R	6.54	18.10
T10H	16.52	45.75
T20R	11.88	32.90
T20H	18.54	51.34

Table 17: numerical values of absorbed energy. 6 m/s impact velocity. 36.11 J impactor initial kinetic energy.

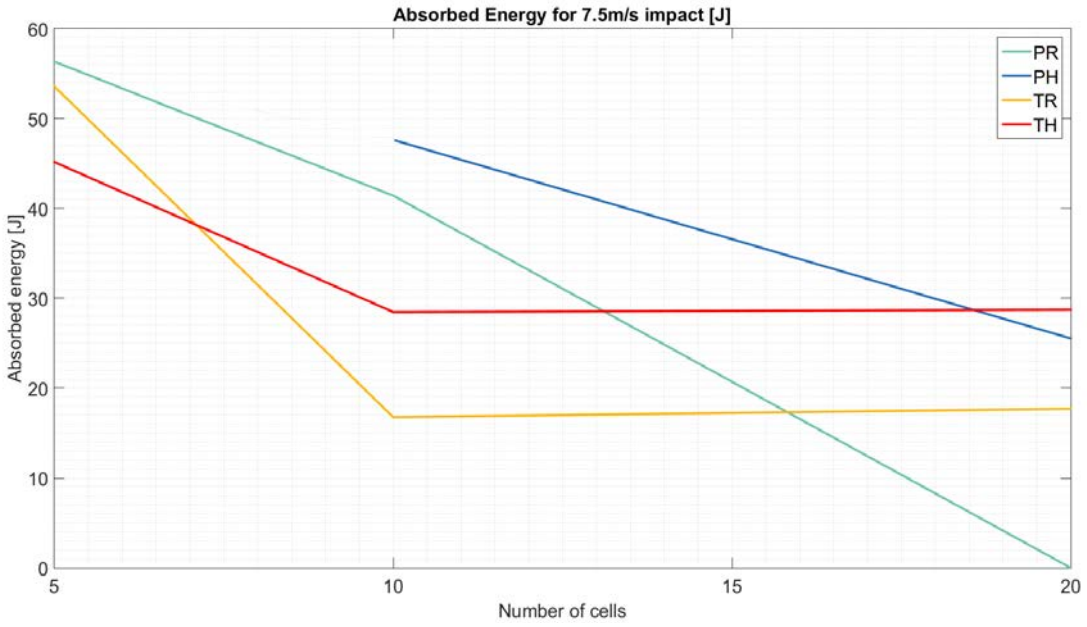

Figure 66: 2D plots for absorbed energy values. 7.5 m/s impact velocity.

STRUCTURE TYPE **Prismatic-shape cells**	**Absorbed energy [J]**	**Absorbed percentage [%]** **Impactor initial kinetic energy = 100%**
P05R	56.32	99.82
P05H	-	-
P10R	41.43	73.42
P10H	47.63	84.42
P20R	0.00	0.00
P20H	25.53	45.25
Tetrahedral-shape cells		
T05R	53.58	94.96
T05H	45.16	80.05
T10R	16.77	29.72
T10H	28.47	50.46
T20R	17.71	31.38
T20H	28.73	50.92

Table 18: numerical values of absorbed energy. 7.5 m/s impact velocity. 56.42 J impactor initial kinetic energy.

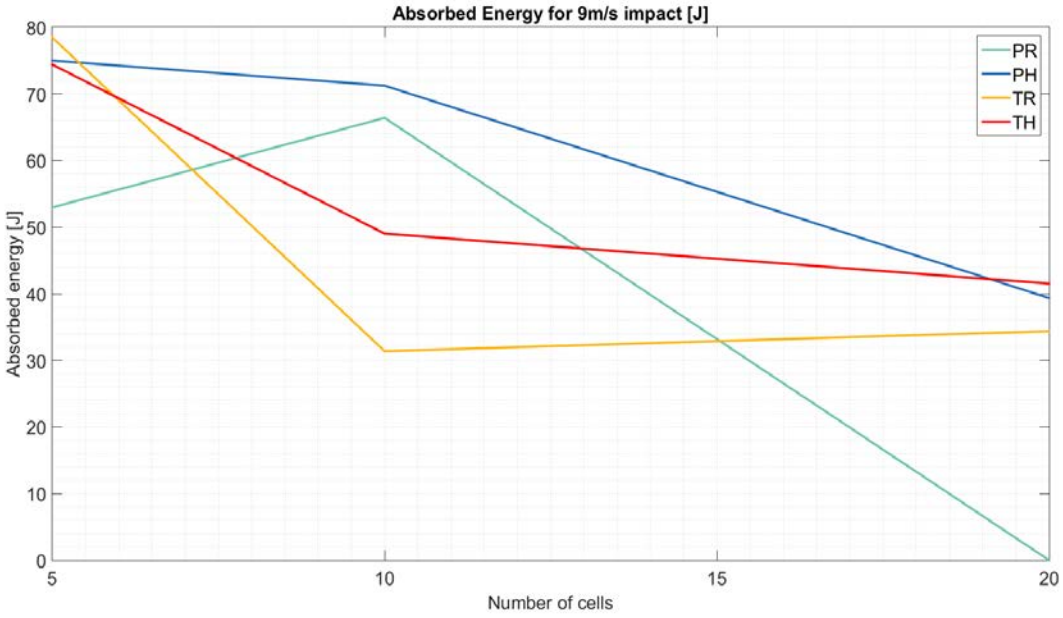

Figure 67: 2D plots for absorbed energy values. 9 m/s impact velocity.

STRUCTURE TYPE **Prismatic-shape cells**	**Absorbed energy [J]**	**Absorbed percentage [%]** **Impactor initial kinetic energy = 100%**
P05R	52.95	65.17
P05H	74.98	92.28
P10R	66.39	81.71
P10H	71.24	87.67
P20R	0.00	0.00
P20H	39.35	48.43
Tetrahedral-shape cells		
T05R	78.44	96.54
T05H	74.39	91.56
T10R	31.38	38.62
T10H	49.02	60.33
T20R	34.38	42.31
T20H	41.51	51.09

Table 19: numerical values of absorbed energy. 9 m/s impact velocity. 81.25 J impactor initial kinetic energy.

From the 2D plots and the tables here above it is possible to sum up that:

- hierarchical specimens are always better than their analogous regular dimensions ones except for those with the lowest density tetrahedral-shape cells ;
- the ten through-the-thickness cells specimens are better if the cells have prismatic shape;
- the twenty through-the-thickness cells specimens are better if the cells have tetrahedral shape;
- the five through-the-thickness cells specimens for the highest impact velocity show better results using prismatic-shape cells if only the hierarchical are considered and using tetrahedral-shape cells if only the regular dimension specimens are considered.

In order to have a more immediate understanding of which are the best structures in these terms, it is useful to compute the percentage of worsening of the different structures with respect to the best absorbing specimen.

This percentage has been computed as:

$$worsening\ \% = 100 - 100 \cdot \frac{energy\ absorbed\ by\ the\ specimen\ in\ exam}{energy\ absorbed\ by\ the\ best\ absorbing} \quad (6)$$

In this computation, the specimens which leave the impactor going towards the anvil after their failure (P05R for *7.5 m/s* and *9 m/s* velocities) have not been considered. This is because they appear to be highly absorbing but they are also useless since the impactor, even though with lower velocity, continues to move towards the anvil.

IMPACT VELOCITY: 6m/s **STRUCTURE TYPE: Prismatic-shape cells**	**Percentage of worsening with respect to the best absorbing specimen [%]** **Best absorbing specimen: T05R**
P05R	-
P05H	-
P10R	47.23
P10H	12.70
P20R	100.00
P20H	54.27
STRUCTURE TYPE: Tetrahedral-shape cells	
T05R	0.00
T05H	25.14
T10R	81.03
T10H	52.06
T20R	65.53
T20H	46.20

Table 20: percentages of worsening in absorbed energy. Impact Velocity 6 m/s.

IMPACT VELOCITY: 7.5 m/s STRUCTURE TYPE: Prismatic-shape cells	Percentage of worsening with respect to the best absorbing specimen [%] Best absorbing specimen: T05R
P05R	-
P05H	-
P10R	22.68
P10H	11.10
P20R	100.00
P20H	52.35
STRUCTURE TYPE: Tetrahedral-shape cells	
T05R	0.00
T05H	15.70
T10R	68.70
T10H	46.86
T20R	66.95
T20H	46.38

Table 21: percentages of worsening in absorbed energy. Impact Velocity 7.5 m/s.

IMPACT VELOCITY: 9 m/s STRUCTURE TYPE: Prismatic-shape cells	Percentage of worsening with respect to the best absorbing specimen [%] Best absorbing specimen: T05R
P05R	-
P05H	4.42
P10R	15.37
P10H	9.19
P20R	100.00
P20H	49.83
STRUCTURE TYPE: Tetrahedral-shape cells	
T05R	0.00
T05H	5.16
T10R	60.00
T10H	37.51
T20R	56.17
T20H	47.08

Table 22: percentages of worsening in absorbed energy. Impact Velocity 9 m/s.

Obviously, the values equal to 0% in the tables 20-22 are those relative to the best absorbing specimen while the values equal to 100% are those relative to the worst specimens that almost do not absorb energy at all.

Specimens with five through-the-thickness cells, not considering the best absorbing

T05R, worsen the absorption of energy between 4.42% and 15.70%. Those with ten cells through the thickness worsen the absorption between 9.19% and 81% depending on the cells geometry. Specimen with twenty cells through the thickness may vary the worsening between 46% and 100%.

With the exception of the specimens with five cells through the thickness, the hierarchical specimens are always better than their analogous specimens with homogeneous dimensions of the cells. In particular it may be noted that for the specimens with ten through-the-thickness cells there are minor differences between regular and hierarchical specimens using prismatic-shape cells; for the twenty through-the-thickness specimen, instead, there are minor differences between regular and hierarchical specimens using the tetrahedral-shape cells.

3.3.2 Specific Absorbed Energy

As stated above, the specimens have different masses because the overall dimensions of the specimens are kept constant and the struts have the same diameter; thus, more struts mean more mass.

It might be useful to evaluate the absorbed energy for unity of mass of the lattice structure. To do this, it has been computed the specific absorbed energy (SAE), previously defined.

In table 23 the masses of each specimen are reported.

MASSES OF SPECIMENS **STRUCTURE TYPE: Prismatic-shape cells**	**Specimen mass [g]**
P05R	14.93
P05H	14.93
P10R	50.18
P10H	50.18
P20R	182.88
P20H	182.88
STRUCTURE TYPE: Tetrahedral-shape cells	
T05R	38.87
T05H	39.47
T10R	145.95
T10H	148.91
T20R	565.95
T20H	579.10

Table 23: masses of the specimens.

The surfaces in 3D plots highlight how the parameters influence the SAE for each impact velocity. In this plots too, it has been removed the unreliable results of the simulations that do not last enough for getting back constant velocity at the impactor.

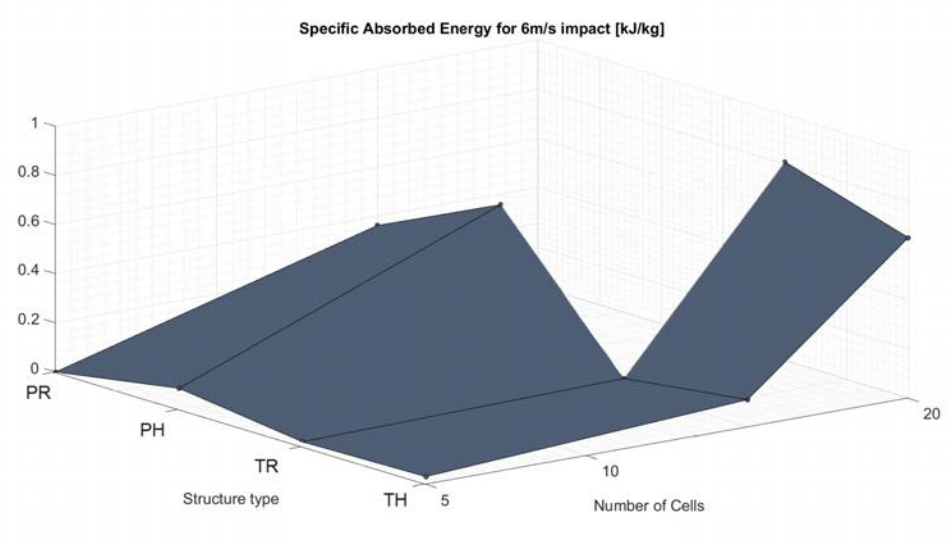

Figure 68: specific absorbed energy values. 6 m/s impact velocity.

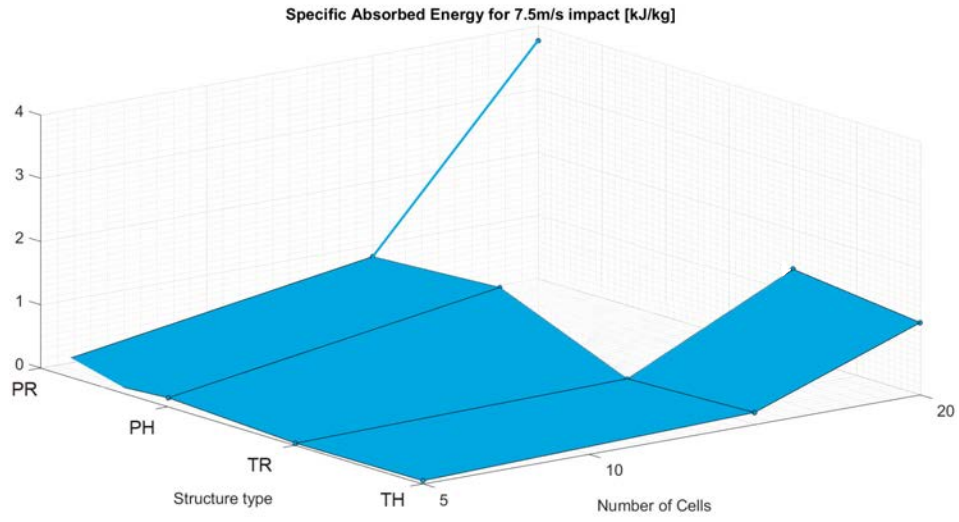

Figure 69: specific absorbed energy values. 7.5 m/s impact velocity.

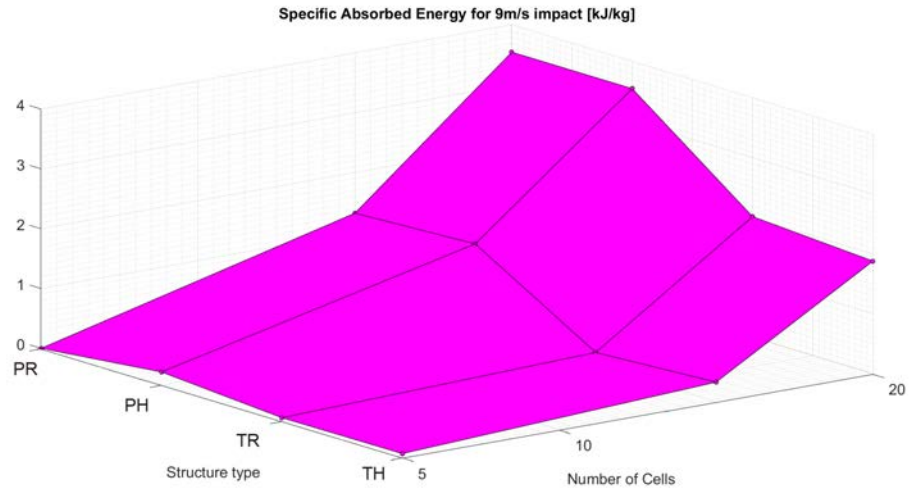

Figure 70: specific absorbed energy values. 9 m/s impact velocity.

In these surfaces the structures affected by errors due to the not-perfectly reached constant velocity (T05R, T05H for the *7.5 m/s* impact and P05H, P10H, T05R, T05H for the *9 m/s* impact) are reported to keep continuity with absorbed energy discussions previously made.

For all the impact velocities it is possible to derive the same comments:

- increasing the number of cells through the thickness is responsible for a decrease of energy absorbed by one kilogram of lattice structure;
- there are not large difference between the usage of regular or hierarchical structures if the shape of the cells is the same;
- larger differences are visible between the usage of prismatic-shape and tetrahedral-shape cells.

For the SAE too, in order to provide quantitative discussions, it is reported the sections of the above plots and the tables with the obtained numerical values.

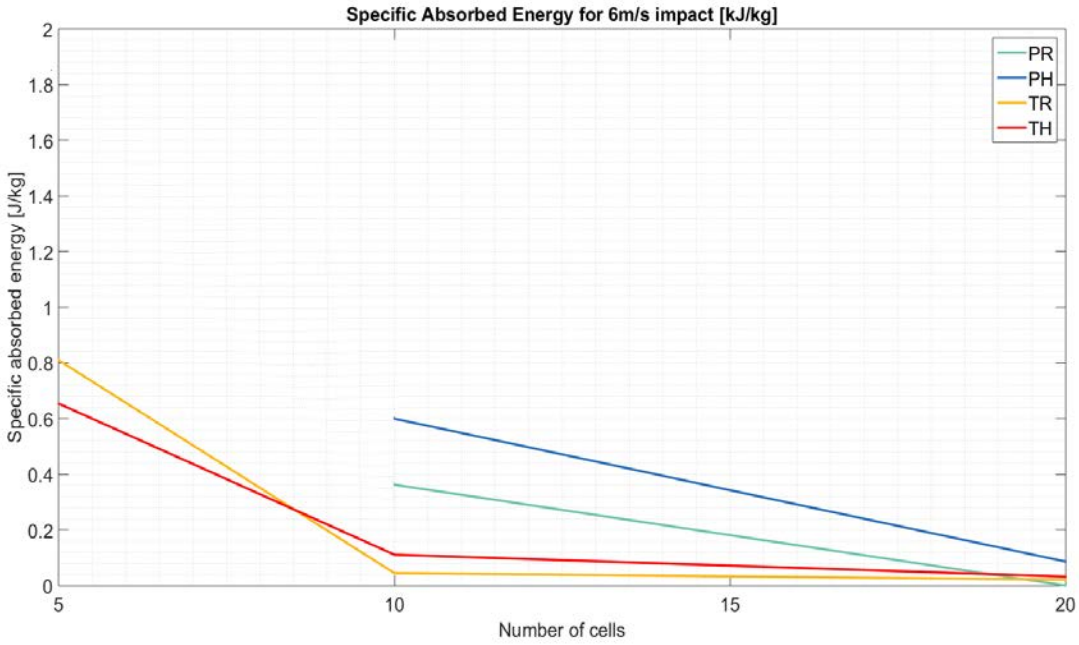

Figure 71: 2D plots for specific absorbed energy values. 6 m/s impact velocity.

IMPACT VELOCITY: 6 m/s **STRUCTURE TYPE: Prismatic-shape cells**	**Specific absorbed energy [kJ/kg]**
P05R	-
P05H	-
P10R	0.363
P10H	0.600
P20R	0.000
P20H	0.086
STRUCTURE TYPE: Tetrahedral-shape cells	
T05R	0.809
T05H	0.654
T10R	0.045
T10H	0.111
T20R	0.021
T20H	0.032

Table 24: numerical values of specific absorbed energy. 6 m/s impact velocity.

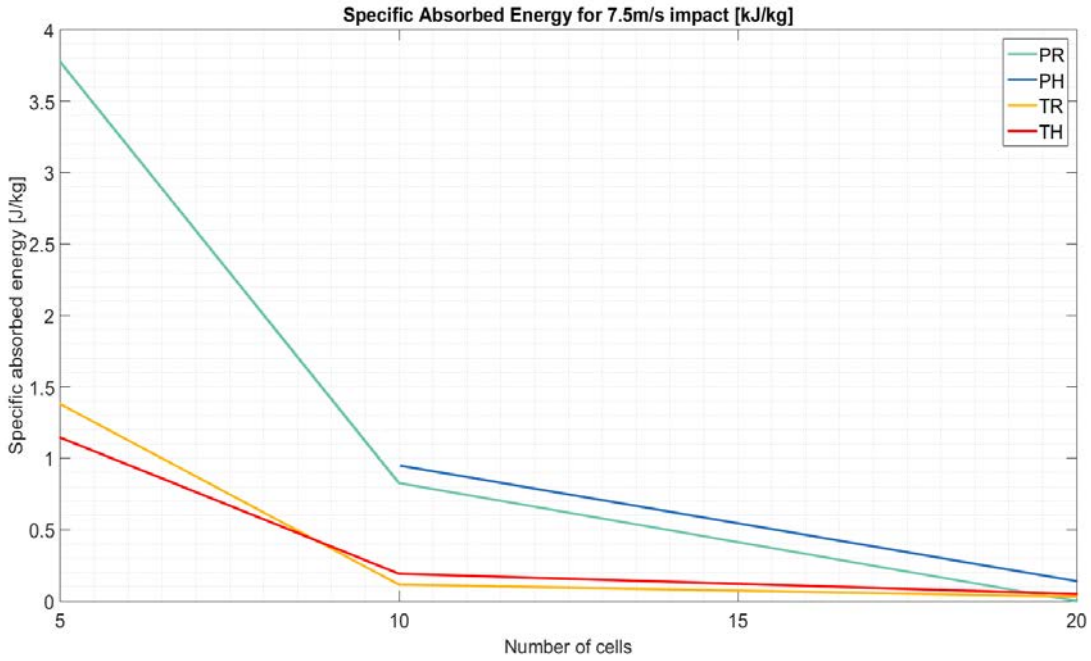

Figure 72: 2D plots for specific absorbed energy values. 7.5 m/s impact velocity.

IMPACT VELOCITY: 7.5 m/s **STRUCTURE TYPE: Prismatic-shape cells**	**Specific absorbed energy [kJ/kg]**
P05R	3.773
P05H	-
P10R	0.826
P10H	0.949
P20R	0.000
P20H	0.140
STRUCTURE TYPE: Tetrahedral-shape cells	
T05R	1.378
T05H	1.144
T10R	0.115
T10H	0.191
T20R	0.031
T20H	0.050

Table 25: numerical values of specific absorbed energy. 7.5 m/s impact velocity.

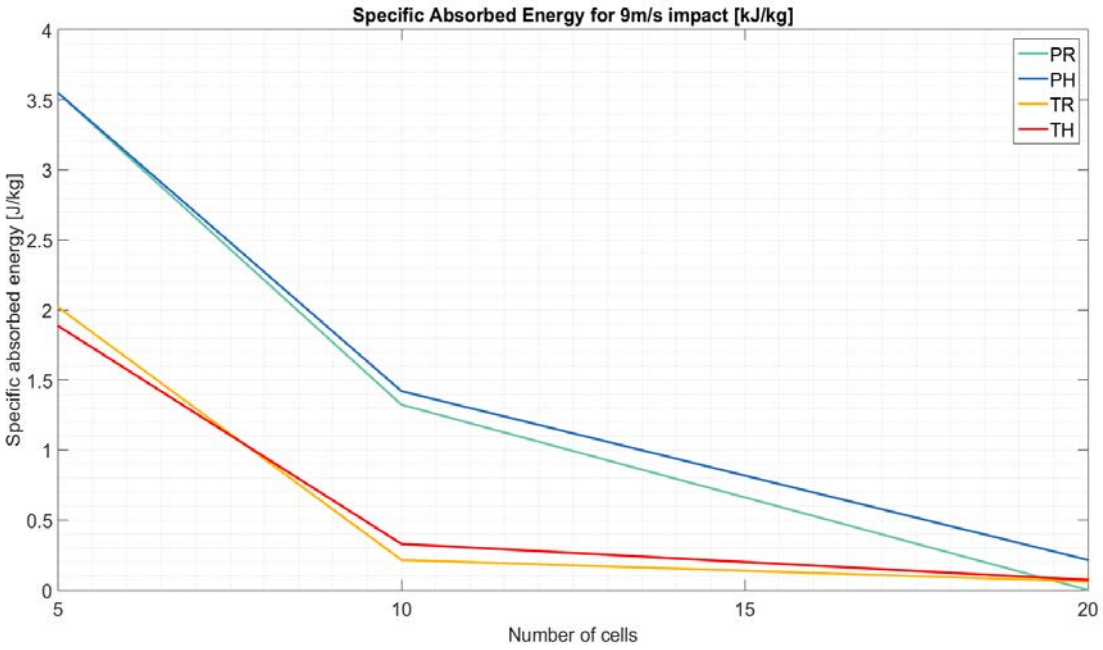

Figure 73: 2D plots for specific absorbed energy values. 9 m/s impact velocity.

IMPACT VELOCITY: 9 m/s **STRUCTURE TYPE: Prismatic-shape cells**	**Specific absorbed energy [kJ/kg]**
P05R	3.547
P05H	3.547
P10R	1.323
P10H	1.420
P20R	0.000
P20H	0.215
STRUCTURE TYPE: Tetrahedral-shape cells	
T05R	2.018
T05H	1.885
T10R	0.215
T10H	0.329
T20R	0.061
T20H	0.072

Table 26: numerical values of specific absorbed energy. 9 m/s impact velocity.

These results are useful to relate achievements in terms of absorbed energy with the mass of protective devices that may be realized with these structures. This relation is important in particular for helmets studies; it is important for a helmet, since it is placed on the head, to be lightweight and to have not too big dimensions.
As anticipated from the 3D plots, it is now possible to confirm that the maximum differences between the results are mainly related to different shape and number of cells rather than if they own homogenous or hierarchical dimensions.
It is interesting to note the only specimens showing better results for the regular dimensions cells rather than the hierarchical ones are those with five tetrahedral cells through the thickness.

Like the previous sets of results it is now considered the SAE with disadvantage percentages of all the structures compared to that best-resulting for each of the three impact velocities.
The worsening percentage is computed similarly to equation (6):

$$worsening\ \% = 100 - 100 \cdot \frac{SAE\ of\ the\ specimen\ in\ exam}{SAE\ of\ the\ best\ absorbing\ specimen} \quad (7)$$

In this computation too, the simulations in which the impactor is left to go towards the anvil after the failure of the specimens (P05R for 7.5m/s and 9m/s velocities) have not been considered.

IMPACT VELOCITY: 6 m/s STRUCTURE TYPE: Prismatic-shape cells	**Percentage of worsening with respect to the best absorbing specimen [%] Best absorbing specimen: T05R**
P05R	-
P05H	-
P10R	55.10
P10H	25.93
P20R	100.00
P20H	89.35
Tetrahedral-shape cells	
T05R	0.00
T05H	19.25
T10R	94.47
T10H	86.29
T20R	97.41
T20H	96.04

Table 27: percentages of worsening in specific absorbed energy. Impact Velocity 6 m/s.

IMPACT VELOCITY: 7.5 m/s STRUCTURE TYPE: Prismatic-shape cells	Percentage of worsening with respect to the best absorbing specimen [%] Best absorbing specimen: T05R
P05R	-
P05H	-
P10R	40.10
P10H	21.13
P20R	100.00
P20H	89.87
Tetrahedral-shape cells	
T05R	0.00
T05H	16.99
T10R	91.66
T10H	86.13
T20R	97.73
T20H	96.40

Table 28: percentages of worsening in specific absorbed energy. Impact Velocity 7.5 m/s.

IMPACT VELOCITY: 9 m/s STRUCTURE TYPE: Prismatic-shape cells	Percentage of worsening with respect to the best absorbing specimen [%] Best absorbing specimen: T05R
P05R	-
P05H	0.00
P10R	62.70
P10H	59.97
P20R	100.00
P20H	93.93
Tetrahedral-shape cells	
T05R	43.11
T05H	46.86
T10R	93.94
T10H	90.72
T20R	98.29
T20H	97.98

Table 29: percentages of worsening in specific absorbed energy. Impact Velocity 9 m/s.

It is to be noticed the best absorbing specimen for the 9m/s impact is the P05H instead of T05R that is the best for *6 m/s* and *7.5 m/s* impacts.

In general, obviously excepting the best specimens, those ones with five through-the-thickness cells worsen the SAE by a minimum of 17% to a maximum of 46.86%. These specimens, considering separately each one of the impact velocities, provide the minor worsening.

Ten through-the-thickness cells specimens provide a SAE worsening which stands almost between 25% and 63% for the prismatic-shape cells and between 86% and 95% for the tetrahedral-shape cells.

The highest densities specimens, as previously seen, are the worst. Their percentage of worsening, considering all the impact velocities, stands between 89% and, obviously, 100%.

4. CONCLUSIONS

Results considerations in terms of transmitted forces may be summarised as follows:

- Increase the number of through-the-thickness cells means to increase the transmitted forces, to make the impacts lasting more time and to reduce the severity of damages in the specimens.
- Specimens with regular dimensions of cells have brittle behaviours that lead to many failed struts.
- Specimens with hierarchical dimensions of cells are more easily deformed with low likelihood of struts failure.
- Increasing the velocity of the impacts leads to more failures and more residual deformations in the specimens;
- Hierarchy have different influence in different structure densities: the hierarchy worsen the transmission of forces with five through-the-thickness cells; it improves the performance of shearing force transmission and worsen the normal force transmission with ten and twenty cells through the thickness.
- Shearing forces are always about an order of magnitude greater than the normal ones; this means the resultant force is always very close to the shearing one, both in behaviour and in the reached values .
- For the transmitted peaks of forces, the worst specimen is P20R for each of the impact velocity; the other twenty through-the-thickness cells specimens improve the performances between the 3% and 45%, depending on the impact velocity; ten through-the-thickness cells specimens improve the performances between 52% and 87%, depending on the impact velocity; five through-the-thickness cells specimen, depending on the impact velocity, improve the performances between 68% and 92%, P05R is not consider because of its complete failure.

Results considerations in terms of absorbed energy may be summarised as follows:

- Increase the number of through-the-thickness cells means to decrease the energy absorption.
- Keeping the same cell-shape, except for specimens with five cells through the thickness, using hierarchical dimensions brings to improve the absorbed energy.
- Impact velocity does not modify these trends.
- Prismatic-shape cells are better than tetrahedral-shape ones in ten through-the-thickness cells specimens.
- Tetrahedral-shape cells are better than prismatic-shape ones in ten through-

the-thickness cells specimens.

- For the specimens with the five through-the-thickness cells, prismatic-shape cells are better than tetrahedral-shape ones only for the specimens with hierarchical dimensions.
- The best specimen is T05R; the others with five cells through the thickness worsen the absorption of energy between 4.42% and 15.70%; specimens with ten through-the-thickness cells worsen between 9% and 81%; highest density specimens worsen between 46% and 100%.
- Considering the SAE, it decreases if the number of cells through the thickness are increased.
- SAE of specimens with same-shape cells is not largely different considering regular or hierarchical dimensions of the cells.
- The usage of prismatic-shape cells are much more effective than that of tetrahedral-shape cells in terms of SAE.
- The best performing specimens for SAE are the T05R for 6m/s and 7.5m/s impacts and the P05H for the 9m/s impact; in general, the worsening is kept between 17% and 46.86% for the specimens with five cells through the thickness; it is maintained between 25% and 63% for the specimens with ten through-the thickness prismatic-shape cells and between 86% and 95% for the specimens with ten through-the-thickness tetrahedral-shape cells; it is kept between 89% and 100% for the specimens with twenty cells through

All of these considerations may drive to the choice of the best structures based on the requirements for the application.

The prismatic-shape cells with five through-the-thickness structures do not provide protection because they tend to a complete crush and make too low resistance against the impactor.

For the purpose to transmit the lower possible forces, the optimal structures are those which can ensure the stop of the impactor with a contemporary low transmission of loads.

Structures that respond better to the just mentioned requirement are those presenting the most severe plastic deformations after the impact. However, they can be considered only for application where the importance of effective protection justifies the change of absorbing device after each impact, since, after it, they are no longer good for the

absorption.

In applications where the absorbing device cannot be frequently changed it is necessary to use structures which recover well after the impact without large residual plasticities. The behaviours of the structures do not change widely where the velocity of the impact is increased, the changes mainly regard the values of the transmitted forces and the severity of the damages.

The structures that appear to be the best for the transmission of the lowest possible force peaks and to be not completely crushed or folded are the T05R, T05H, P10R and P10H. These structures ensure the stop of the impactor and thus represent good trade-offs.

For the purpose to absorb the highest possible energy, the best trade-offs for both absolute absorbed energy and specific absorbed energy are the specimens P05H, P10H, T05R and T05H. However, considering the P05H is completely folded during the impact, it is better not to use it in order to do not accept the risk of contact between impactor and anvil.

Finally, it appears the best lattice structures that provide protection against oblique impacts, both in terms of transmitted forces and absorbed energy, are those with five tetrahedral-shape cells through the thickness (T05R, T05H) and that one with ten hierarchical prismatic-shape cells through the thickness (P10H).

5. BIBLIOGRAPHY

1. L. Di Landro, G. Sala, D. Olivieri, Deformation mechanism and energy absorption of polystirene foams for protective helmets, Polymer Testing 21 (2002) 217-228.

2. S.P. Soe, P. Martin, M. Jones, M. Robinson, P. Theobald, Feasibility of optimising bicycle helmet design safety through the use of additive manufactured TPE cellular structures, Int. J. Adv. Manuf. Technol. 79 (2015) 1975-1982.

3. A. Cernicchi, U. Galvanetto, R. Olsson, Virtual testing of composite motorcycle helmets, Int. J. Mod. Phys. B 22 (2008) 1705-1711.

4. L. Cui, S. Kiernan, M. D. Gilchrist, Designing the energy absorption of functionally graded foam materials, Materials Science and Engineering A 507 (2009) 215-225.

5. X. Zhang, H. Zhang, Optimal design of functionally graded foam material under impact loading, International Journal of Mechanical Sciences 68 (2013) 199-211.

6. M. A. Forero Rueda, L. Cui, M. D. Gilchrist, Optimisation of energy absorbing liner for equestrian helmets. Part I: Layered foam liner, Materials and Design 30 (2009) 3405-3413.

7. M. A. Forero Rueda, L. Cui, M. D. Gilchrist, Optimisation of energy absorbing liner for equestrian helmets. Part II: Functionally graded foam liner, Materials and Design 30 (2009) 3414-3419.

8. T. A. Schaedler, C.J. Ro, A. E. Sorensen, Z. Eckel, S. S. Yang, W. B. Carter, A. J. Jacobsen, Designing Metallic Microlattices for Energy Absorber Applications, Advanced Engineering Materials 16(3) (2014) 276-283.

9. J. Brennan-Craddock, D. Brackett, R.Wildman, R. Hague, The design of impact absorbing structures for additive manufacture, Journal of Physics: Conference Series 382 (2012) 012042.

10. M. Mohsenizadeh, F. Gasbarri, M. Munther, A. Beheshti, K. Davami, Additevely-manufactured lightweight Metamaterials for energy absorption, Materials and Design (2018) 521-530.

11. S. Banerjee, On the mechanical properties of hierarchical lattices, Mechanics of Materials 72 (2014) 19-32.

12. F. Sun, C. Lai, H. Fan, D. Fang, Crushing mechanism of hierarchical lattice structure, Mechanics of Materials 97 (2016) 164-183.

13. S. F. Khosroshahi, S. A. Tsampas, U. Galvanetto, Feasibility study on the use of a hierarchical lattice architecture for helmet liners, Materials Today Communications 14 (2018) 312-323.

14. N. J. Mills, S. Wilkes, S. Derler, A. Flisch, FEA of oblique impact tests on a motorcycle helmet, International Journal of Impact Engineering 36 (2009) 913-925.

15. C. Ling, J. Ivens, P. Cardiff, M. D. Gilchrist, Deformation response of EPS foam under combined compression-shear loading. Part I: Experimental design and quasi-static tests, International Journal of Mechanical Sciences 144 (2018) 480-489.

16. C. Ling, J. Ivens, P. Cardiff, M. D. Gilchrist, Deformation response of EPS foam under combined compression-shear loading. Part II: High strain rate dynamic tests, International Journal of Mechanical Sciences 145 (2018) 9-23.

17. C. Ling, P.Cardiff, M. D. Gilchrist, Mechanical behaviour of EPS foam under combined compression-shear loading, Materials Today Communications 16 (2018) 339-352.

Acknowledgements

For this thesis I would like to thank Prof. Galvanetto and Siamak Farajzadeh Khosroshahi PhD for the support and the suggestions during these months of work.